國 立 交 通 大 學

材料科學與工程學系奈米科技碩士班

碩士論文

交流電動力輔助之阻抗式生醫感測研究

Study of AC electrokinetics assisted impedance biosensors

研 究 生：潘俊良

指導教授：許鉦宗 博士

中華民國 一百 年 十一 月

交流電動力輔助之阻抗式生醫感測研究

Study of AC electrokinetics assisted impedance biosensors

研究生：潘俊良　　Student：Chun-Liang Pan

指導教授：許鉦宗 教授　　Advisor：Prof. Jeng-Tzong Sheu

國立交通大學

材料科學與工程學系

奈米科技碩士班

碩士論文

A Thesis

Submitted to Graduate Program for Nanotechnology

Department of Materials Science and Engineering

College of Engineering

National Chiao Tung University

in partial Fulfillment of the Requirements

for the Degree of Master

in Nanotechnology

November, 2011

Hsinchu 300, Taiwan, Republic of China

中華民國 一百 年 十一 月

交流電動力輔助之阻抗式生醫感測研究

研究生：潘俊良　　指導教授：許鉦宗 教授

國立交通大學

材料科學與工程學系奈米科技碩士班

摘　　要

食物中毒案例於全世界的發生率愈來愈高且也愈來愈受重視，其原因主要都是細菌對食物的汙染。在多數有害細菌之中，有病原性的腸炎弧菌在台灣及美國所引起的病發案例最為多數。傳統和現今應用於感測細菌的方式通常需要數天的時間來完成。相較於發展中的生物感測器偵測病原，則可大大地縮短偵測時間。本研究利用電阻抗方式感測貼附於金電極表面的腸炎弧菌，然而為了縮短腸炎弧菌貼附於金電極表面的時間，使用在微流道系統施加不均勻電場所產生的交流電動力濃縮細菌。本研究之生醫感測元件以半導體元件製程製作金電極於二氧化矽基材上。新的電極設計利用圓形電極裡的內圓電極換成指叉式型式。此設計是為了同時具備聚集細菌及感測細菌之效果。為了使聚集的細菌固定在晶片表面，對金電極修飾有專一性的抗體使其與腸炎弧菌有共價鍵連接。我們也利用氧化還原、螢光修飾及 TMP 的顯色機制確認晶片上所修飾的化學分子和生物分子。檢測細菌的晶片會與微流道系統作結合，在輸送細菌於晶片表面的同時，施加適當的電壓及頻率使溶液產生交流電動力以聚集細菌置電極內圓。然後量測細菌貼附於電極表面後的阻抗，再與細菌貼附於晶片之前的阻抗值比較，計算出變化量。本研究以不同大小電極檢測腸炎弧菌，發現當電極面積對流道腔體體積之比率愈大，其阻值變化量愈大。對不同濃度的感測，本系統的最低極限為 10^5cfu/mL。最後以量出的阻抗值對一等效電路作模擬，分析電路裡造成阻值改變的元件。等效電路的模擬結果可看出，細菌貼附於晶片表面主要導致表面電容的改變。另外，選擇性感測也呈現在此研究中，當大腸桿菌與腸炎弧菌同時混入溶液一起感測時，其阻值變化量接近單測腸炎弧菌之變化量。

Study of AC electrokinetics assisted impedance biosensors

Student: Chun-Liang Pan Advisor: Dr. Jeng-Tzong Sheu

Submitted to Graduate Program for Nanotechnology

Department of Material Science and Engineering

National Chiao-Tung University

ABSTRACT

Foodborne disease is becoming one of the major crises on human health. *Vibrio parahaemolyticus,* one of the pathogens, is becoming a highest risk source in food poisoning worldwide. The conventional bacterial detection methods such as immunology-based methods are not fast enough and require a few days for a reply. Hence, biosensing techniques with rapid, sensitive, and accurate detection have attracted much attention recently. Among different sensing techniques, impedimetric sensor adopted in this study is becoming popular due to its simplicity in device preparation. In this thesis, study of *Vibrio parahaemolyticus* trapping mechanisms on the gold electrode via AC electrokinetics was investigated. The detection was fulfilled using impedance analysis in a microfluidic system. A novel configuration of electrode was designed and proposed for its advantages in combining bacteria trapping and detection. To enhance the specificity, *Vibrio parahaemolyticus* specific antibody was modified onto the gold electrode for bacteria immobilization. Cyclic voltammetry, fluorescence imaging, and TMP were applied to identify the quality of the surface modifications. The functionalized chip was then integrated into microfluidic system for bacteria transport. The time needed for bacteria immobilization was reduced by AC electrokinetics manipulation. The concentrated bacteria were detected by impedance analysis. An electrical circuit model was also constructed and compared with the experimental data. In spite that the detection was only at a level of 10^5cfu/mL, according to analysis, device with larger ratio of electrode surface to volume of microfluidic channel could enhance sensitivity. In addition, the selectivity was also investigated by simultaneous detection of analyte with *Vibrio parahaemolyticus* and non-pathogenic bacteria, X1 Blue *E.coli*.

誌謝

回顧碩士班兩年多的生活，對於一位從技職體系畢業的學生而言，跨領域的論文研究充實了碩士生涯、收穫到豐富知識也結交了許多朋友。以前對生物跟化學的認識有限也害怕學習相關的內容，但有了工程的專業背景，切入生物相關的研究也就變得容易多了，這些都要感謝曾在實驗上幫助過我的人。感謝指導教授許鉦宗博士，提供豐富的實驗資源，且總是盡心地跟我們討論實驗研究，讓我知道如何邏輯地作實驗跟分析實驗結果，學習成為一位真正的專家。在實驗室研究期間，很感謝振嘉學長，一直找出我實驗的癥結，以淵博的專業知識與多年的歷練，給予正確的研究看法與方向，從學長身上學到了很多東西。感謝皓恆學長，一直把實驗室跟學弟妹的事情擺在第一位，每次都大方地的跟我討論實驗。感謝博鈞學長和東裕學長用心傳授半導體製程技術、以及振翔學長在化學上的教導。謝謝志偉學長和一起實驗的同伴新怡、子萱、于聖、儒政和承樺，那不眠不休趕實驗的日子，因為有了你們參與，不覺得孤單。也因學弟妹，宜澤、珮琳、華安、宗翰和崇陞，在實驗上的輔佐與支持，才能努力到現在。還要感謝應化系的李耀坤老師和生科所吳東昆老師在生物化學上指導以及論文上的指證與見解提供。而這兩年來也學到了很多分生實驗技術，謝謝模元郁茹同學在化學方面的幫忙，當然也很感謝裕國學長、文鴻學長與程翔學長，你們的生物分析專業知識，使我獲益良多。尤其是裕國學長，為了幫我取抗體，犧牲的許多小老鼠，真的很抱歉。謝謝李耀坤實驗室、吳東昆實驗室與廖奕翰實驗室的學長姐同學學弟妹的陪伴，使本來無趣的碩士生涯變得豐富又有趣。另外感謝實驗室的 AFM 小房間，在作實驗疲憊之於可以有個舒服的空間可以休息，雖然裡面總是很冷。最後感謝我的家人，爸爸、媽媽和姊姊，因為你們這長久以來的關懷、照顧和鼓勵，讓我無憂無慮的在新竹生活，順利完成碩士學業。

TABLE OF CONTENT

LIST OF TABLES

LIST OF FIGURES

Chapter 1 Introduction

1-1 Research Background and motivation

To secure health of human beings is the fundamental of pathogens detection. Foodborne disease infected by pathogen has being a serious threat for decades in public health. Most of the diseases are caused commonly by the pathogenic bacteria, including *Escherichia coli* O157:H7, *Salmonella* Typhimurium, and *Vibrio parahaemolyticus.* One pathogenic bacteria, *Vibrio parahaemolyticus* was normally found in many species of fish, shellfish, and crustaceans in marine environments, shown in Figure 1-1. They survive in warm saline water with a temperature ranging from 5 to 43 degree Celsius. When infected, *Vibrio parahaemolyticus* causes watery diarrhea with abdominal cramping, nausea, vomiting, fever and chills. Usually these symptoms occur within 24 hours after ingestion. Illness is usually self-limited within 3 days. Due to the change of diet and the global warning, *Vibrio parahaemolyticus* is becoming a highest risk in food poisoning both in United State(Figure 1-2) and Taiwan(Table 1-1), Thus, the development of rapid, sensitive and specific detection as an assay is important to respond effectively.[1, 2]

Biosensors have a wide range of applications for diseases detection and diagnosis. The biosensor is an analytical device, which converts a biological response into an electrical signal. It consists of two main components: the biorecepter element, which recognizes the target analytes, and the transducer element, for converting the recognition event into a measurable electrical signal. The bioreceptor can be a tissue, microorganism, cell, enzyme, antibody etc. The transduction may be optical, electrochemical, piezoelectric, and micromechanical combinations. All the biosensors were designed for fast detection, specificity, sensitivity, accuracy, and capacity to

detect small amounts of target in samples.[3]

The impedimetric detection is a potential technique for biosensors with advantages of low-cost, miniaturization, and flexibility. It can integrate with other analytic methods for higher sensitivity. The detection of bacterial cells using impedance analyzer is well-known.[4, 5] However, performance of the previous studies may be so far limited due to time and diffusion even the analytes are close to sensing surface. In the case of fluidic system applications for biomolecular detection, the targets displacement is dominated by diffusion of its nature. To overcome the constraints of biosensing, the sensing signal enhancement with AC electrokinetics is necessary and reduces the time of detection greatly.

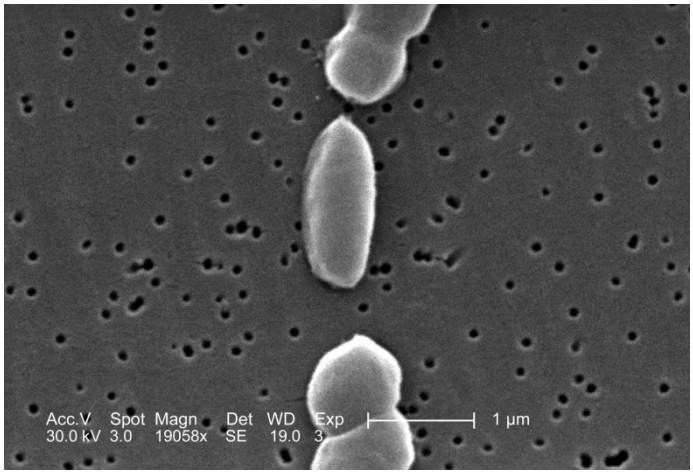

Figure 1-1 SEM image of *Vibrio* para*haemolyticus*.[1]

Table 1-1 Statistics of pathogen infection in Taiwan in 2010. [2]

台灣地區食品中毒案件病因物質分類統計表（民國 99 年） 單位：案，人				
病因物質		案件數	患者數	死者數
細菌	小計 [2]	170	3664	1
	腸炎弧菌	60	478	0
	沙門氏桿菌	27	777	0
	病原性大腸桿菌	11	256	0
	金黃色葡萄球菌	41	902	0
	仙人掌桿菌	46	1982	0
	肉毒桿菌	8	11	1
	其他 [3]	5	470	0

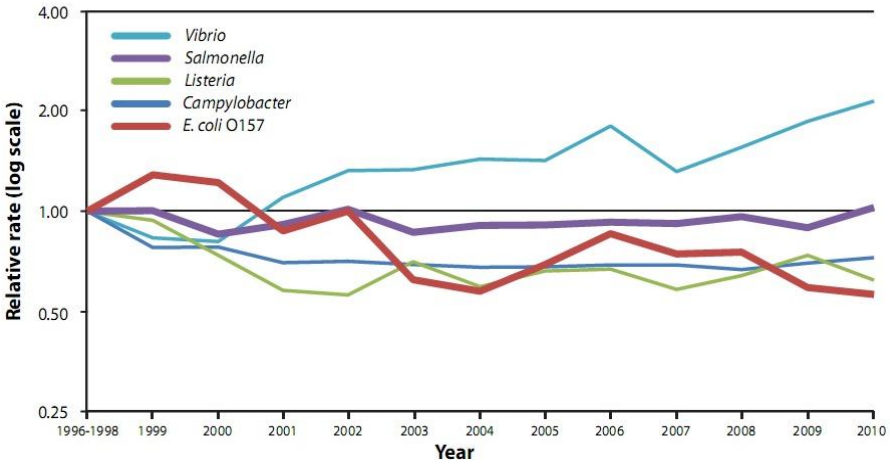

Figure 1-2 Relative rate of laboratory-confirmed infections with *Campylobacter, E. coli O157, Listeria*, *Salmonella, and Vibrio*, compared with 1996-1998 rates by years. [1]

1-2 Bacteria detection via Impedance analyzer

The recognition of pathogenic bacteria can help control the poisoning foods and prevent the foodborne diseases. Indeed, a wide range of biosensors in current on bacteria detection, such as surface plasmon resonance(SPR)[6], quartz crystal microbalance(QCM)[7], and electrochemical impedance spectroscopy(EIS), are mostly adapted to detect bacteria. The advantages of these methods are simple and rapid compared with conventional systems such as Enzyme-linked immunosorbent assay(ELISA)[8] and polymerase chain reaction(PCR) /DNA array[9], which are limited by length of sensing time and portability for biochemical testing procedures.[3]

The previous studies, Yang et al. in 2004 used indium tin-oxide(ITO) interdigitated electrode for the detection of viable *Salmonella typhimurium* in milk.[10] The impedance growth curves, against bacteria growth time, were recorded at four frequencies (10Hz, 100Hz, lkHz, and 10kHz) during the growth of *S.typhimurium*. It was observed that impedance did not change until the cell number reached 10^5-10^6 cfu/mL(determined by the plating method). The greatest change in impedance was observed at 10Hz. Figure 1-3 shows the results presented by Yang. He also fabricated a label-free electrochemical immunosensor for detection of *E coli* O157:H7 by immobilizing anti-E. coli antibodies on the surface of ITO interdigitated electrode and measuring impedance change in the presence of a redox probe label-free detection of *Salmonella* cells in DI water. Figure 1-4 shows the bacteria attachment on the ITO electrode and measured via redox probe.[11]

Suehiro et al. in 2001, 2003, and 2006 studied the issue of capturing bacterial cells on the surface of electrodes using dielectrophoresis(DEP).[12, 13, 14, 15] The concentration of bacteria formed pear chain between electrodes followed by an

impedance measurement, shown in Figure 1-5(a). The detection system was able to detect 10^5 cfu/mL in 10 min. The group has also presented specificity improvement by immobilization of antibody on DEP devices in a microfluidic environment, shown in Figure 1-5(b). This study was published as a proof of concept and only a high concentration (10^6 cfu/mL) of *E.coli* cells was demonstrated. (in Figure 1-6)

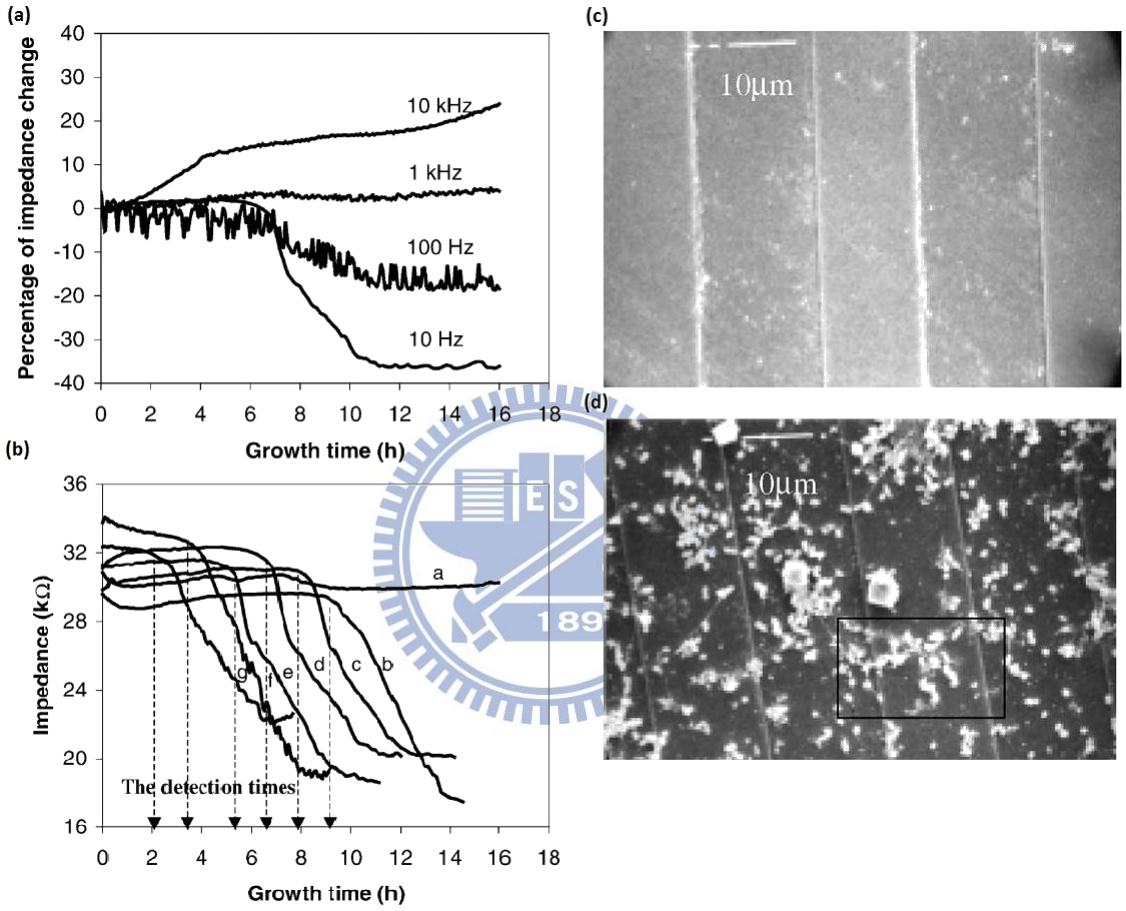

Figure 1-3 (a) Changes in impedance of the IME impedance sensor during the Bacterial growth in selective solution recorded at different frequencies. Initial *Salmonella* cell number: 2.06×10^2 cfu/mL (b) a group of impedance growth curve during the growth of *Salmonella*, recorded at 10Hz. Initial cell number : a:control, b: 4.8×10^0, c: 2.84×10^1, d: 1.75×10^2, (e): 5.4×10^3, f: 5.3×10^4, g: 5.4×10^5 cfu/mL; AC amplitude: 5mV (c) SEM micrograph before test (d) after the test of bacteria growth (initial number:$1.76*10^2$cfu/mL).[10]

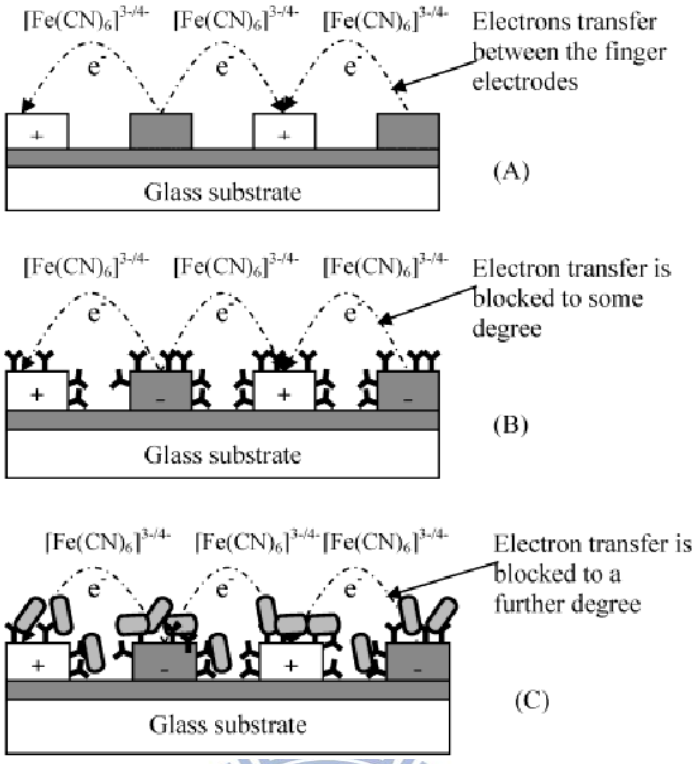

Figure 1-4 The principle of the direct impedance immunosensor with interdigitated electrode.[11]

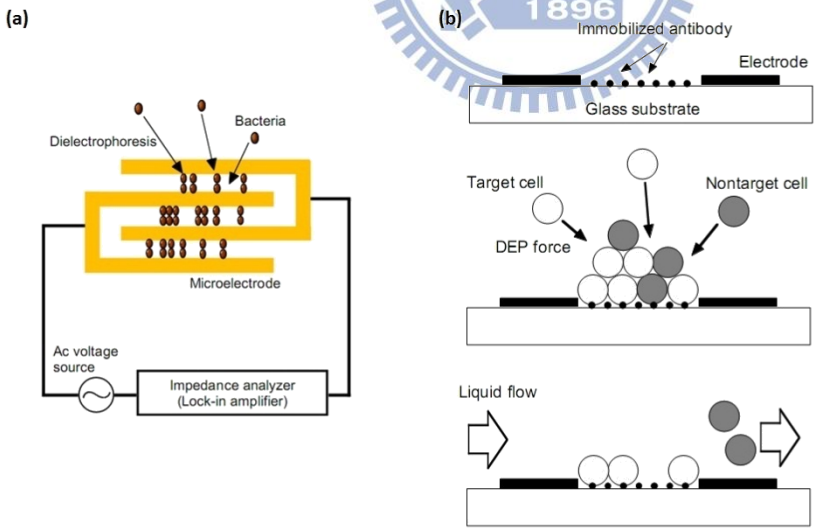

Figure 1-5 (a) Dielectrophoresis based impedance detection system (b) selective impedance analysis based on Dielectrophoresis using immobilized antibody.[13]

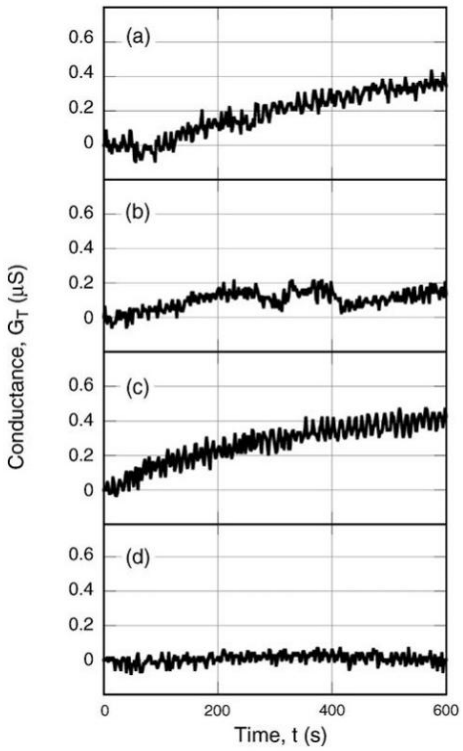

Figure 1-6 Real-time Conductance inspected in 0.1M mannitol solution for (a) blank electrode (b) with antibody modification (c) *E. coli* suspension without antibody modification (d) *E. coli* suspension without antibody modification. (1V, 10kHz, 10min).[13]

1-3 Electrodes configuration of microfluidic system for bioelectronics detection

There are plenty of studies about the concentration of bioparticles using AC electrokinetics on electrodes with various configurations, such as parallel integrated, castellated, potential-well, quadrupole, and concentric. AC electrokinetics as an approach in microfludic system for particles manipulation has also been reported by several research teams. AC electrokinetics can induce non-uniform AC electric field above electrodes. P. K. Wong had used the circular electrode (Figure 1-7) to concentrate the samples into the region at center of electrode, which has a advantage of smaller target preparation, such as E. coli Bacteria, quantum dot, and DNA, showed as Figure 1-8 and Figure 1-9.[16, 17, 18] Also, multiple interdigited electrode arrays in previous researches were widely used as impedance analyzer. The impedance spectroscopy in microfluidic system often uses the parallel interdigited electrode for incubation of the analytes. It has been present advantages of low ohmic drop, fast response of steady-state, and well performance in detecting small amounts of products.[19] Figure 1-10 shows the experimental set up of impedance measurement with interdigitated electrode.

In this work, concentric electrode combined with inside parallel integrated electrode enhances the capability of target concentration and bioassay. The bacteria were concentrated onto the inner circular electrodes, and impedance measurement was performed by using inner interdigitated electrode inside the inner circular.

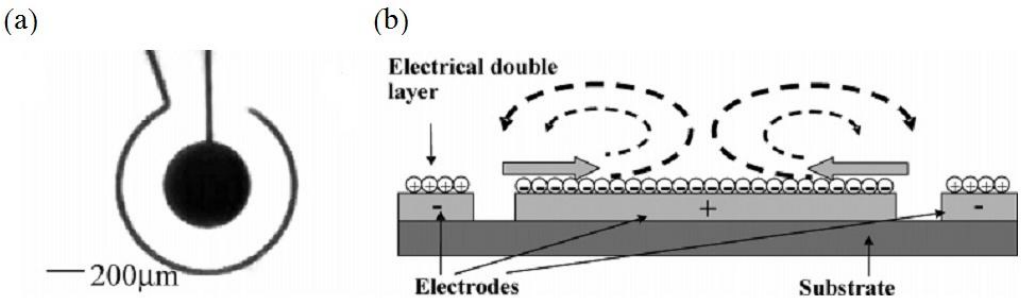

Figure 1-7 (a)Electrode design of the AC electroosmotic processor (topview). (b) Schematic (side view) illustrating electrode polarization and formation of AC electroosmosis.[18]

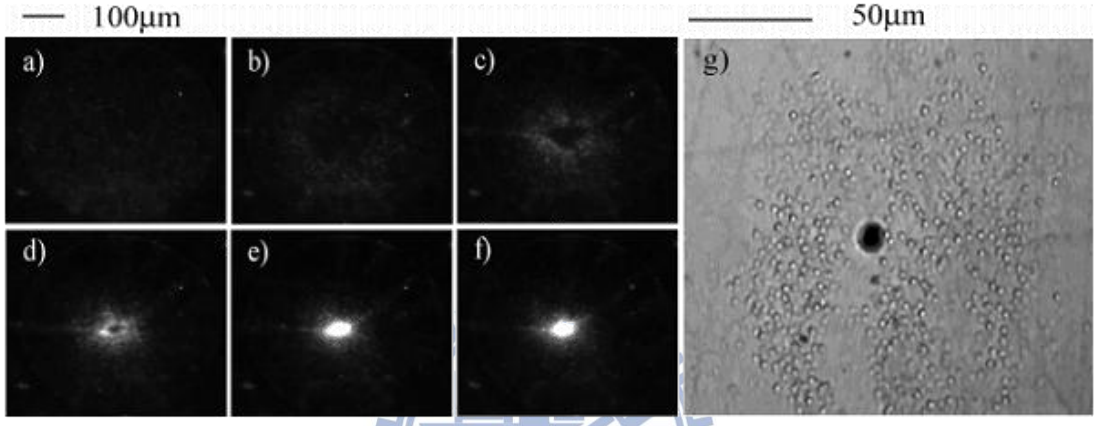

Figure 1-8 Particles concentration (a-f) Video time series showing concentration of 200-nm fluorescence particles on the central electrode each picture is separated by 10s. (g) Concentration of *E.coli* bacteria at the center of the central electrode.[18]

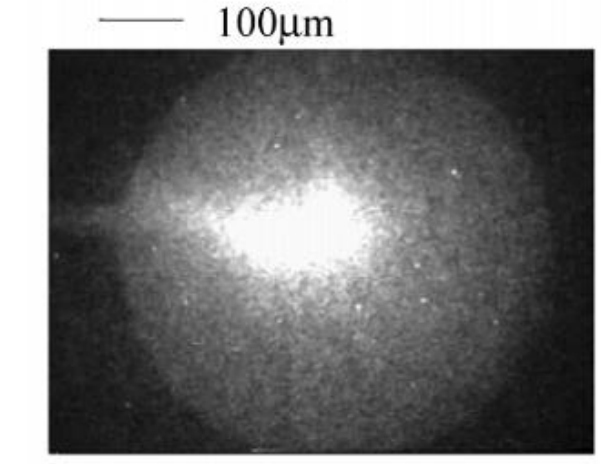

Figure 1-9 Fluorescence image demonstrating concentration of double-stranded λ phage DNA molecules (48.5kbp) on the central electrode.[18]

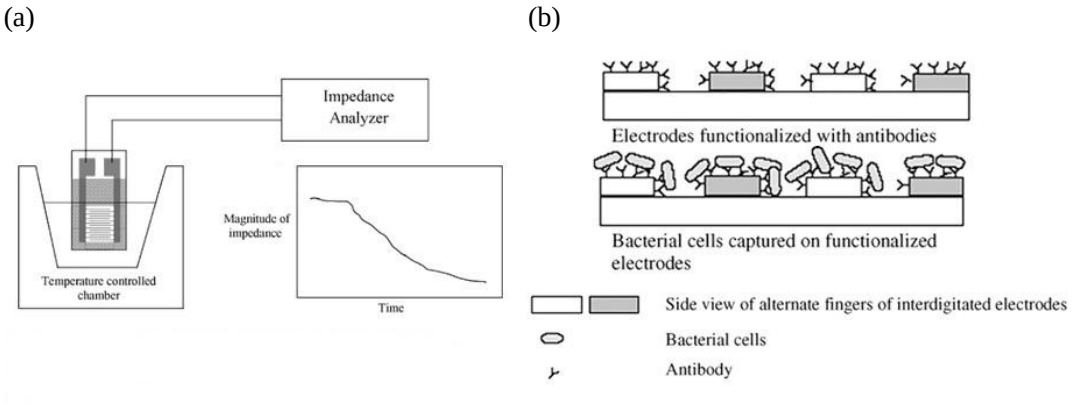

Figure 1-10 (a) The experimental set up of impedance measurement with interdigitated electrode for bacteria growth (b) impedance response with time for the growth of bacteria.[19]

1-4 AC electrokinetics in Microfluidics system

In microfluidic system, the phenomena under AC electric field that involve the interactions among applied electric fields , ions suspended in solution, and polarized particles result in ions and particles movement. There are three dominant mechanics during the AC signal applying, dielectrophoresis(DEP), AC Electroosmosis(ACEO), and electrothermal effect actuating motion of solid bodies(micro-/nano-particles or bio-particles) in the process of applied electric field.[20, 21] The AC electrokinetics physically displaces particles and induces fluidic flow duo to the controllable parameters, such as voltage, frequency, electrode size, etc.[22] Electroosmosis is the motion of fluid induced by tangential electric field at the surface of electrode due to ionic movement in the electrical double layer (Figure 1-11(a)). Dielectrophoresis occurred during non-uniform signal applied in the solution as suspended particles is polarized. The polarized dipoles difference of dielectric particles between the interface inside and outside give rise to a net force, either toward the strong electric field, called Positive DEP(p-DEP), or away from electric field, called negative DEP(n-DEP), on the particles(Figure 1-11(b)). Electrothermal fluid is generated by electric field from the temperature heating of the fluid and the gradient in local conductivity and permittivity (Figure 1-11(c)). In this thesis, AC electrothermal effect is negligible due to the low conductivity of medium and undesirable mechanism while trapping the particles. These experiments reduce the response time by relying on forces integrated with electroosmosis and dielectriophoresis on analytes. The parameters are with low potential and low frequency that can induce merely dielectrophoresis on particles and electroosmosis in electrical double layer, but prevent the electrothermal fluid in the microfuidic cell. The potential application of AC electrokinetics can facilitate methods for

manipulating biological objects.[23, 24] Efficient bioparticles manipulation can shorten the detection time and improve the sensitivity.[25, 26]

In the article, bacteria were trapped onto the center of the inner electrode, experiencing a balance force from dielectrophoresis induced by polarized particles and drag force by AC electrosomsis under non-uniform electric fields without using bulk fluidic. It can largely reduce the time for immobilization of bacteria and enhance the sensitivity.

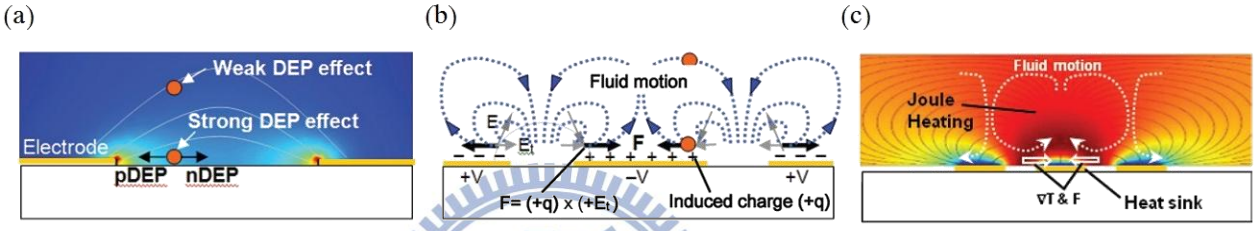

Figure 1-11 AC eletrokinetics behaviors (a)Dielectrophoresis (b)AC electroosmosis (c)Electrothermal effect.[22]

1-5 Structure of the thesis

This thesis reported enhancement of biosensor via AC electrokinetics on bacteria detection. We detected the *Vibrio parahaemolyticus* as pathogenic analytes via impedance biosensor and AC electrokinetics was adopted to enhance the capture of bacteria. First, a new configuration of electrodes for diagnosis was fabricated and simulated by COMSOL V. 4.2 for analysis of electric field and AC electroosmosis. Second, the chip was cleaned and functionalized by chemical molecules ion gold electrode with confirm using characteristic methods. The specific biomolecules that recognize *Vibrio parahaemolyticus* uniquely was immobilized on the electrode before detection. Third, the AC electrokinetics was involved for bacteria trapping and the

impedance was analyzed through electrodes. Modeling using equivalent circuit was also adopted to justify the impedance spectroscopy from the measurement. Finally, to confirm the selectivity and specificity in *Vibrio parahaemolyticus* detection, a non-pathogenic *E.coli* bacteria was mixed with *Vibrio parahaemolyticus in the analyte* for detection. Figure 1-12 illustrates the experimental flowchart on achieving *Vibrio parahaemolyticus* detection.

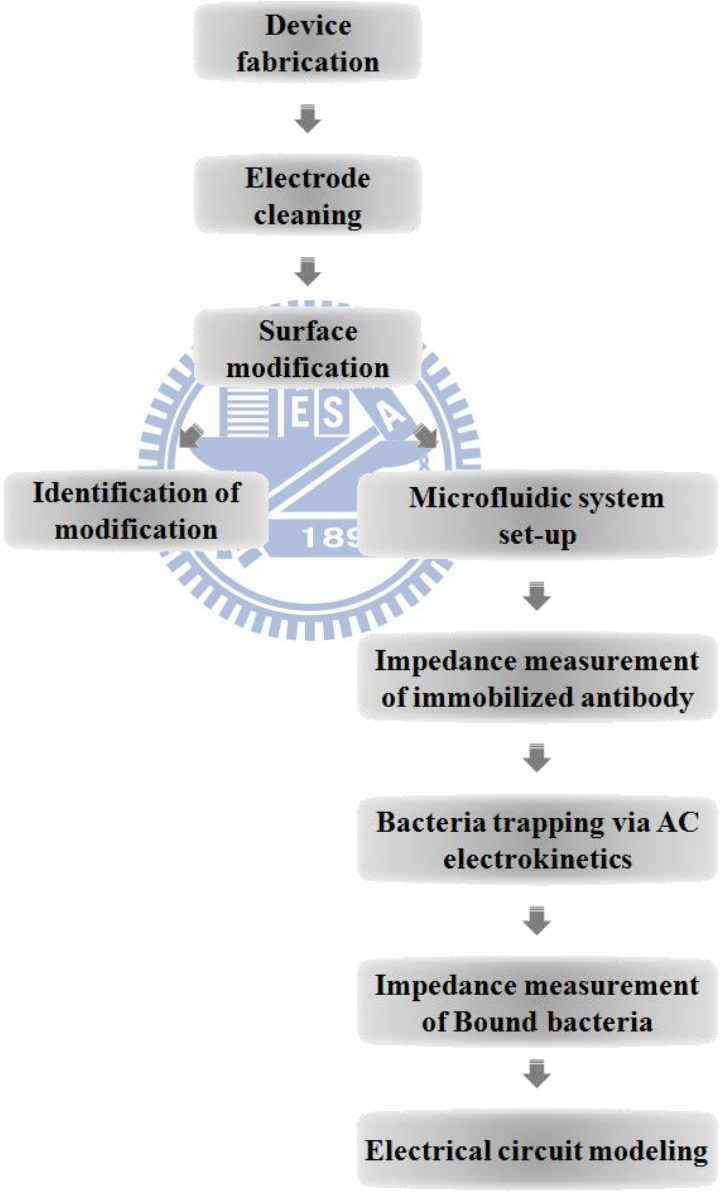

Figure 1-12 Experimental flowchart of this thesis.

Chapter 2 Theoretical reviews

2-1 Fluid motion

In incompressible fluid dynamics, the behavior and velocity of the flow can be described by Navier- Stokes Equation:

$$\rho\left(\frac{\partial v}{\partial t}+v\cdot\nabla v\right)=-\nabla p+\eta\nabla^2 v+F_{body} \text{ ---------- (1)}$$

where ρ is the density of medium($^{\mathrm{Kg}}/_{\mathrm{m}^3}$), v the velocity of flow($^{\mathrm{m}}/_{\mathrm{s}}$), p the pressure(Pa), η the viscosity(Pa · s) and F_{body} a body force term($^{\mathrm{F}}/_{\mathrm{m}^3}$) The Navire-Stokes equation is derivative from Newton's Second Law, $ma=F$. On a hand, the left side of equation due to the inertia of whole fluid describes acceleration of transient and convection. On the other hand, the right side is the sum of pressure, viscous forces and the body forces. For laminar flow of microfluidic system the Reynold number(Re) expressing the ratio of inertial forces(convection acceleration) to viscous forces, is low, so the inertia terms are neglected. Considering the steady flow in addition, the Navier-Stokes equation is written:[27]

$$0=-\nabla p+\eta\nabla^2 v+F_{body} \text{ ---------- (2)}$$

The equation presents the motion of fluid and gives the velocity for a given body force in the microfluidic channel.

2-2 Electrical double layer

In an electrochemical system, an ideal polarized electrode involves no charge can be transferred across the electrode-solution interface. As a potential is applied to the electrode, charges (counter ions) will aggregate in the electrode surface until the potential drop across the capacitor satisfies the applied potential. The region of liquid near to the interface has a higher density of counter ions. The result in the change of distribution of ions near the surface is influenced by the distribution of electrode signal. The charges exist on the metal, the excess or deficiency of electrons and resides accumulating in a thin layer (< 0.01 nm) on the metal surface. The charges in the solution are made up of an excess of cations or anions in the vicinity of the electrode surface. The whole array of charged species existing at the metal-solution interface is called the electrical double layer (EDL).[28, 29]

Electrical double layer consist in the presence of several layers. In the further consideration of EDL model in Figure 2-1, the inner layer closest to the electrode contains specifically adsorbed solvent molecules and other species is called stern layer. The stern layer can be subdivided into two regions, which is the inner and outer layer. The inner surface of which is named inner Helmholtz plane, composed of solvent molecules and other specifically absorbed species. The bound solvent ions as outer layer, outer Helmholtz plane, of stern layer samples which are not absorbed specifically but attracted in electrostatic forces from the charged metal. Due to the thermal agitation of solution, excess charges distributed in the extend region from outer Helmholtz plane to solution bulk form a diffuse layer. This model is presented in Figure 2-1.

The volume of double layer is dependent on the pH and ionic strength of the solution. To calculate the potential distribution of the electrical double layer,

Poission-Boltzman equation is given to describe the varieties of electrostatics potential of charged atoms in the space,

$$\nabla^2\psi = \frac{d^2\psi}{dz^2} = -\frac{q}{\varepsilon_0\varepsilon_r}\sum_i n_i^{\infty} z_i exp[-z_i q\psi(z)/k_B T] \text{---- (3)}$$

where ψ is the electric potential due to surface charge, q is electric charge, n is the ion concentration, z is the ion valence. The Poission-Boltzman equation can be solved by assuming generally the relation with respect to smaller α, which leads to the Debye-Huckel approximation

$$\nabla^2\psi = \frac{d^2\psi}{dz^2} = \kappa^2\psi(z) \text{---------- (4)}$$

and the potential distribution is

$$\psi(z) = \psi_s exp\,(-\kappa z) \text{---------- (5)}$$

where

$$\kappa = \left(\frac{e^2\sum_i n_i^{\infty} z_i^2}{\varepsilon_0\varepsilon_r k_B T}\right)^{1/2} \text{----------(6)}$$

κ is called Debye-Huckel parameter. The potential decays exponentially in the diffuse layer with a characteristic distance by Debye length $\lambda_D = \kappa^{-1}$. This value correlates the thickness of electrical double layer.[29]

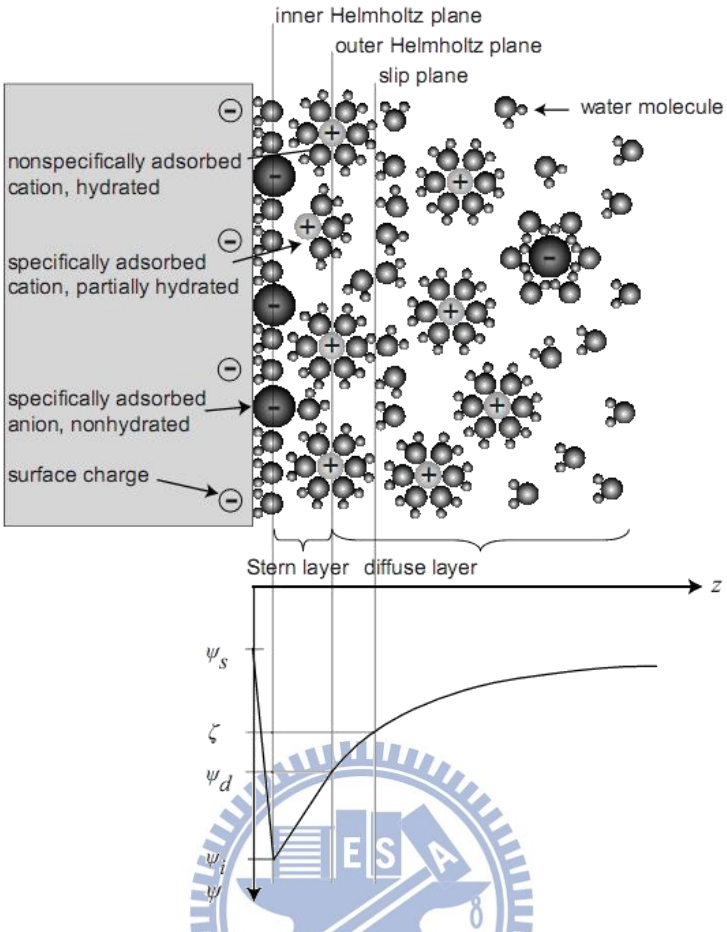

Figure 2-1 Model of the solid-electrolyte interface with corresponding potential ψ v.s. the distance from electrode to wall. The electrode is illustrated with a negative surface potential ψ_s . The inner Helmholtz plane layer ψ_i consists of nonhydrated coions and counterions, whereas the outer Helmholtz plane layer ψ_d is built up of only hydrated ounterions.[29]

2-3 AC electrokinetics:

2-3-1 AC Electroosmosis

When the potential is applied on a electrode in the solution, explained in Figure 2-2, the electrical double layer (EDL) is established and accumulated uniformly and the microfluidic cell is also supplied by external electrical power as a electrostatic body force E_{ext}. There is a tangential component of electric field, $E_{ext,wall}$. Here considering the steady isobaric flow in x-direction along the surfaces (such as electrodes), with velocity and potential gradient remaining in y-direction, the equation (2) is simplified: [27]

$$0 = \eta \frac{\partial^2 v}{\partial y^2} + \rho_E E_{ext,wall} \text{ ----------(7)}$$

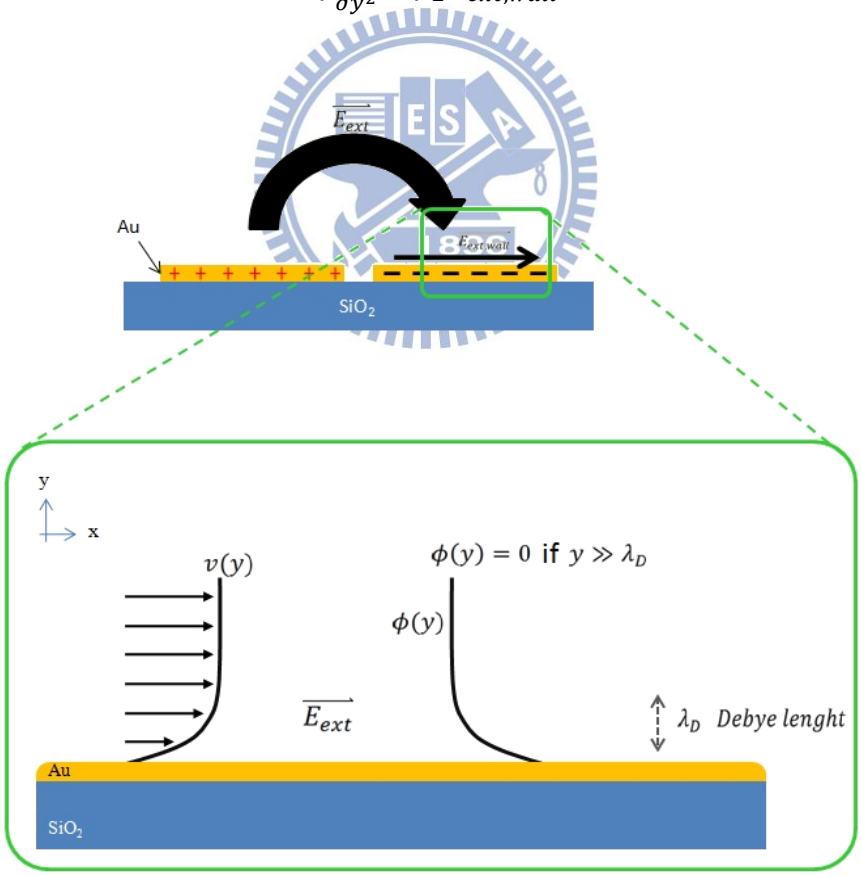

Figure 2-2 Velocity, Coulomb force, and electrical potential in an electroosmotic flow.

The term, $\rho_E E_{ext}$, is induced Coulomb force by electric field applied on the electrical double layer. In further detail of Coulomb force, the charge density around the EDL can be gotten by Poisson equation, ϕ is the potential of bulk solution, ρ_E the charge density of medium, and ε electrical permittivity of solution:

$$\nabla^2\phi = -\frac{\rho_E}{\varepsilon} \text{----------(8)}$$

the equation (8) is to substitute ρ_E in equation (7):

$$0 = \eta\frac{\partial^2 v}{\partial y^2} - \varepsilon\frac{\partial^2\phi}{\partial y^2}E_{ext,wall} \text{----------(9)}$$

Rearranging equation (9)

$$\eta\frac{\partial^2 v}{\partial y^2} = \varepsilon\frac{\partial^2\phi}{\partial y^2}E_{ext,wall} \text{ ---------- (10)}$$

This differential equation can be solved via boundary conditions at the electrode ($y = 0$) and the bulk solution($y \gg \lambda_D, y = \infty$) point with the definition $\phi = \phi_0$ and $\phi = 0$:

$$\eta v = \varepsilon E_{ext,wall}\phi + C_1 y + C_2 \text{---------- (11)}$$

It makes velocity:[30]

$$v = \frac{\varepsilon E_{ext,wall}}{\eta}(\phi_0 - \phi) \text{ ---------- (12)}$$

where the v, ε, $E_{ext,wall}$, and η are the electroosmosis velocity, permittivity of medium, the tangential electric field on the surface, and the viscosity. $\phi_0 - \phi$ is defined as potential that represents the potential drop cross the electrical double layer. ϕ_0 is a potential at the surface and ϕ is another potential as a function of distance in y-direction. Equation (12) is the solution of the electroosmotic flow, that involving fluidic flow in the solution after the external work of electric applied. The free

charges within the diffuse layer of electrical double layer move due to the electric field direction, tangential component, on the surface turning out electroosmosis. The mechanism was generally observed and accounted for in DC field. However, AC field providing a non-uniform field can also generate the fluidic flow locally relating to the charges of the double layer. As voltage is applied, it causes an electrical double layer outside the electrode surface. If ignoring the formation of stern layer in electrical double layer and assuming a linear approximation of diffuse double layer, like the chart in Figure 2-4, we consider a specific capacitance dropped across entire double layer, which is

$$C_S = \frac{\varepsilon}{d} \text{---------- (13)}$$

here C_S is surface capacitance(F/m^2), d the Debye length(m). Owing to the surface charge density, the capacitance can be rewritten as a ratio of charge to potential:

$$\frac{Q_S}{\zeta} = C_S \text{---------- (14)}$$

Where $Q_S$is the electrode surface charge density(C/m^2) and ζ is the zeta potential(V) which describe equivalent potential of diffuse layer. Here the zeta potential drop from the electrode surface to potential defined point, ϕe^{-1}. The interval is same as Debye lenght(Figure 2-4). In the linear approximation the zeta potential is proportional to surface charge density in the diffuse double layer:

$$\frac{Q_S}{C_S} = \frac{Q_S}{\frac{\varepsilon}{\kappa^{-1}}} = \zeta \text{---------- (15)}$$

and

$$\frac{Q_S}{\kappa} = \varepsilon\, \zeta \text{---------- (16)}$$

where κ is the reciprocal Debye length. In term of velocity resulted from interaction

of ions in double layer

$$v = \frac{\varepsilon E_{ext,wall}}{\eta}\zeta \text{ ---------- (17)}$$

also

$$v = \frac{\varepsilon E_{ext,wall}}{\kappa\eta}Q_S \text{ ---------- (18)}$$

In microfluidic system, generating a non-uniform electric field between electrodes can model as a circuit, including a series of solution resistance and surface capacitance at either double layer on the electrode surface. Figure 2-3 show a two dimensional system with a semircular circuits.[31]

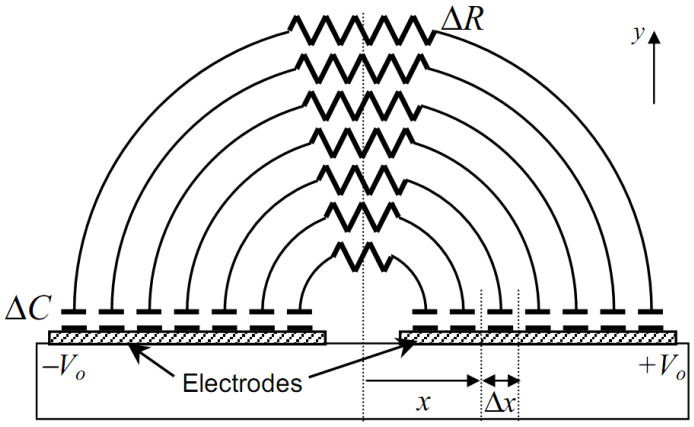

Figure 2-3 Approximate circuit diagram for two long coplanar plateeletrodes specrated by narrow gap.

The solution resistance and double layer capacitance is with a value

$$\Delta R = \rho\frac{L}{A} = \frac{\pi x}{\sigma_m dx} \quad \text{and} \quad \Delta C_S = \frac{\varepsilon A}{d} = \varepsilon\kappa dx$$

Here, x is cross-sectional position and start from the center of the gap between electrodes and d expresses the length of electrodes into the page.

Since eletroosmosis is affected exactly by the behavior of ions motion in the double layer. The potential with a time-averaged value, i.e. root mean square value V_0 cross the double layer can be driven via voltage dividing:

$$\phi_{EDL} = V_0 \frac{{}^{1}/_{j\omega\Delta C_S}}{{}^{2}/_{j\omega\Delta C_S} + \Delta R} \quad \text{---------- (19)}$$

Resistance and capacitance parameters substitute the function

$$\phi_{EDL} = \frac{V_0}{2 + j\omega\pi({}^{\varepsilon}/_{\sigma_m})\kappa x} \quad \text{---------- (20)}$$

The total surface charge distribution and tangential electric field in x-direction can be evaluated from this model as $Q_S = \varepsilon\kappa\phi_{EDL}$ and $E_{ext,wall} = \frac{\partial\phi_{EDL}}{\partial x}$. The time averaged electroosmosis velocity from $v = \frac{E_{ext,wall}Q_S}{\kappa\eta}$ yields:[30]

$$\langle v \rangle = \frac{1}{2} Re\left\{\frac{E_{ext,wall}Q_S}{\kappa\eta}\right\} = \frac{\varepsilon {V_0}^2 \Omega^2}{8\eta(1+\Omega^2)^2} \text{---------- (21)}$$

where

$$\Omega = \frac{1}{2}\pi\kappa x \frac{\varepsilon}{\sigma_m}\omega \quad \text{---------- (22)}$$

Moreover, diagram outlining of AC electroosmosis is patterned at Figure 2-5. Its mechanism report the charges above electrode surface shift from the edge of electrode to the center. The ion movement induces and exerts net drag force due to medium viscoity. The forces acted on the double layer generate bulk fluid motion, rotational motion, on the electrode surface toward the center of electrode. The direction of the flow would not be alternative with electrical potential change since co-ions and counter-ions switch transiently as well due to applied electric field and the tangential component.

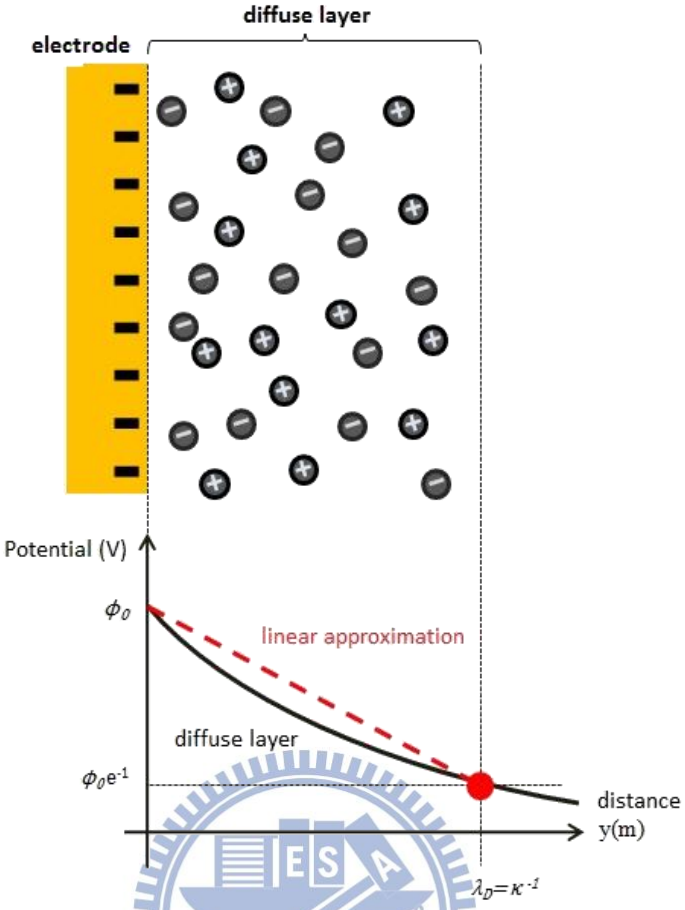

Figure 2-4 Schematic diagram for concentration of ions close to a charged surface in solution. Also shown is the distribution of potential with distance from electrode surface.

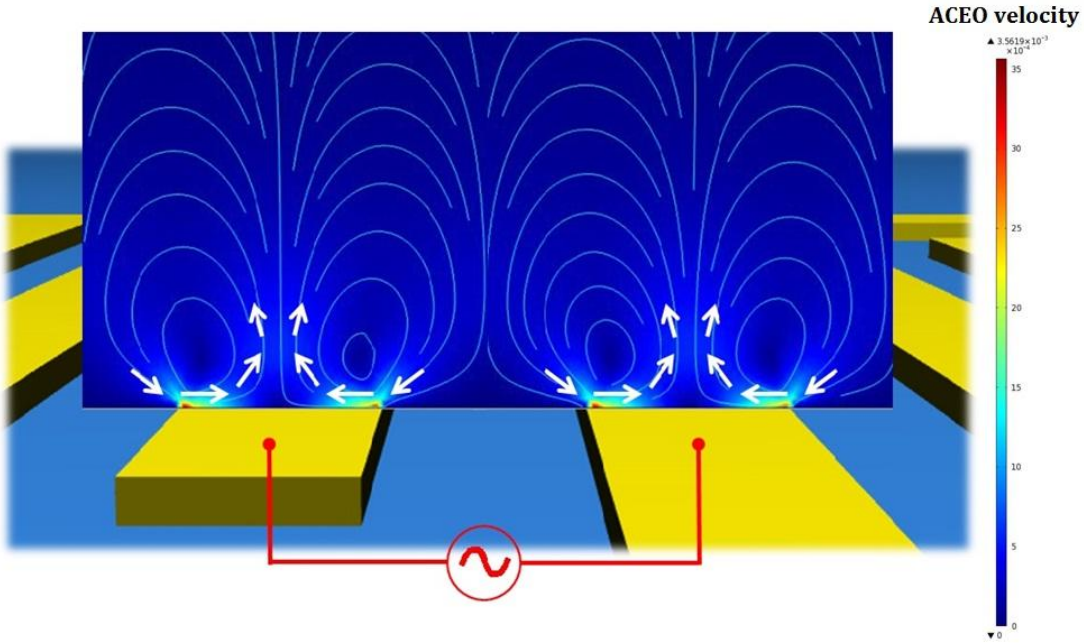

Figure 2-5 Behaviors of ACEO on two electrodes applied different signal.

2-3-2 Dielectrophoresis

Dielectrophoresis(DEP) describes the motion of polarizable particles under a non-uniform electric field. It always employs in an alternative current (AC) to produce the non-uniform electric field. Depending on electrical and polarized properties of the medium around particles and particles inside it can be attractive or repulsive, which termed negative and positive dielectrophoresis. Figure 2-6 shows that particles move toward the field in Positive DEP. The negative DEP causes movement in reverse.

In electric field $\vec{E}$ .a dielectric particles can be induced with dipole moment $\vec{p}$ proportional to the electric field, $\vec{E} \propto \vec{p}$. The constant of proportionality depends on the geometry of the particles in general. The force of dipole is given by $\vec{F} = \overrightarrow{(p} \cdot \nabla)\overrightarrow{E}$. Combining two equation above with using a spherical particles of radius r and dielectric constant ε_p as model and accounted for the solution permittivity ε_m , the force acting on a spherical particles is given by[27, 31]

$$\vec{F}_{DEP} = 2\pi r^3 Re[CM(\omega)]\nabla|E_{rms}|^2 \text{---------- (23)}$$

where the $Re[CM(\omega)]$ is real part of Clausius-Mossotti (CM)-factor, which is frequency dependant. The CM-factor reflecting the effective polarizability of the particles and medium depends on the complex permittivity:

$$CM = Re\left(\frac{\varepsilon_p{}^* - \varepsilon_m{}^*}{\varepsilon_p{}^* + 2\varepsilon_m{}^*}\right) \text{---------- (24)}$$

The complex permittivity, ε^*, as a function of the frequency of AC signal, is a measure of the permittivity and conductivity of particles and medium, $\varepsilon^* = \varepsilon - i\frac{\sigma}{\omega}$. For the spherical particles, the CM-factor ranges from *-0.5* to *+1*. Positive value of CM-factor means that the motion of the particles are toward higher electric field

strength in the direction, this is so-called the positive DEP, while negative DEP occur when the direction toward lower field strength and the CM-factor has negative value.

For ellipsoidal particles, such as *E. coli* and *vibrio parahaemolyticus*, it has an extend value range of CM-factor. The dipole of ions gets along with axes of ellipsoid. An ellipsoid with three orthoghonal axes a, b, and c, the volume(m^3) is

$$V_{ellipsoid} = \frac{4\pi abc}{3} \text{ ---------- (25)}$$

and the time average dielectorphoresis on an ellipsoid particle[20, 32, 33]

$$F_{DEP_{ellipsoid}} = \pi abc\varepsilon_m \mathrm{Re}[\widetilde{CM}]\nabla|E|^2 \text{ ---------- (26)}$$

For the solid prolate ellipsoid, the CM-factor along axis is given by

$$Re[\widetilde{CM}] = \frac{\varepsilon_p{}^* - \varepsilon_m{}^*}{(\varepsilon_p{}^* - \varepsilon_m{}^*)A_\alpha + \varepsilon_m{}^*} \text{ ---------- (27)}$$

α = a,b,c

A_α is a component of the depolarization factor along any one of the three axis of ellipsoid(a,b,and c). The $Re[\widetilde{\mathrm{CM}}]$ for ellipsoid can take account of ellipsoidal shape of cell. A_α is for a prolate spheroid with semi axes $a \gg b = c$ has been described as

$$A = \frac{q}{(q^2-1)^{3/2}} ln\left(q + \sqrt{q^2-1}\right) - \frac{1}{q^2-1} \text{ ---------- (28)}$$

where $q = \frac{a}{b}$

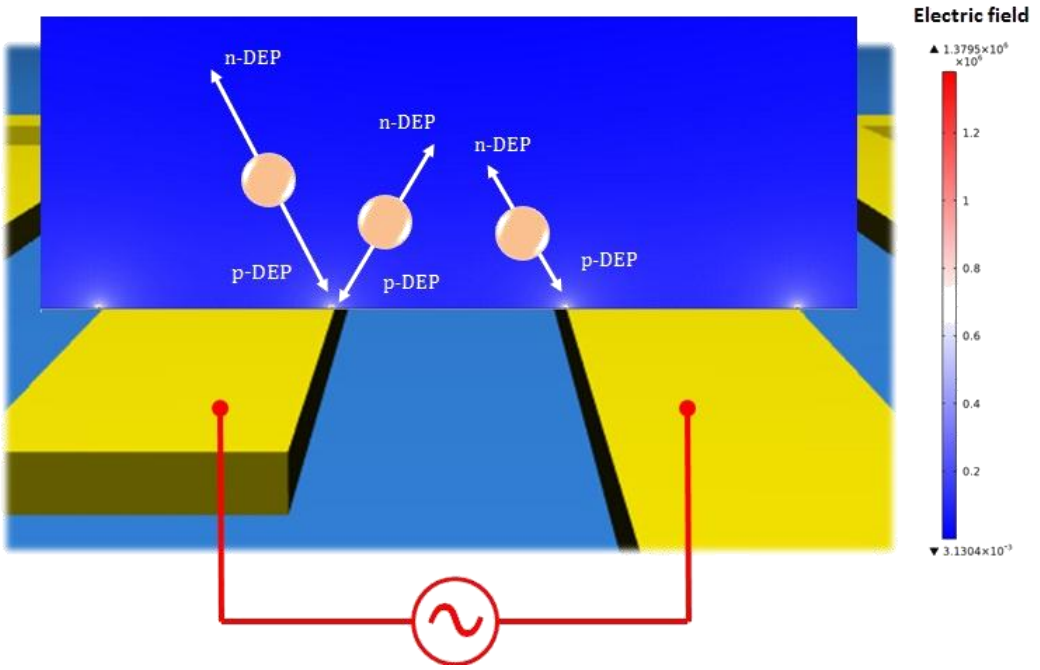

Figure 2-6 Behaviors of particle movement under force of DEP.

2-4 Electrochemical methods

The electrochemical techniques here perform using a 3-electrode cell. The cell is consist of a working electrode, usually, a counter electrode, usually in Pt material, a reference electrode, usually in Ag/AgCl in saturated KCL, an electrolyte solution; and redox reactive species (Figure 2-7). Working electrode is usually Au surface in commercial assay, counter electrode in Pt material and a reference electrode Ag/AgCl in saturated KCL. Potential is measured between working electrode and reference electrode. However, the current is measured between working electrode and counter electrode.

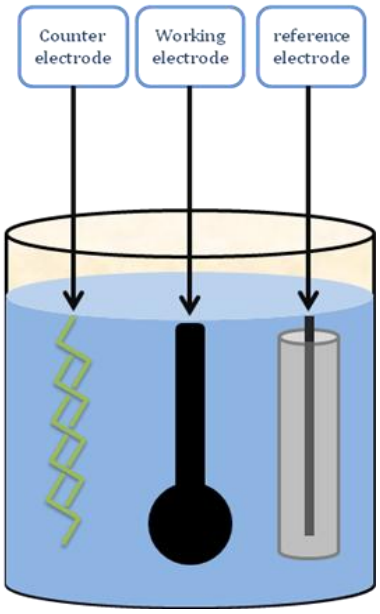

Figure 2-7 Electrochemical cell system. Three electrodes put in the electrolyte is made up by working electrode, Au patterned on SiO_2 chip; counter electrode, Pt wire; and Ag/AgCl reference electrode in 3M KCl solution.

The Cyclic Voltammetry can measure the varieties of current of distinguish analytes during pre-determined range of potential is applied. The voltage signal is triangular wave. In forward scan of input wave, cathodic potential increases and current increases as concentration of active species in solution become lower. After reaching the highest potential, the reverse scan provides the potential with anodic direction and the oxidation occurred in working electrode (Figure 2-8).

(a) (b)

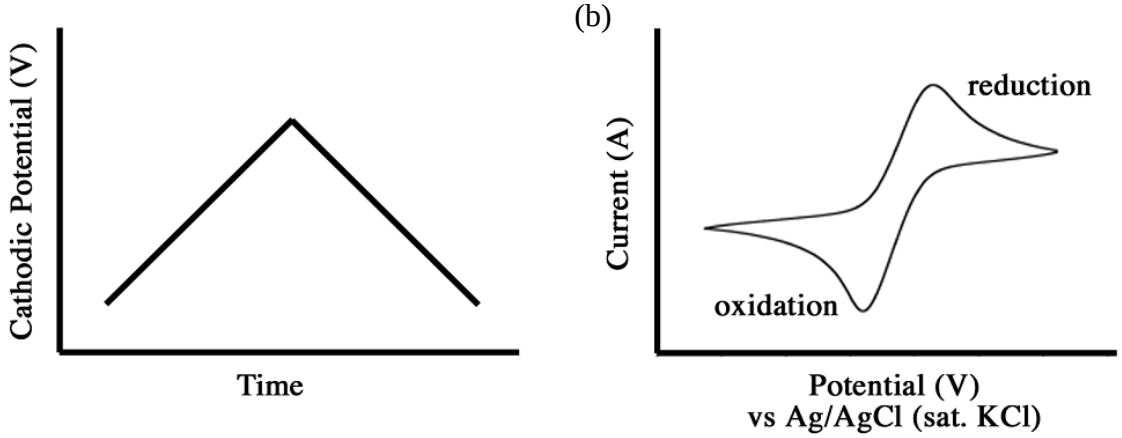

Figure 2-8 Cyclic voltammetry curves for (a) applied potential sweep and (b) measured current response.

2-5 Impedance measurement

Impedance measurement are made using AC signal, where the current oscillates in a sinusoidal function from as low as a less hundred to nearly 100,000 Hz in different measurements. As applied AC current to the electrode system and measure the AC voltage across the electrodes, the impedance is simply given by AC equivalent Ohm's Law:

$$Z = \frac{V}{I} \text{ ---------- (29)}$$

The instrument is capable of monitoring both magnitude of voltage and the phase change of voltage relative to the phase of current. Combining these parameters, the impedance can be broken down into two parts: one due to pure resistance and the other to the reactance of the system. The reactive part (X_c) in this case is due to the capacitance (C) associated with the medium around metal surfaces. The signal of impedance received from the electrode as a simple circuit both in series and parallel of resistances and reactive part.

For the circuit, the impedance of each element are given by:

$$R = \frac{V_{(in\ phase)}}{I} \text{ ---------- (30)}$$

$$X_C = \frac{V_{(out\ of\ phase)}}{I} \text{ ---------- (31)}$$

X_C depends on the AC frequency(*f*) is given by

$$X_C = \frac{1}{2\pi fC} \text{---------- (32)}$$

and total impedance (*Z*) is given by

$$Z = \sqrt{(R)^2 + {X_C}^2} \text{---------- (33)}$$

Chapter 3 Experimental set-ups

3-1 Materials

The following materials and chemicals are used:

Potassium hydroxide(KOH), Potassium ferrocyanide, bovine serum albumin(BSA), N-hydroxy-succinimide 97% (NHS) and 1-ethyl-3-(3-dimethylamino-propyl) carbodiimide (EDAC) were purchased from Sigma-Aldrich . carboxytetramethyl-rhodamine succinimidyl ester (5(6)-TAMRA,SE) were obtained from AnaSpec, Inc. 11-mercaptoundecanoic acid(11-MUA) and 3-mercaptopropanol(3-MPOH) were provided by laboratory of Prof. Yaw-Kuen Li in Department of Applied Chemistry, NCTU. *Vibrio parahaemolyticus* and Polyclonal antibody of *Vibrio parahaemolyticus* purified by mouse Immunoglobulin G was prepared by laboratory of Prof. Tung-Kung Wu in Department of Biological Science and Technology, NCTU. Phosphate buffer was prepared as 4.4 mM Na_2HPO_4 and 1.4 mM KH_2PO_4.

3-2 Design and Fabrication of electrodes for biosensing

3-2-1 Patterned electrodes Device

Geometry, area and gap between electrodes are important parameters that influence the function of AC electrokinetics. In the interest of the bioparticles and micro- or nano- particles manipulation and concentration, the concentric electrode was designed.[18] The interdigitated electrode for analytes detection in microfluidic system was beneficial for the impedance spectroscopy.[19] In this work, concentric electrode combined with inside interdigitated electrode was designed as shown in Figure 3-1. AC electrokinetics manipulation and impedance measurement was integrated together in this device. The size of the circular electrode part was defined for the effective trapping and for electrical impedance measurement. Due to the biomolecular modification onto the electrode, the material of external surface of electrode is limited to gold, which has also a great biocompatible affinity. Gap distance and interdigited arrays size influence the scale of impedance. Devices with 5-um gap and 5-um-electrode width were optimized for impedance measurement.

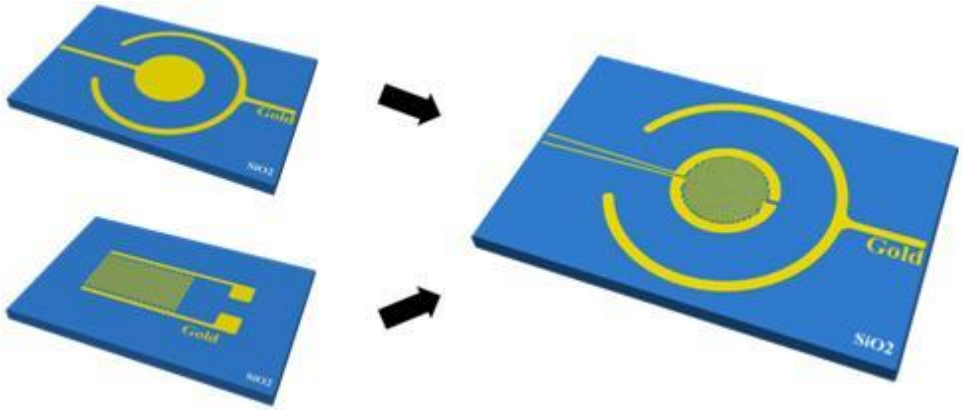

Figure 3-1 Innovative integration for electrodes. Right side as a device for detection.

3-2-2 Electrode preparation

Each device used wet SiO_2(wet oxide) as substrate. A thin layer of titanium(Ti) of 30 nm and gold(Au) of 300 nm in thickness were then deposited on SiO_2 with the procedures of thermal coating by *CHIPBOND Technology Corporation*. Then, Au-Ti film electrode was printed by photolithography and etched by wet-etching processes:

I. Coating the positive photoresist(6400) by spinner

II. Soft bake

III. Exposure

IV. Development and fixing

V. Gold etching with KI:I_2:DI water = 68 mg: 17 mg: 24 mL

(shake the etchant gently during etching the gold)

VI. Ti etching with DHF:H_2O_2:DI water = 1 mL:1 mL:80 mL

Finally, the photoresist on the electrodes was dissolved by acetone as shown in Figure 3-2.

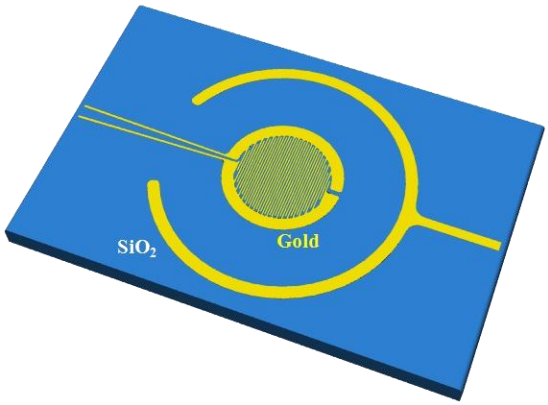

Figure 3-2 Electrode configuration.

3-2-3 Definition of the sensing area for impedance analysis

For impedance analysis, the area of electrode dominates the measurement as well. Though the microfluidic channel was used, various sizes of channel made artificially had effect the measurement. Hence, the SU-8 2005 (negative photoresist) as passivative layer created same area in all electrodes and reduce the effect on impedance measurement. A 5-μm SU-8 layer was patterned via photolithography. The defined SU-8 pattern was shown in Figure 3-3. The processes were depicted as followed:

I. Spin coating the SU-8: 500 rpm for 10 sec; 3000 rpm for 30 sec.

II. Soft bake: 65℃ for 60 sec; 95℃ for 120 sec; 65℃ for 60 sec.

III. Exposure (with light intensity 130 millijoule per square centimeter).

IV. Hard bake: 65℃, 60 sec; 95℃,600 sec; 65℃, 60 sec.

V. Development: 40 sec with SU-8 developer.

VI. Definition: 30 sec with IPA.

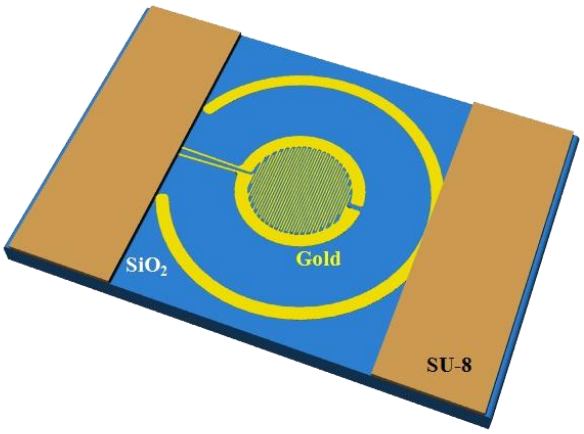

Figure 3-3 Sensing area definition of the chip after SU-8 passivation.

3-3 Preparation of Self-assembly monolayer modification

3-3-1 Gold electrode cleaning methods

A clean gold surface provides a better interaction with thiol molecules during SAM process, which is also beneficial to electrochemical detection and impedance spectroscopy.[34, 35] Previous study had shown technique for cleaning gold electrodes. The gold electrodes were cleaned sequentially by following processes:

I. The bare gold chip was first cleaned by immersing chip in isopropanol and ethanol for 10 min each within 2 min sonication.

II. After rinsed with DI water, sample was immersed in a solution of 50mM KOH with 25% H_2O_2 for 10 min.

III. After the treatment described above, sample was in 50mM KOH and connected to a potentiostat. The electrode potential was swept from -200 mV to -2000 mV (vs. Ag/AgCl) at 20 mV/s scan rate, and then rinsed in DI water again.

IV. Blow dry with N_2.

3-3-2 Preparation of mixed SAMs on gold electrode

The alkanethiol layer was modified onto the gold electrode by the self-assembly techniques. A SAM as linker molecule, 11-Mercaptoundecanoic acid(MUA), on the gold surface was modified to connect the proteins or other biomolecule via covalent bond.[36] In previous attempts, however, using a thiol mixture with a 4:1molar ratio of 3-mercaptopropionic acid(3-MOPHA) as a spacer to 11- mercaptoundecanoic acid(11-MUA) immobilized proteins for antibody detection exhibits a better performance than homogeneous SAM since the mixed SAM s reduces the steric hindrance caused by the carboxylic-terminated groups of SAMs.[37] Therefore, we designed a kind of mixed SAM, including hydroxyl- and carboxylic-terminated thiol for covalent bond with anti-*Vibrio Parahaemolyticus* antibody. The antibodies of bacteria were then exposed on the thiol-functionalized gold electrode. As a result, the biocompatible layer formed on gold surface for *Vibrio Parahaemolyticus* capturing. Figure 3-4 shows a cartoon flowcart of the surface modification. The processes:

I. The cleaning gold electrode was immersed 8 mM 3-MPOH and 2 mM 11-MUA mixing thiol at absolute ethanol for 12 hours at room temperature
II. Gold electrode were washed by sonication in ethanol, followed several times by ethanol and DI water
III. The 50 mM EDAC and 30 mM NHS in 1xPBS for 30 min was attached the NHS group to –COOH terminated thiol on the gold electrode at room temperature and then the chip was washed by 1xPBS and DI water.
IV. *Vibrio Parahaemolyticus* antibody with a concentration of 100 μg/mL in 1xPBS injected into the channel through fluidic flow and incubated for 6 hours at 4℃

V. The PBS and the DI water rinsed the chip

VI. After microfluidic channel made up, BSA with 1mg/mL for blocking was incubated in the chamber for 1hour and washed with 1xPBS and 0.01xPB.

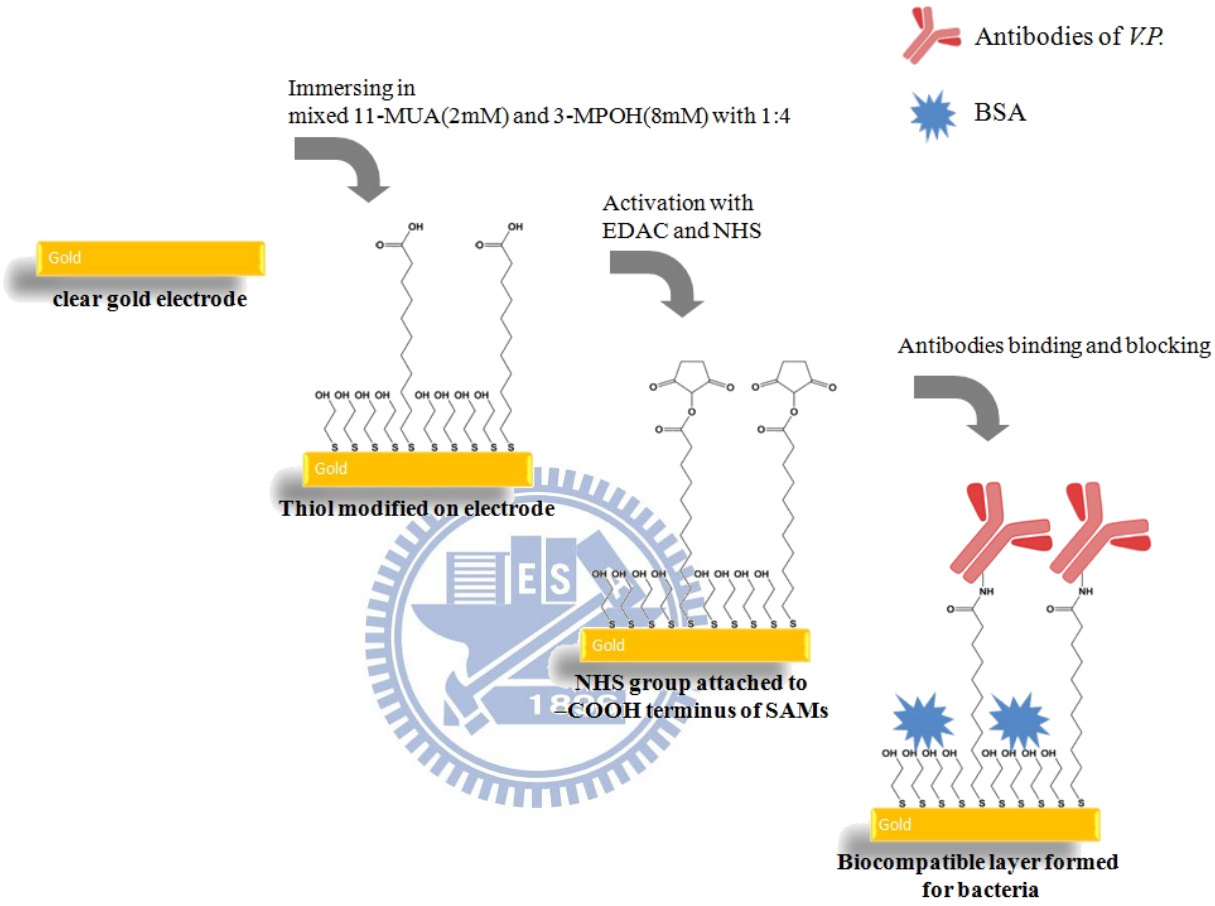

Figure 3-4 Processes of modification: the clean gold electrode was modified by 11-MUA/3-MPOH mixed solution to assemble the carboxylate-thiol layer. EDC/NHS activated the carboxylate group for antibodies binding. After immobilizing the antibodies, the BSA was followed to block remain area of nonbinding.

3-4 Surface molecular identification on Gold electrode

3-4-1 Electrochemical method for 11-MUA and 3-MPOH identification

Cyclic voltammetry is an electrochemical technique that probes the reduction and oxidation of the redox active species in the solution with the electrode. The stability of structural SAM on the gold electrode can be analyzed by CV method.[35] Three electrode cells were comprised. Gold electrode with patterns on the SiO_2 substrate was as a working electorde. A Pt wire and Ag/AgCl metal in 3 M KCL was also prepared as counter electrode and a reference electrode. During the CV scan, shape of I-E curve between the barely clean gold electrode and SAM–coveraged gold electrode would get a strong difference. The gold electrodes with SAM blocking the redox currents influences the electrons transfer in CV scan. The investigation gave the identification of the MUA/MH coating on the gold electrode. CV measurement was achieved by a CH Instruments Model 600B potentiostatic (CH Instruments, Austin,TX) with parameters:

1. Electrolyte and redox active species: 1xPBS(pH7.6) with 30 mM potassium ferrocyanide($K_3Fe(CN)_6$)
2. Scan range: -0.4 V ~ 0.8 V
3. Scan rate: 100 mV/s

3-4-2 Fluorescence labeling

Antibody of *Vibrio Parahaemolyticus* at concentration of 100 ug/mL was applied to NHS group on surface of electrode. Carboxytetramethyl-rhodamine succinimidyl ester (5(6)-TAMRA,SE) were diluted to 1 mg/mL in 1xPBS. The solution within rhodamine put on antibody-modified electrode to carry out the binding reaction.[38] The reaction took 4 hr. PBS with 0.5% tween 20 and D.I water rinse heavily on the chip, followed by dry N_2. Images of labeled antibody were obtained by fluorescent microscopy(Zeiss AX10). A filter of 515-560 nm was used for exciting the rhodamine. The binding method was show in Figure 3-5.

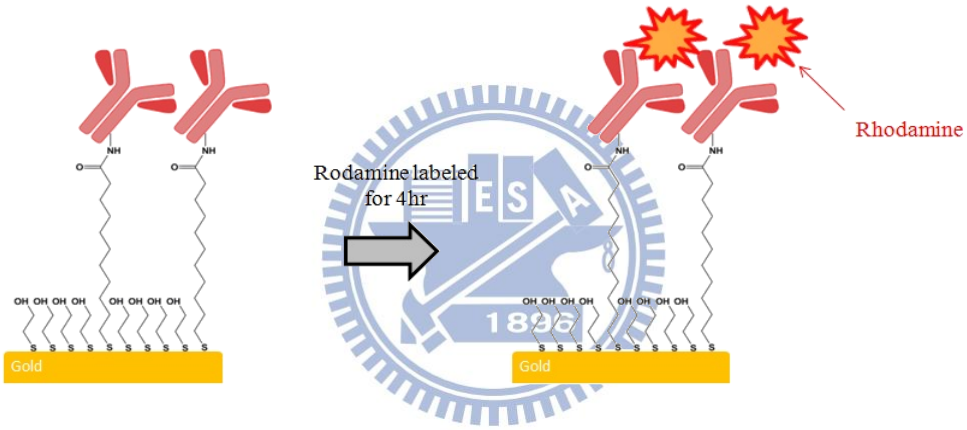

Figure 3-5 Process of sample preparation for fluorescence imaging. After binding antibodies on the electrode, the Rhodamine was labeled on antibodies for fluorescence detection.

3-4-3 TMB development

TMB solutions are chromogenic reagents for horseradish peroxidase(HRP) enzyme, wildly utilized in ELISA techniques normally. In the presence of HRP, the peroxide active the enzyme and thus convert TMB into a blue byproduct. The incubation for 6 hr with HRP conjugated second antibody on to the no-patterned gold electrode, which was immobilized antibody in previous. Figure 3-6 demonstrates the

antibody modified on the thiol-modified electrode. After incubation of HRP-conjugated second antibody on the first-antibody modified electrode for 6 hr, the chip was washed with PBS/0.05% Tween-20 and D.I. water. Subsequently, the TMB substrate was dropped on the chip for a while and the measurable color-changed solution was then taken to read absorbance at 450nm wavelength. Here, the negative comparison was experimented by taking the absorbance change at 450nm for the electrode without antibody modification.

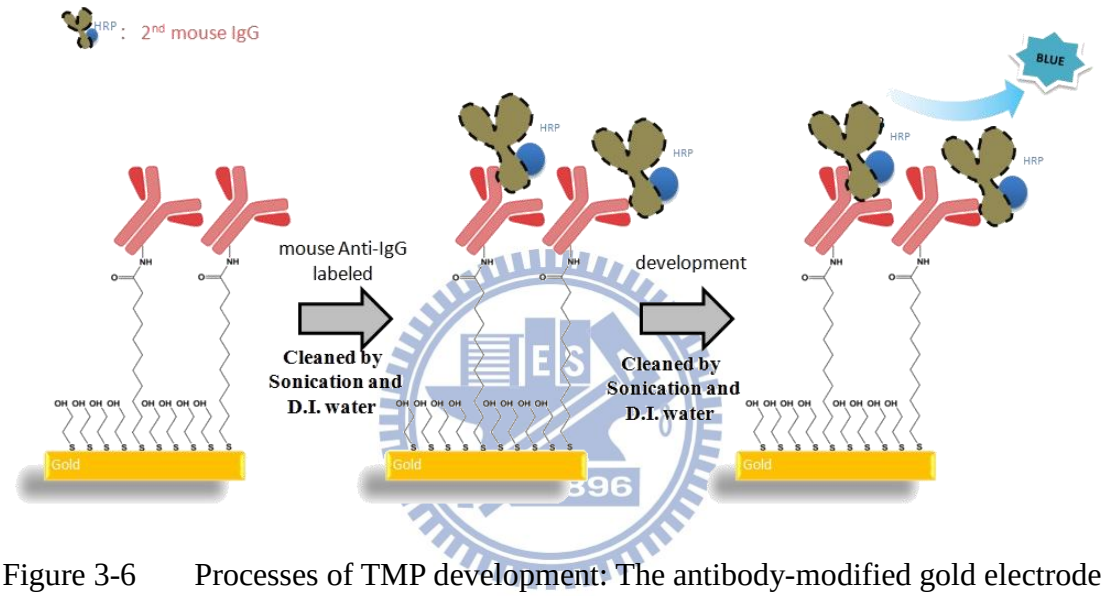

Figure 3-6 Processes of TMP development: The antibody-modified gold electrode was followed by incubating the second antibody. Then the TMP substrate was dropped on the electrode and developed.

3-5 Microfluidic channel and detection system set up

In recent years, the interest in the bacteria or cell detection using microfluidic system increase dramatically. Microfluidic channel was used for the stability and enhancement of biosensing. The integration of bacteria detection with microfluidic enables a faster detection. We use a simple microfluidic system to combine the chip and facilities for bacterial transport and detection.

3-5-1 Microfluidic settlement

Following the modification of biomolecular on the gold electrode of chip, the chip was located by a Teflon O-ring and acrylic broad to make a microfludic chamber. The advantage of being removable and reusable Teflon ring on the top of the chip gives a compliance of experimental channel. Teflon at 1mm thickness was taken to a well with a volume of 25 uL.Figure 3-7(a) illustrates schematics of chamber settlement. Teflon tube was then inject into the chamber as inlet and outlet for sample delivery. The chip after settlement placed at the PCB, shown in Figure 3-7(b). Bovine serum albumin (BSA) was injected into chamber for blocking before measuring 0.01xPhosphate buffer as baseline.

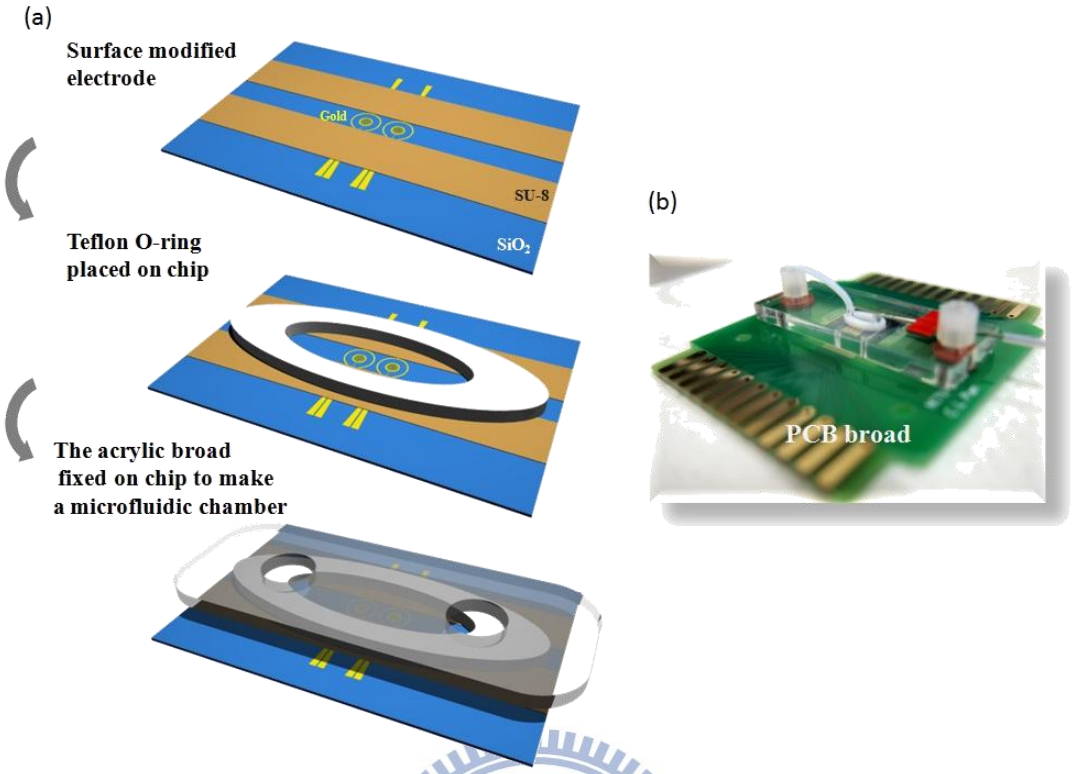

Figure 3-7 Processes of microfuidic system set-up (a) fabrication of microfluidic channel . (b) completion of microfluidic chip.

3-5-2 Processes of detection in microfluidic channel

Due to the design of electrode configuration, the electrical connection for bacteria trapping and bacteria detection is different. In order to manipulate the bacteria to the inner circular of gold electrode, inner electrode was connected with functional generator reverse to outer ring of electrode, shown in Figure 3-8(a). However, measuring bacteria immobilizing on the electrode was completed by linking either side of pad in inner electrode to impedance analyzer, shown in Figure 3-8(b).

Phosphate buffer diluted 100 times is as solution for whole detections. The solution did not react electrochemically with electrodes during trapping and detection. In this bioassay, Peristaltic pump for sample delivery was connected to inlet and outlet port and make the flow through the channel at rate of uL per minute, shown in

Figure 3-9. The all assays of detection were investigated under microscopy. Figure 3-10 also states the process of detection. A modified- antibody electrode without AC electrokinetics was also inspected for comparison. Figure 3-10 shows the pictures of detection system.

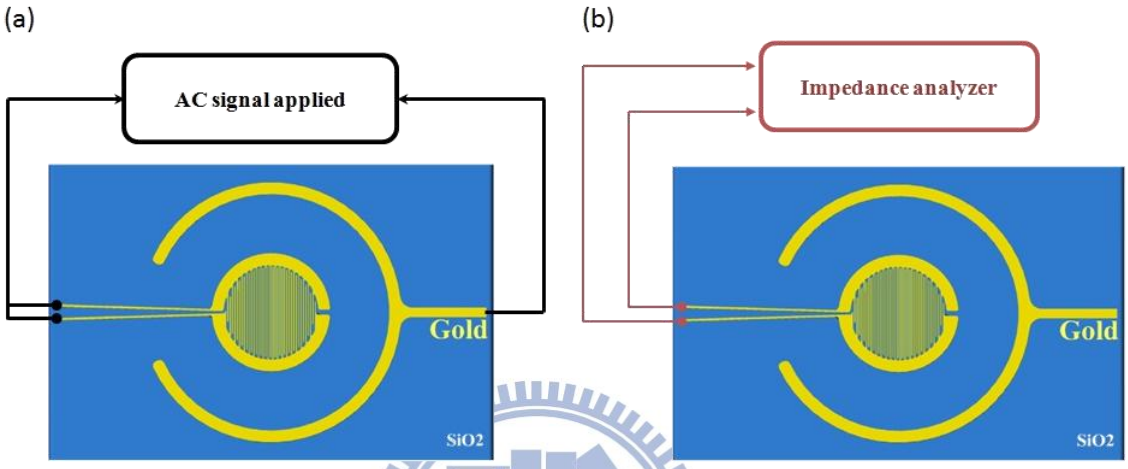

Figure 3-8 Connection for (a) bacteria trapping (b) bacteria detection by electrode.

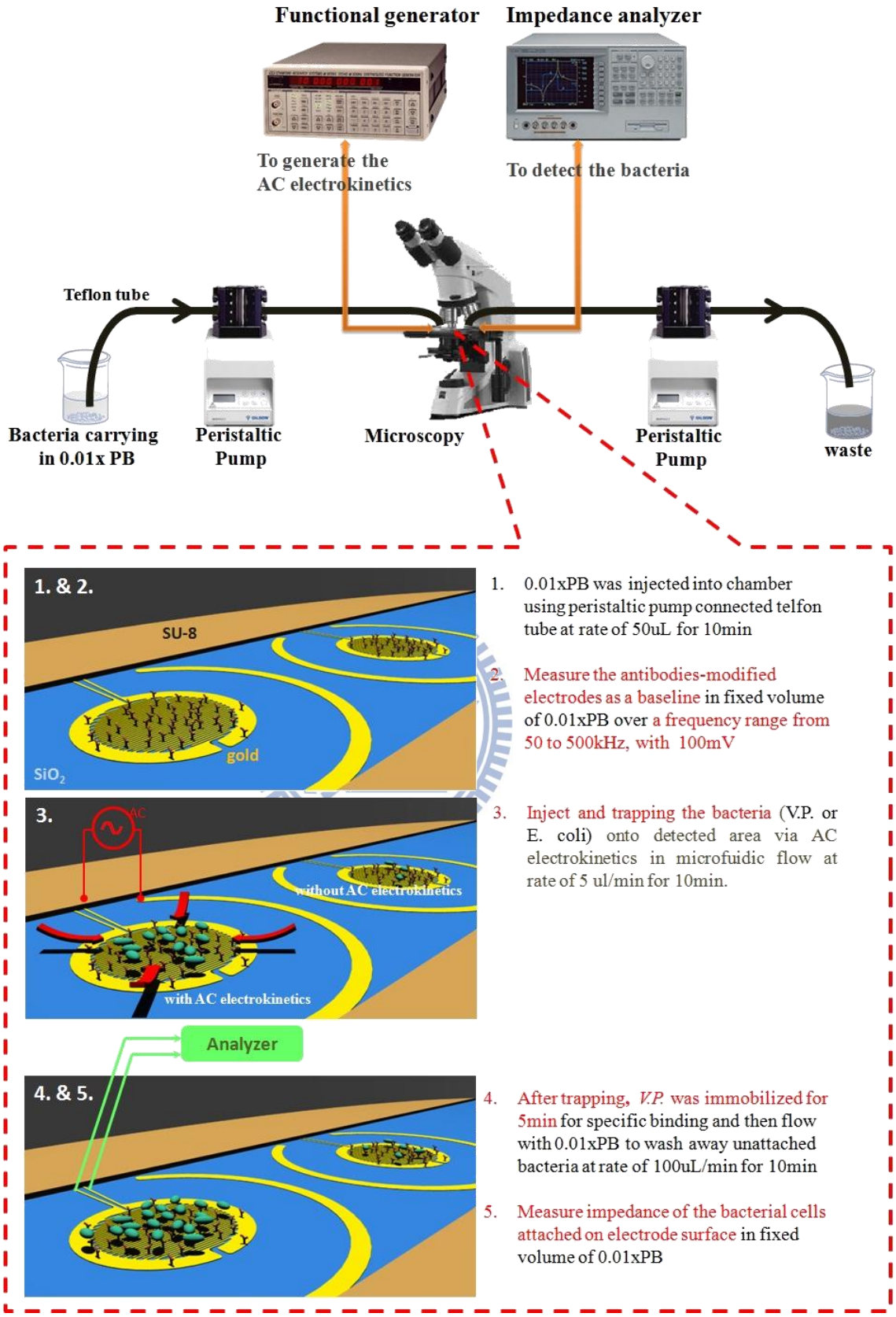

Figure 3-9 Schematics illustration of assay.

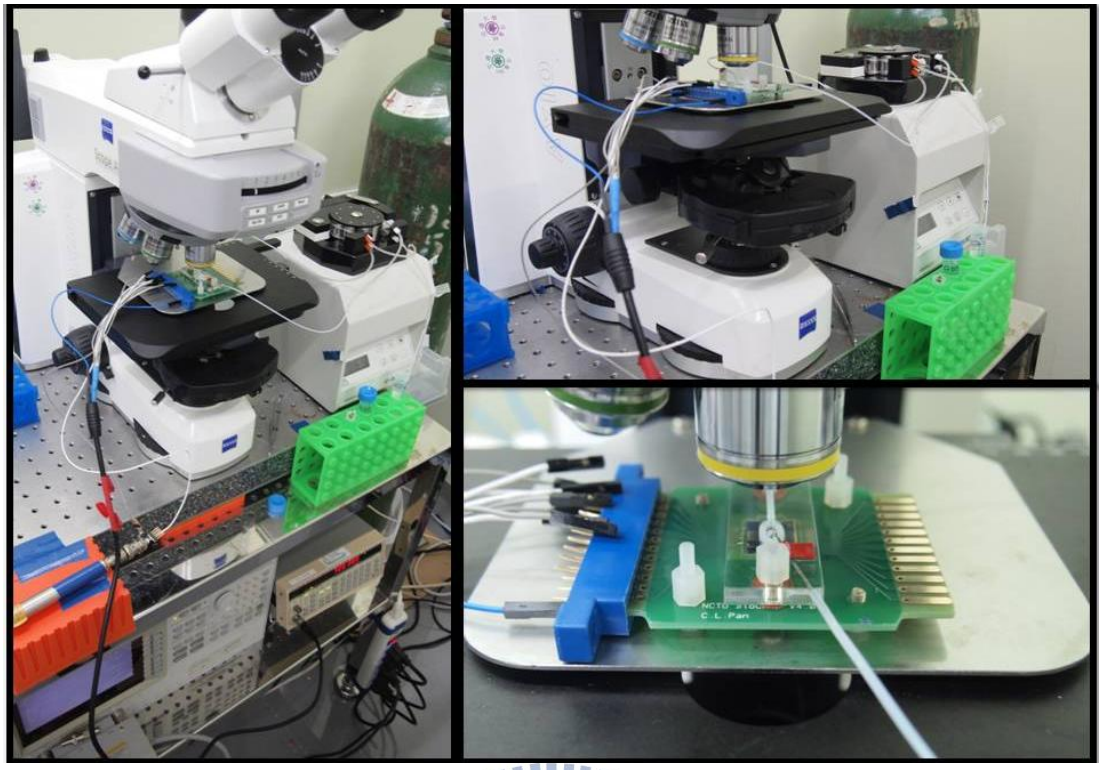

Figure 3-10 Pictures of the whole system.

3-6 Bacteria preparation

The fresh *Vibrio Parahaemolyticus* and *E coli* XL1-Blue strain were taken from frozen stock and then cultured in the solution of Tryptic Soy Broth (TSB) with 3% sodium chloride, and Luria Broth (LB) containing 20μg/ml tetracycline at 37℃ for 6 hour, respectively, until the value of OD_{600} reach about of 0.97 (10^9cfu bacteria). The bacteria were collected and diluted 100 fold in phosphate buffer that do not affect the electrode surface after applying via oscillate voltage. The bacteria were then trapped though AC electrokinetics and the impedance were sequentially detected.

3-7 AC electrokinetics manipulation for analyte trapping

After antibodies were immobilized onto microelectrode surface, the AC electrokinetics processed so that only antibody specific bacteria can be left on the inner surface effectively even the electric field unapplied. The article demonstrates the enhancement of the binding of anayltes with its antibody via AC electrokinetics. The mechanism assist to reduce binding time. Several researches of AC electrokinetics forced on bioparticles trapping onto center of circular electrode. The designed electrode using in this detection, however, has not been applied for the bacteria or other bioparticles trapping. Here we show the approachable AC eletroosomosis and electric field by COMSOL V.4.2 simulation on the electrodes to make sure the probability of bacteria trapping.[22] The ideal result for bacteria trapping is manipulating it onto inner surface of electrode, depicted in Figure 3-11. There is one size of inner electrodes with diameters 500 μm, and each contains the interdigited electrode with 5 μm width and 5 μm gap. The diameter of outer electrode is 1050 with width 50 um.

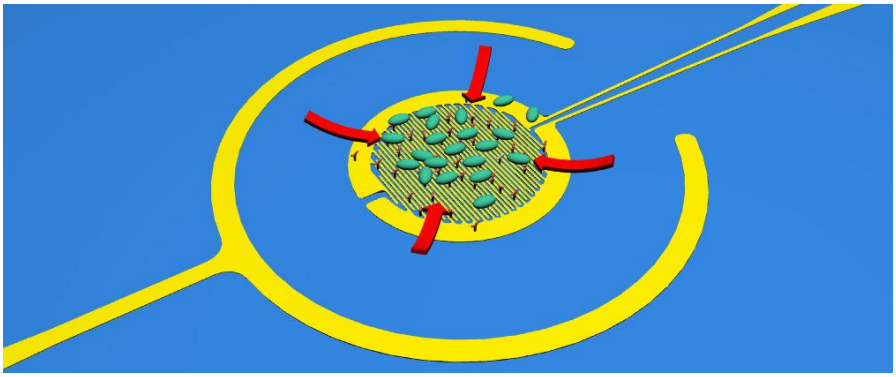

Figure 3-11 Bacteria trapping via AC electrokinetics enhancement.

3-8 Impedance measurement

Each detection method used Agilent 4294A impedance analyzer with two-end measurement. The data were collected via Labview programming. A set of inner circular electrodes was actuated with AC electrokinetics and another set of electrode was without AC electrokinetics as control part. The sensor detects the changes of dielectric properties of electrode surface up to analytes binding. Bactria were dragged in fluidic flow channel at various dilution ($10^{5\sim}10^{7}$cfu/mL) and mixed (*Vibrio Parahaemolyticus*+*X*L1 Blue *E coli)* solution. The baseline was established by the flow flushed thought the antibody-functionalized electrode.

3-8-1 Parameters for impedance measurement

For frequency sweep measurement, the impedance was measured from 50 Hz to 500 kHz with oscillate voltage 100mV. Diluted Phosphate buffer with 100 times as a solution for measurement without and with bacteria. The fixed volume of solution was used to steady while measurement.

3-8-2 Normalized impedance change as impedance analysis

Using antibody-modified electrode to binding the bacteria without AC electrokinetics enhancement was used as control. To observe the effect of Bacteria binding, the magnitude of impedance was compared for bacteria binding in the presence of AC electrokinetics to antibody modified on electrode. Introducing a Normalized impedance change (NIC) as a function of frequency range from 50 Hz to 500 kHz and drawn based on the difference of magnitude of impedance with respect to the baseline. The value of NIC was given by following formula:

$$NIC = \frac{Z_{sample} - Z_{baseline}}{Z_{baseline}} \times 100\%$$

where $Z_{baseline}$ is the magnitude of impedance for antibody-modified sample and

Z_{sample} is the magnitude of impedance for a sample containing bacteria, *Vibrio Parahaemolyticus* and *X*L1 Blue *E coli*.

3-8-3 Equivalent circuit

In impedance analyzer as biosensor, total impedance of medium cannot directly be calculated from input voltage and current. Another alternative method, an equivalent circuit, can fit the experimental data. The information of equivalent circuit characterizes physical response of electrical parameters owing to the impedance change.

The electrical parameters used in the experiments were designed and fitted including bulk medium resistance (Rsol), double layer capacitance (CPEdl), and medium dielectric capacitance (CPEsol) between the surface of inner interdigitated electrodes , shown in Figure 3-12(a) and (b). When electrodes immerse in solution, it is consider that the bulk medium and electrical double layer in series. Bulk medium with ion species is as a resistance and the polarized interface of electrodes as capacitance. The dielectric capacitor explains dielectric properties of solution surrounding the electrodes. Instead of ideal capacitors, these capacitors mentioned above are described as constant phase element (CPE):[5]

$$Z_{CPE} = \frac{1}{T(j\omega)^p}$$

T and P depend on the environment of medium and interface of electrodes. If p is 1, the CPE is an ideal capacitor. In reverse, p close to 0 means a simple resist emerging. if the equivalent circuit is simulated, the detection plot as a function of frequency can be explained in three distinguishing range(Figure 3-12(c)).[39] The CPE double layer dominates at lower frequency since the higher impedance of interface capacitor. At intermediate frequency, the CPE interface and CPE solution obtain a balance that

causes bulk medium resistance influences the total impedance changes. At higher frequency, the electrical double layer vanishes and impedance of the dielectric capacitor still diminishing, so the dielectric capacitor is become important.[40]

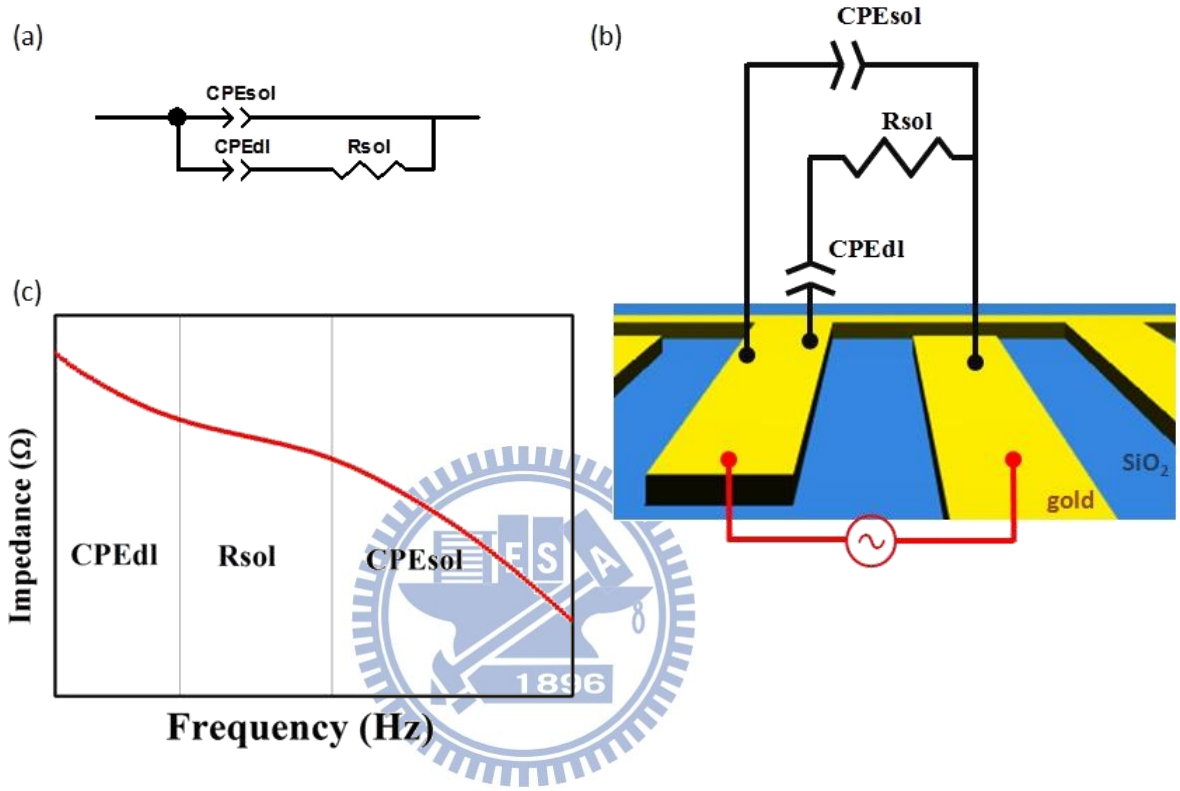

Figure 3-12 (a) Equivalent electrical circuit (b) Equivalent electrical circuit on the chip (c) Impedance spectra divided into dominant element.

Chapter 4 Results and discussion

4-1 Characterization of surface molecular on gold electrode

4-1-1 Electrochemical detection for monolayer coverage on gold electrode

The CV method is capable of analyzing the SAM formation on gold electrode via investigation of moving ability in electrons transfer. Before processing the modification, CV recorded the ions transfer current between the reduction and oxidization at the cleaning gold electrode. It shows the redox species $Fe^{2+/3+}$ converts easily in black line of Figure 4-1. However, the CV curve varies as the electrode is SAM modified. A 2 mM MUA with the spacer 8mM MH monolayer in absolute ethanol were absorbed for 12 hour on the pattern gold electrode with size of inner diameter in 500 um. CV curve for MUA/MH SAM on gold are given in red line of Figure 4-1. During the CV scan, the MUA/MH monolayer insulate the gold surface against the electrons transfer with $Fe^{2+/3+}$ molecule in solution. The anodic and cathodic peak currnet was deceased compared to bare gold electrode. The results effectively identify the MUA/MH monolayer formation on biosensing area.

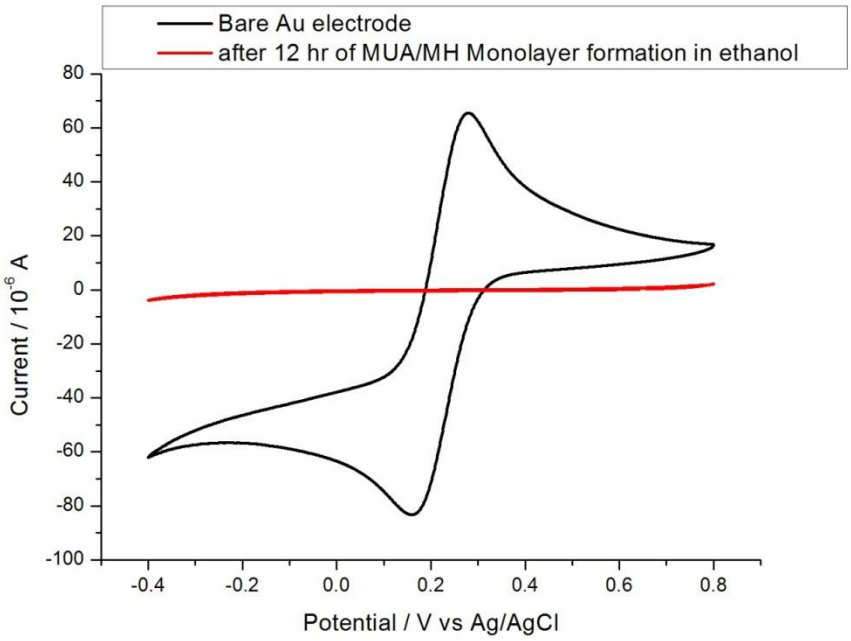

Figure 4-1 Comparison of CV scan (a) before modification with (b) after modification.

4-1-2 Binding of fluorescent dye to Protein on MUA/MH-covered gold electrode

The CV measurement revealed the 11-MUA/3-MPOH thiol layer modified on gold electrode. The COOH-terminal thiols can covalently bind antibody after activating it to NHS-group. To present the antibody of *Vibrio Parahaemolyticus* binding to NHS group on patterned gold electrode, a fluorescent dye performed a visualized study of antibody binding. Rhodamine interaction with and without modified gold electrode were characterized by fluorescence microscopy. Unmodified chip act as a control data. Figure 4-2 and Figure 4-3 show the patterned electrode fixed rhodamine with modified and unmodified antibody. Though the rhodamine on the antibody-modified electrode compared with the control can clearly be observed, the SiO2 substrate still have unstable absorption of Rhodamine.

(a) (b)

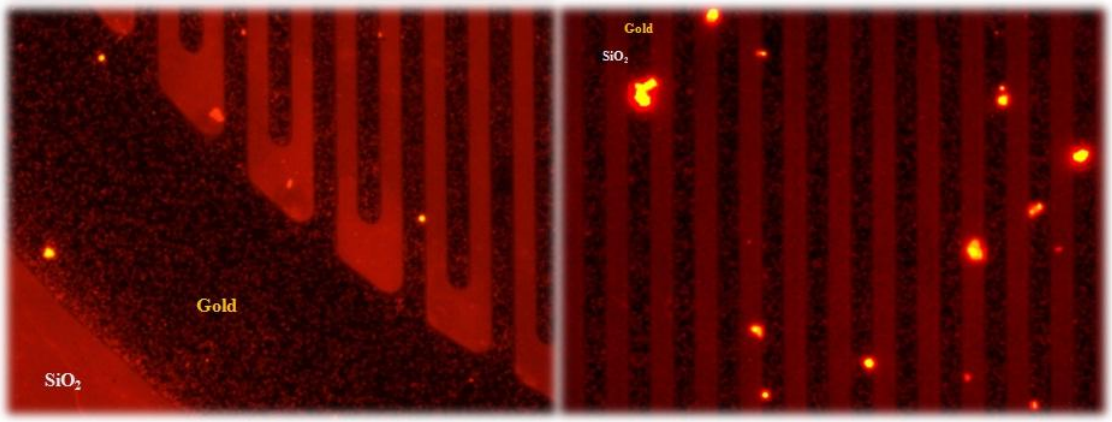

Figure 4-2 Rhodamine fixed on electrode with antibody modification.

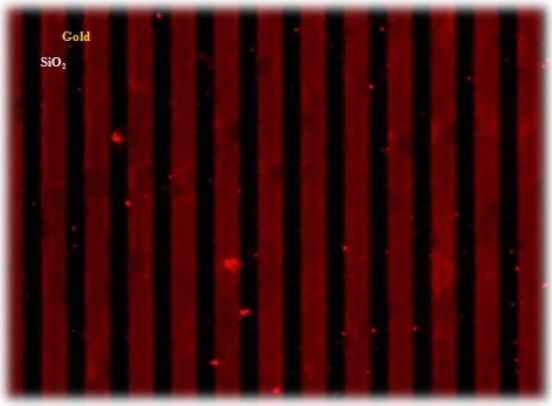

Figure 4-3 Rhodamine fixed on electrode without antibody modification.

4-1-3 HRP development using second antibody

Figure 4-4 depicts the TMB chromogenic resulting of thiol-modified electrode immobilized HRP-conjugated secondary antibody. Under light exposure, the changed color could be visualized. The absorbance at 450 nm was further measured to compare the modification

(a) (b)

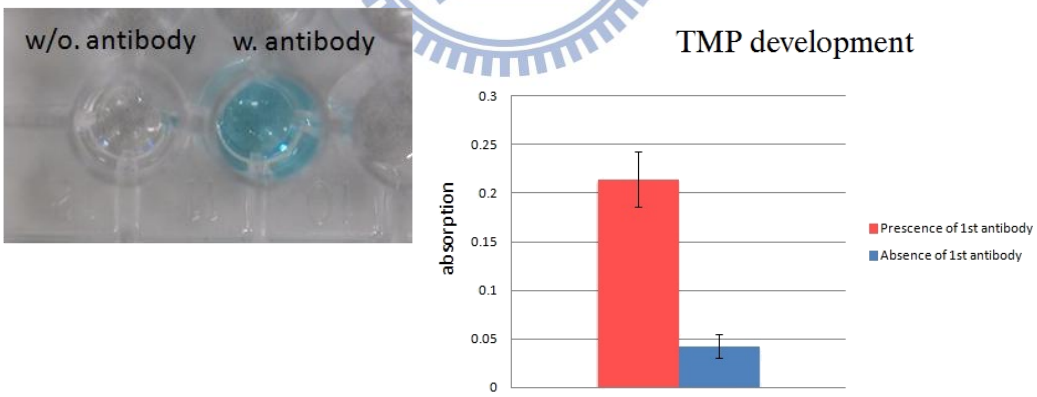

Figure 4-4 (a) TMB chromogenic result on gold electrode without and with antibody modification (b) absorbance at 450nm.

4-2 AC electrokinetics and microfluidic system in bacteria trapping

4-2-1 The behavior of AC electrokinetics in microfluidic channel

Locating bacteria on the inner surface of electrode is the ideal concentration. Appearance of AC electrokinetics results from combination of DEP with ACEO. Figure 4-5(a) depicts the profile of simulated ACEO velocity in the 0.01xPB solution. It may produce ACEO on the surface of electrode(y=0) even if the velocity on gap inside inner interdigitated electrode is zero. Figure 4-5(b) shows profile of ∇E^2. E is electric field and ∇E^2 is proportional to DEP force due to the same parameters of bacteria. We still can get the notice that the DEP is available under this electrode type. In fact, the bacteria can be manipulated on the surface of inner electrode efficiently with 2 Vp-p and 200 Hz. When applied voltage with 2 Vp-p and 30 kHz, the DEP mainly trap the bacteria at electrode edge. The outcome of bacteria manipulation could be set as a function of frequency, in Figure 4-6 and Figure 4-7. At low frequency, the bacteria could be trapped on the inner electrode because of the combination of DEP and ACEO. At high frequency, DEP force dominated in the microfludic flow. Bacteria were dilution in 0.01xPB and non-uniform electric field was applied by 2 V from peak to peak. The sample flow rate was at 5 uL/min.

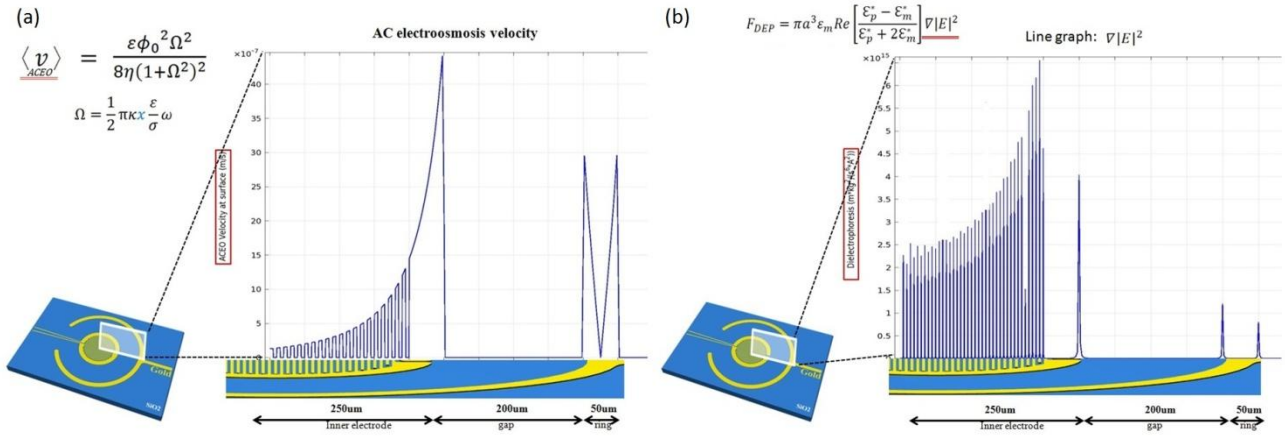

Figure 4-5 Profile of (a) ACEO (b) gradient of quadratic electric field.

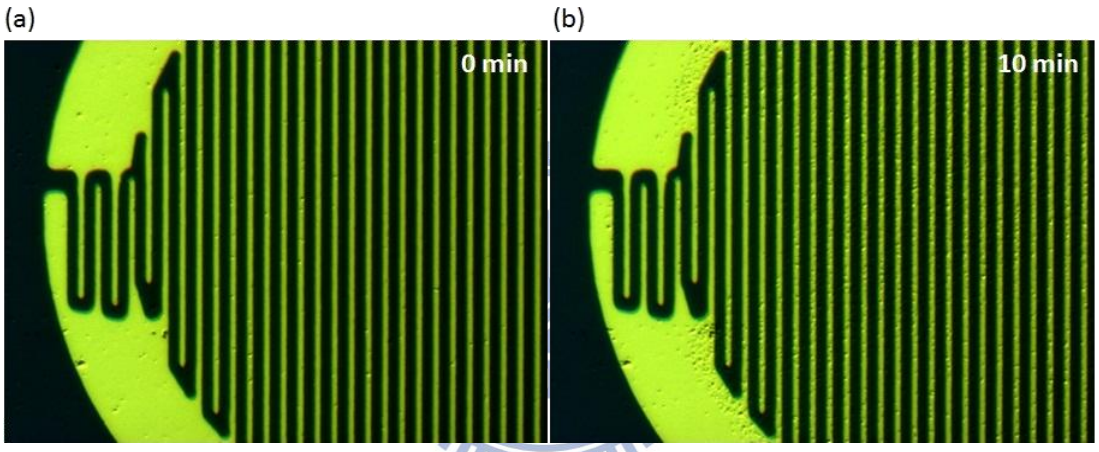

Figure 4-6 Bacteria trapping with 2Vp-p and 200Hz (a)at 0min(b) after 10min.

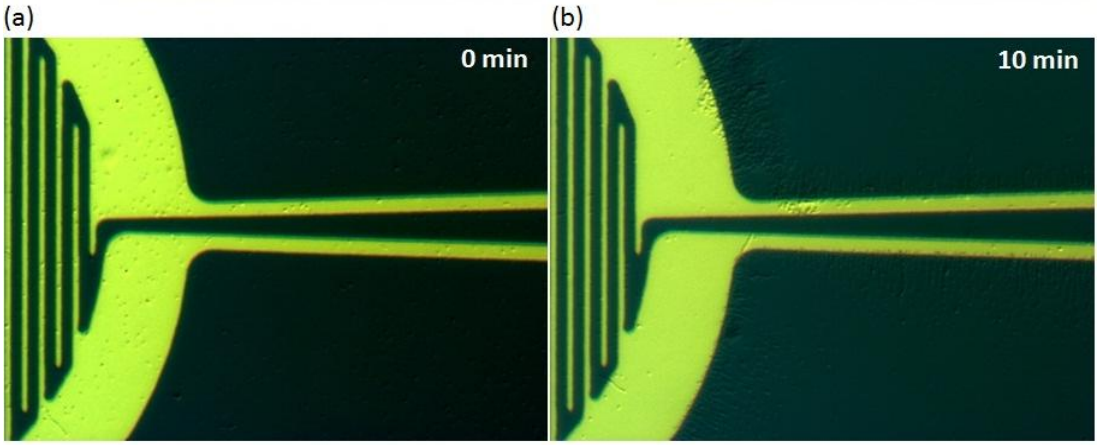

Figure 4-7 Bacteria trapping with 2Vp-p and 30kHz (a)at 0min(b) after 10min.

4-2-2 The influence of flow rate on bacteria trapping

Before bacteria detection, the bacterial cells delivered by tube to microfluidic channel with a rate of flow. The flow rate can affect on the efficiency of bacteria trapping. We use pump to deliver the bacteria in 0.01xPB to microfluidic chamber with different rate and observe the effect on the bacteria concentration on the inner circular electrode. Flow rate at 5, 50, and 100 uL per minute was chosen for monitoring. The results in Figure 4-8 show that the best efficiency of bacteria concentration occurred at flow rate of 5 uL/min. The time for bacteria trapping is 10min by applied voltage 2 Vp-p and frequency 200 Hz.

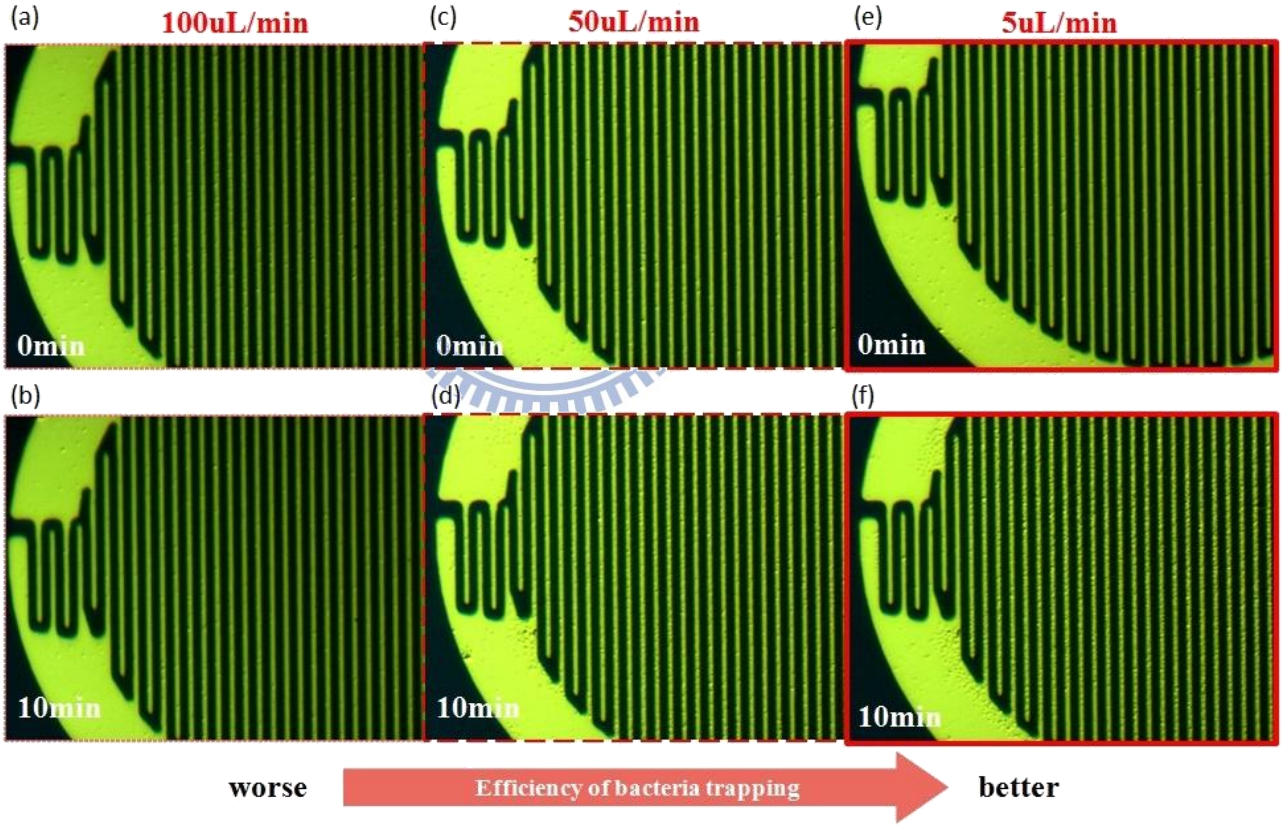

Figure 4-8 Flow rate at 100uL/min (a) before trapping (b)after trapping , flow rate at 50uL/min (c) before trapping (d) after trapping, flow rate at 5uL/min (e) before trapping (f) after trapping.

4-3 Bacteria detection

The AC electrokinetics for *Vibrio Parahaemolyticus* concentration on surface of inner electrode was manipulated successfully by the data above. The impedance change was measured for immobilization of bacteria and accounted for the physical model based on electrical circuit.

4-3-1 Impedance analysis for three types of electrodes

The sizes of electrodes were fabricated for efficient trapping and detection of bacteria. Three sizes of electrodes with different diameter of inner circular electrodes(100 um, 250 um, and 500 um) was investigated for the impedance change. We present electrodes with inner diameter 500 um as electrode A, inner diameter 250um as electrode B, and inner diameter 100 um as electrode C(Figure 4-9). Detection of *Vibrio Parahaemolyticus* at concentration of 10^8cfu/mL was performed for comparison. Applying 2 Vp-p with 200 Hz can concentrate bacteria efficiently for electrode A, 2 Vp-p with 400 Hz for electrode B, and 2 Vp-p with 750 Hz for electrode C. One of the electrodes has largest variation of Normalized impedance change (NIC). The electrode with greatest change allowed it to use for following detection. Figure 4-10, Figure 4-12, and Figure 4-14 show impedance spectra as a function of frequency for individual electrode. Figure 4-11, Figure 4-13, and Figure 4-15 results of Normalized impedance change for each electrode. Experiments of bacteria binding with AC electrokinetics are set against without AC electrokinetics for NIC analysis.

Figure 4-16(a) and (c) which are the SEM images tell the difference between bacteria immobilization bound to functionalized electrode with and without AC electrokinetics. Figure 4-16(b) shows that few bacteria attach to the SiO2 substrate resulting from antibodies not being immobilized on the oxide surface.

Figure 4-9 Different sizes of electrode. (a) inner diameter: 500 um (b) inner diameter: 250 um (c) inner diameter: 100 um.

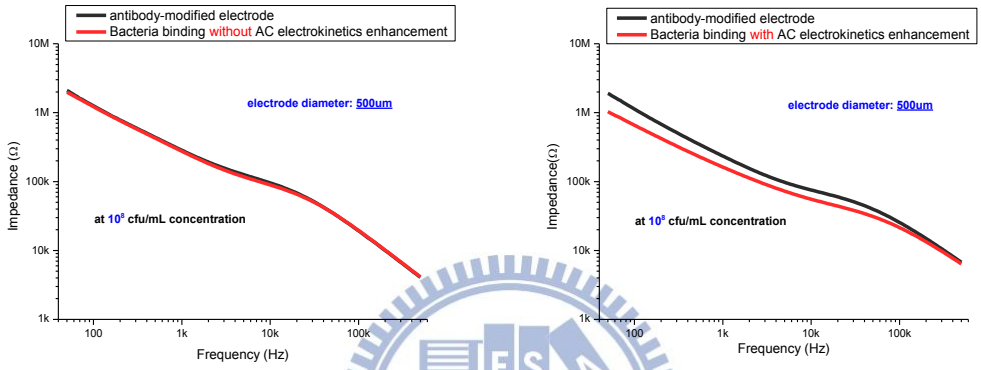

Figure 4-10 Impedance spectra using electrode A.
(left: without AC electrokinetics /right: with AC electrokinetics)

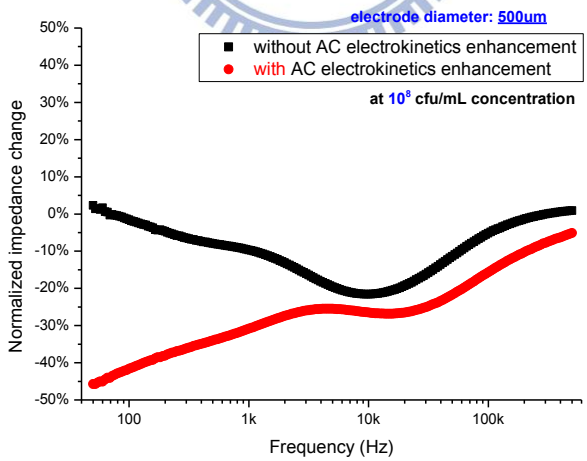

Figure 4-11 Normalized impedance change(NIC) for electrode A .
(blank line: without AC electrokinetics;
red line: with AC electrokinetics)

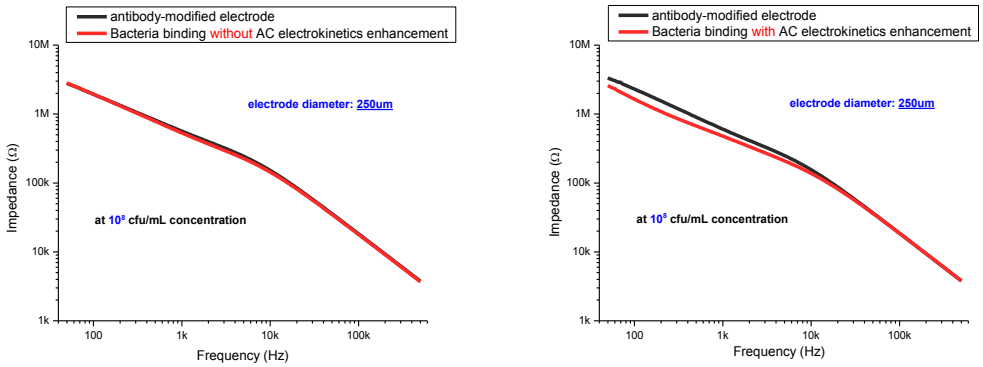

Figure 4-12 Impedance spectra using electrode B.
(left: without AC electrokinetics /right: with AC electrokinetics)

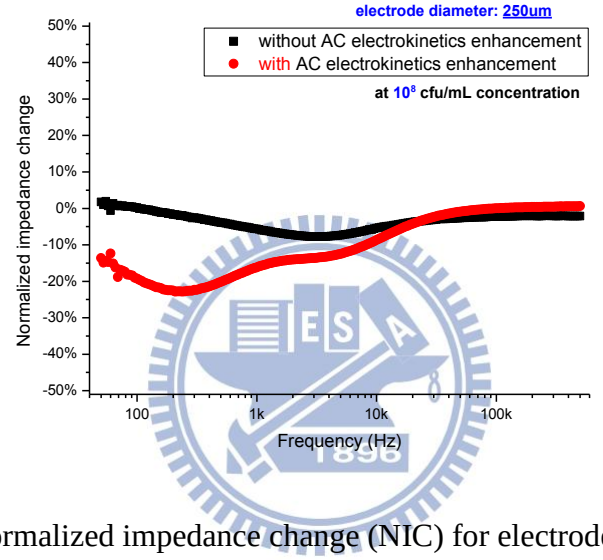

Figure 4-13 Normalized impedance change (NIC) for electrode B.
(blank line: without AC electrokinetics;
red line: with AC electrokinetics)

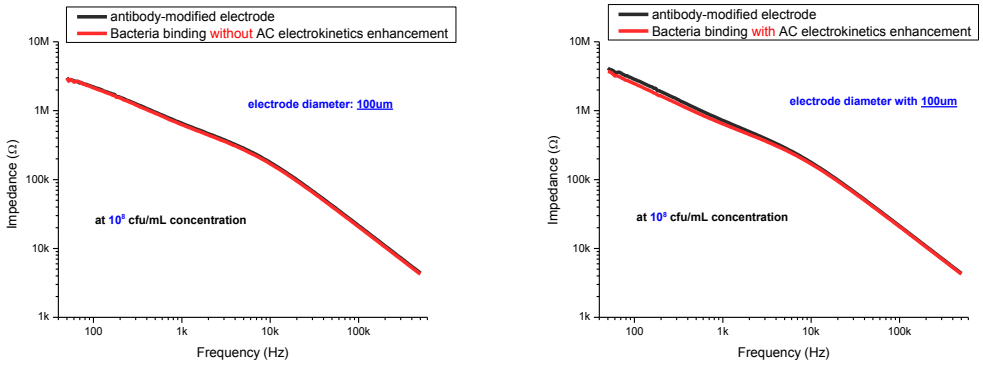

Figure 4-14 Impedance spectra using electrode C.
(left: without AC electrokinetics /right: with AC electrokinetics)

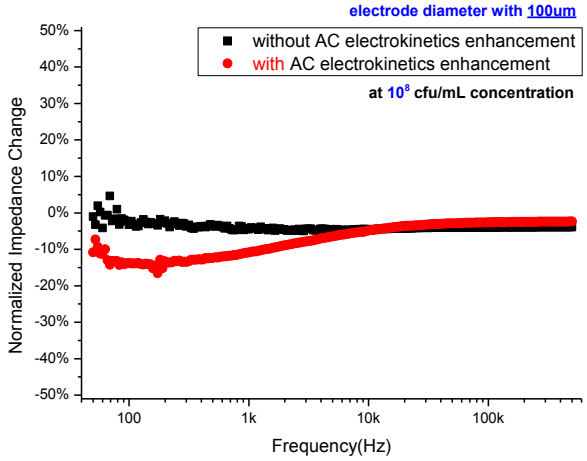

Figure 4-15 Normalized impedance change(NIC) for electrode C. (blank line: without AC electrokinetics; red line: with AC electrokinetics)

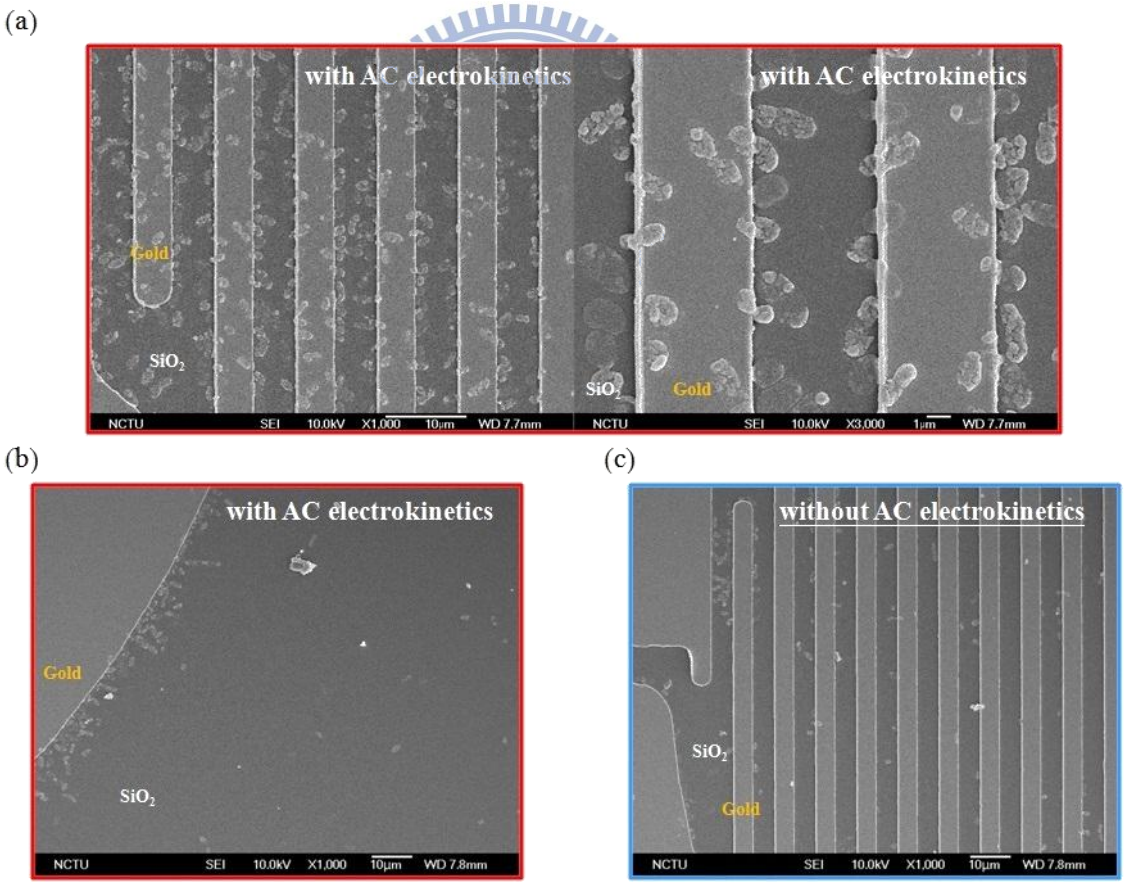

Figure 4-16 SEM images of *Vibrio Parahaemolyticus* bound to antibody-modified electrode surface (a) trapping with AC electrokinetics enhancement (b) edge of electrode (c) trapping without AC electrokinetics enhancement.

All of the impedance spectra from three different sizes of electrodes have the same trend of decreasing value in low frequency after binding with the bacteria. It can be attributed to the change of dielectric properties on electrode surface. The surface of bacteria has many proteins with high conductivity.[40] These charges can gain the conductance around the electrode surface causing total impedance reducing. Compared with value of detection(red line) from Figure 4-10, Figure 4-12, and Figure 4-14, the electrode A gives a greater change in bacteria detection. The AC electrokinetics trapping can actually detect the bacteria in limited time. Figure 4-17 illustrates NIC in three sizes of electrodes. The NIC can obviously tell a major difference on electrode with inner diameter 500 um (electrode A).

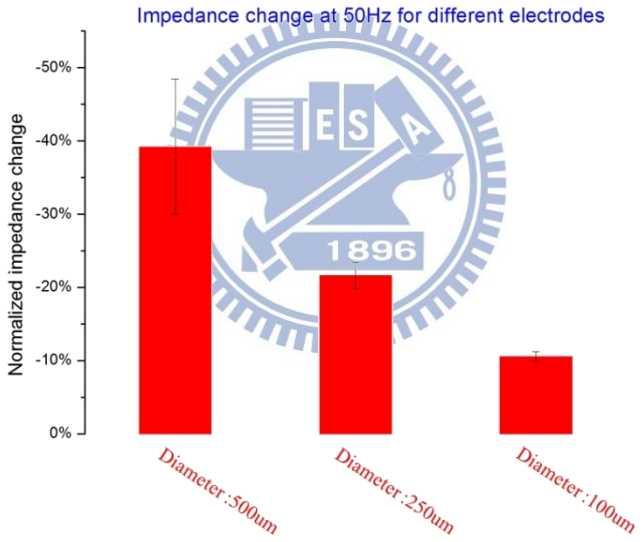

Figure 4-17 NIC of bacteria detection with AC electrokinetics in three sizes of electrodes.

We fitted the impedance data to the electrical circuit model. The value of the element in the circuit with and without bacteria binding can explain the behaviors inside the chamber. The circuit model can fit the measured impedance under 5% error. Figure 4-18(a) Figure 4-19(a), and Figure 4-20(a) are the fitting of the equivalent circuit of 500 um, 250 um, and 100 um of inner diameter electrode. In one hand, thick

gray (antibody-modified) and blue (bacteria binding) line perform the measured data. On the other hand, Thin cyan (antibody-modified) and red (bacteria binding) line are fitting spectra. The impedance spectra of antibody-modified electrodes are fitted by impedance of distinctive elements in Figure 4-18(b), Figure 4-19(b), and Figure 4-20(b). We figure out that the CPEdl at low frequency dominating the impedance value. Frequency ranges from 50 to 1 kHz can play a role for electrode A, 50 to 550Hz for electrode B, and 50Hz to 300Hz for electrode C, collected in Table 4-1. The electrical element from the model in different electrodes is followed by Figure 4-21, Figure 4-22, and Figure 4-23. CPEdl represents capacitance of the electrode surface and its change in three elements is largest due to the attachment of bacteria onto the electrode. The value of each element for different electrode and with/without bacteria binding is showed in Table 4-2. The difference of CPEdl-T before and after bacteria binding for electrode A is evaluated as 2.4 times. Others could be 1.07 times for electrode B and 0.9 times for electrode C.

(a)

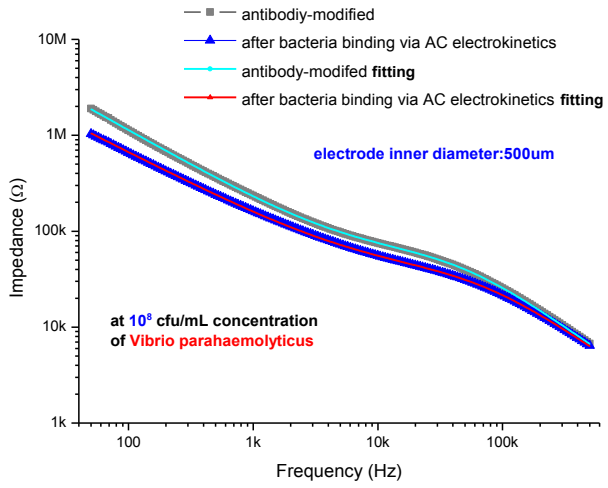

(b)

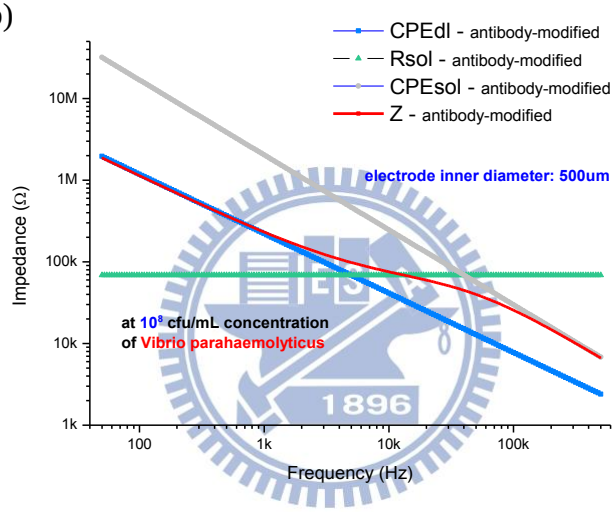

Figure 4-18 Impedance spectroscopy of inner diameter: 500 um (a) Fitting spectra of the measured data (b) Magnitude of three elements in impedance analysis.

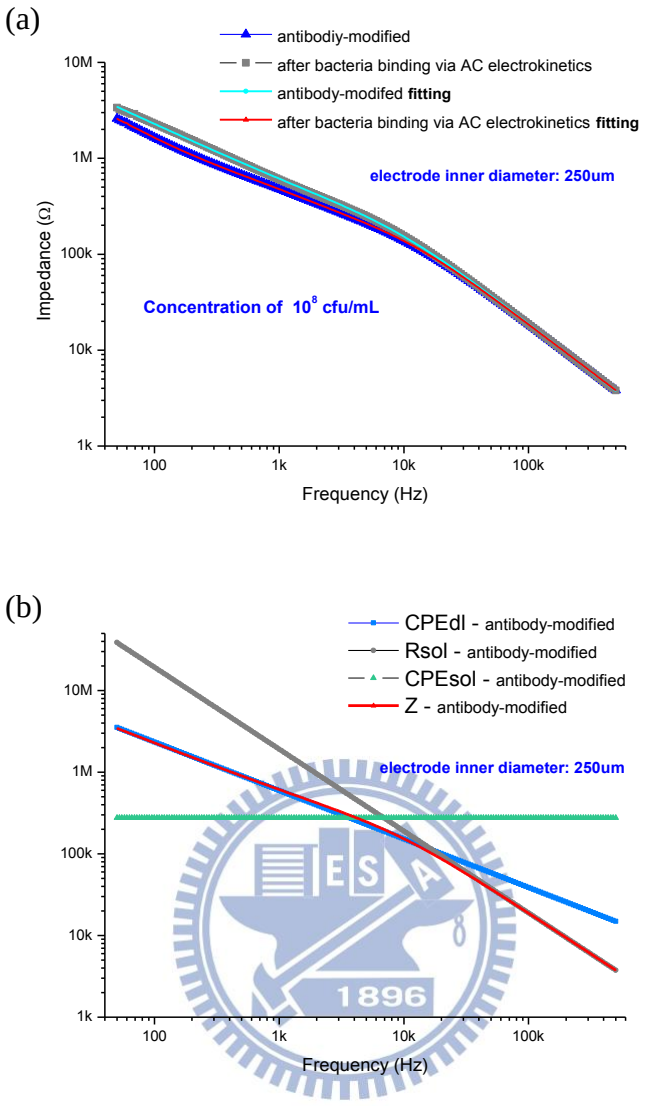

Figure 4-19 Impedance spectroscopy of electrode A (a) Fitting spectra of the measured data (b) Magnitude of three elements in impedance analysis.

(a)

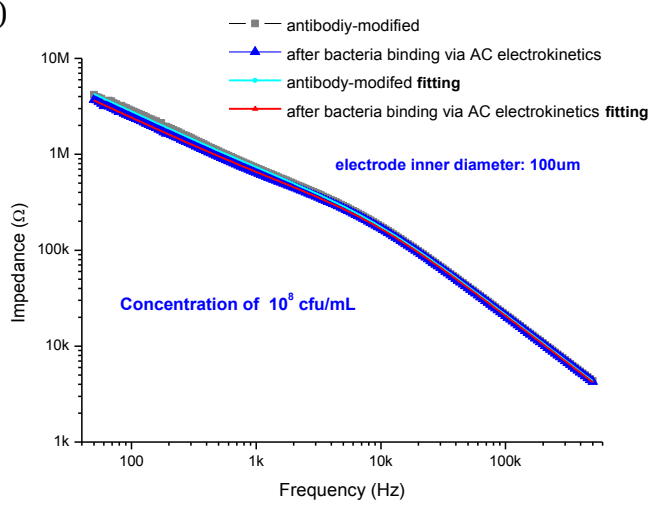

(b)

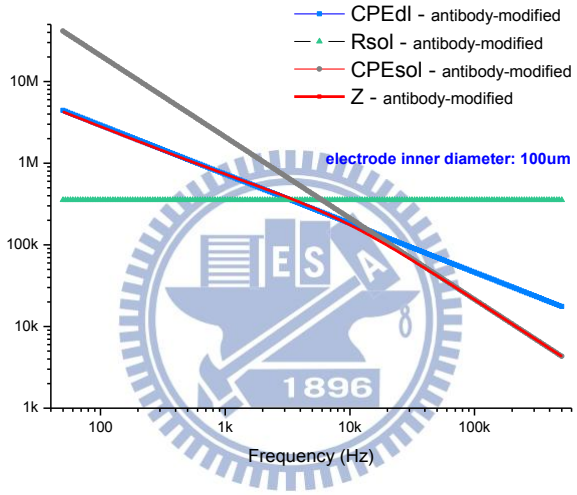

Figure 4-20 Impedance spectroscopy of electrode B (a) Fitting spectra of the measured data (b)Magnitude of three elements in impedance analysis.

Table 4-1 Influence of frequency for each element.

	Inner diameter:500 um	Inner diameter:250 um	Inner diameter:100 um
CPEdl	**50 ~ 1k Hz**	**50 ~ 550 Hz**	**50 ~ 300 Hz**
Rsol	**1k~ 200k Hz**	**550 ~ 60k Hz**	**300 ~ 10k Hz**
CPEsol	**200k ~ 500k Hz**	**60k ~ 500k Hz**	**30k ~ 500k Hz**

Table 4-2 Value of each element for the electrical circuit fitting.

	CPEdl-T	CPEdl-p	Rsol	CPEsol-T	CPEsol-p
Inner electrode diameter : 500 um					
before detection	**8.7701×10^{-9}**	0.72793	68620	1.6052×10^{-10}	0.91754
After detection	**2.0848×10^{-8}**	0.6613	44204	2.3348×10^{-10}	0.8948
Inner electrode diameter : 250 um					
before detection	**9.3361×10^{-9}**	0.59348	276160	8.0934×10^{-11}	1
After detection	**1.00022×10^{-8}**	0.63343	251830	1.0966×10^{-10}	0.98156
Inner electrode diameter : 100 um					
before detection	**1.2653×10^{-8}**	0.76104	94521	9.4923×10^{-11}	0.99394
After detection	**1.1471×10^{-8}**	0.76894	97305	9.5325×10^{-11}	0.99378

(a)

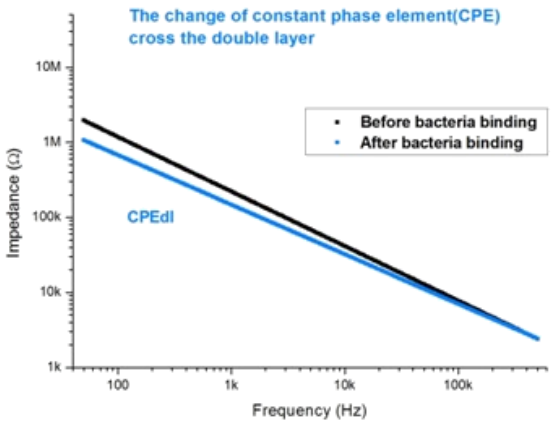

(b)

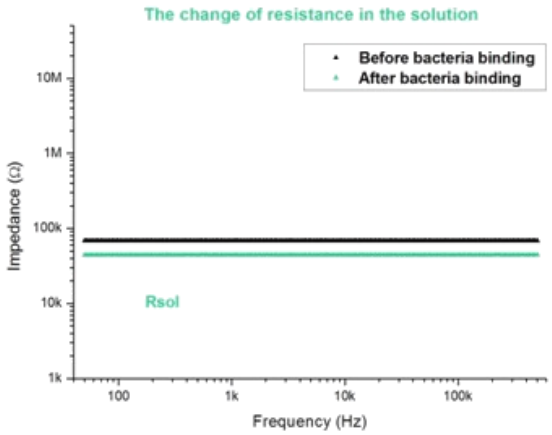

(c)

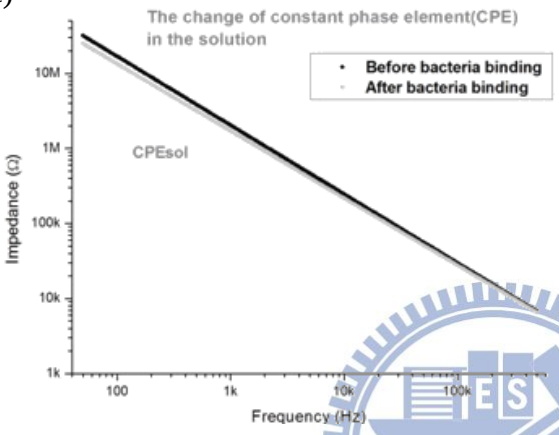

Figure 4-21 Impedance spectroscopy of electrode A (a) impedance of CPE on electrode surface (b) resistance of solution(c) impedance of CPE in the solution.

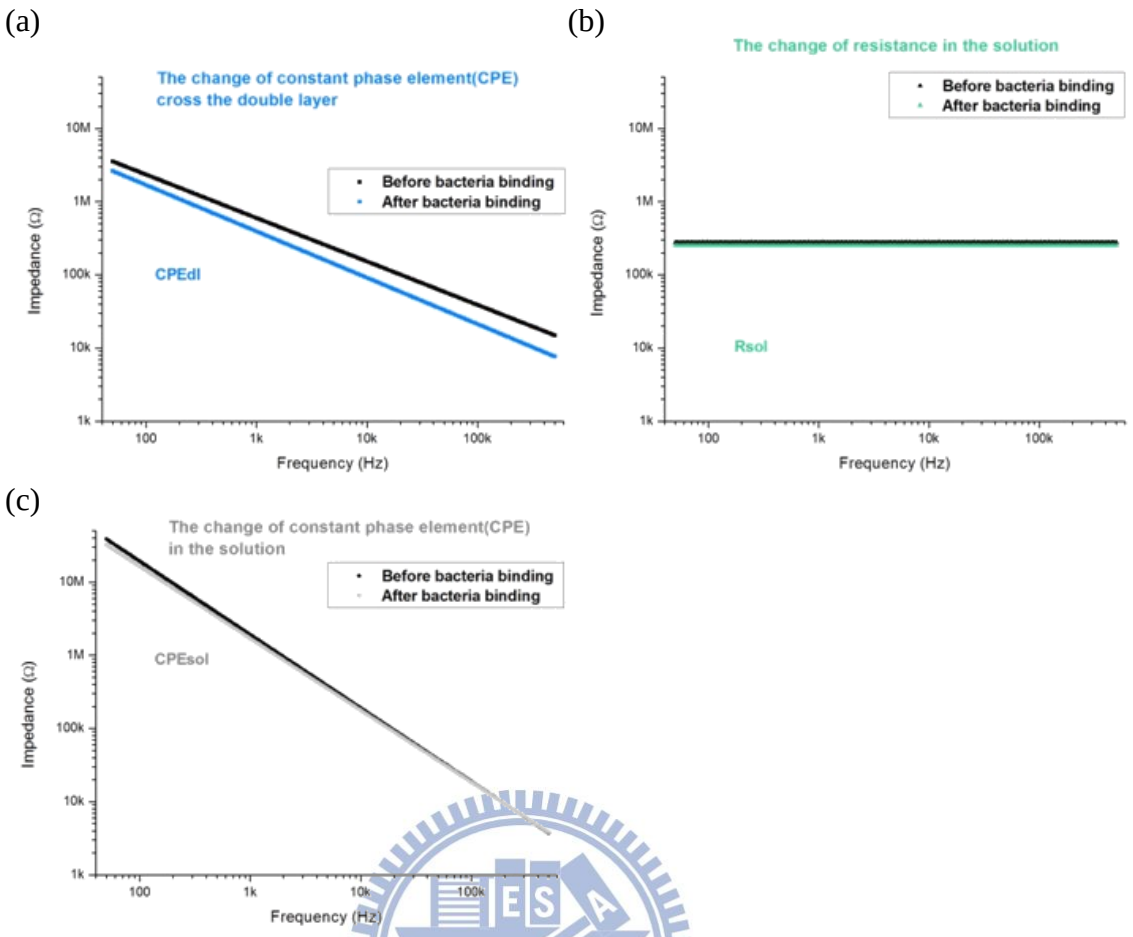

Figure 4-22 Impedance spectroscopy of electrode B (a) impedance of CPE on electrode surface (b) impedance of solution(c) impedance of CPE in the solution.

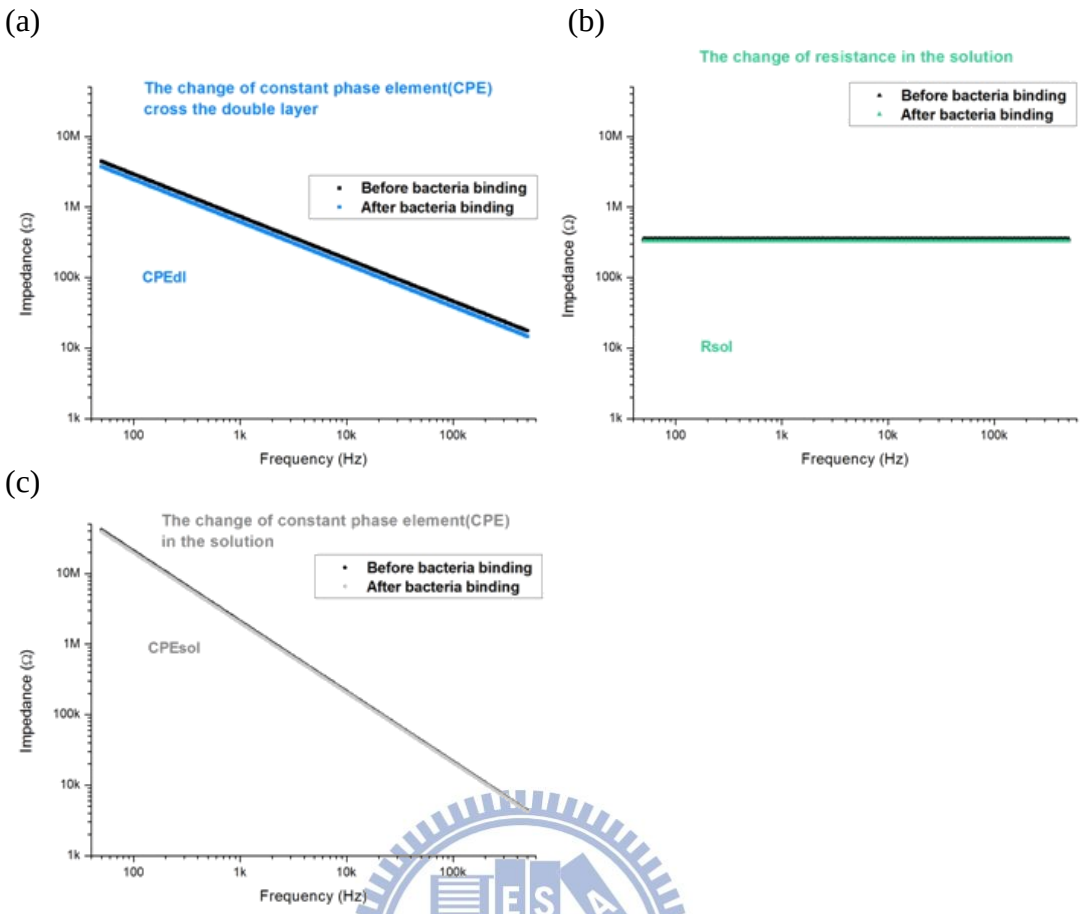

Figure 4-23 Impedance spectroscopy of electrode C (a)impedance of CPE on electrode surface (b) impedance of solution(c) impedance of CPE in the solution.

4-3-2 Impedance analysis on antibody-unmodified chip

The efficiency of bacteria binding was characterized by detection on the antibody-unmodified chip. The detection was gotten by trapping *Vibrio Parahaemolyticus* at concentration of 10^8 cfu/mL with AC electrokinetics compared with trapping without it on electrode A. Figure 4-24 show the results of measurement for antibody-unmodified process. Figure 4-24(a) is the impedance spectra for bacteria binding with excitation. Figure 4-24(b) is control without excitation. The pictures in Figure 4-25 reveal few bacteria under microscopy are still binding after AC electrokintices enhancement and wash. The remaining attachment of bacteria is caused by the polarized effect from the DEP force. The impedance normalized

change(NIC) between the bacteria binding in Figure 4-26 states similar variation, so the gold electrode with antibody modification has beneficial to bind bacteria. We also take the NIC data from the detection of *Vibrio Parahaemolyticus* at concentration of 10^8 cfu/mL on antibody-modified chip for comparison at 50 Hz, shown in Figure 4-27.

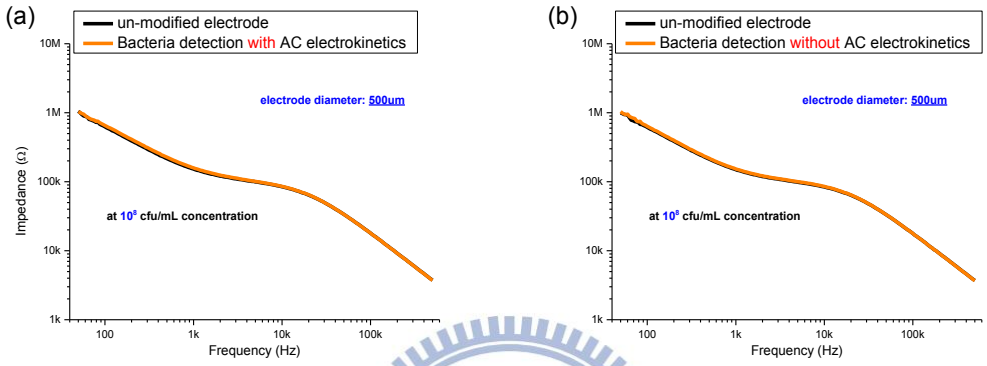

Figure 4-24 Impedance spectra (a)with AC electrokinetics (b) without AC electrokinetics on antibody-unmodified electrode.

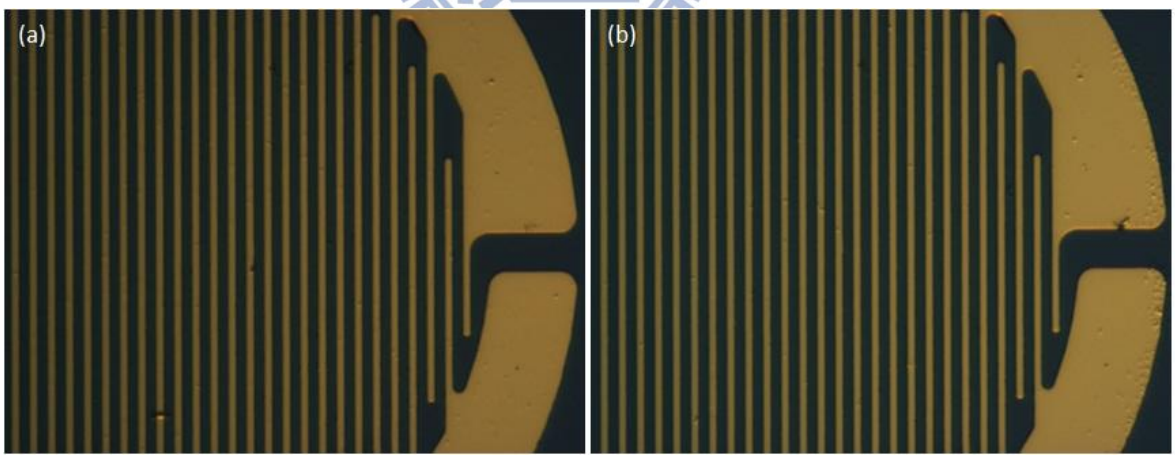

Figure 4-25 Optical images of *Vibrio Parahaemolyticus* attaching on electrode after binding (a) without AC electrokinetics (b) with AC electrokinetics and wash.

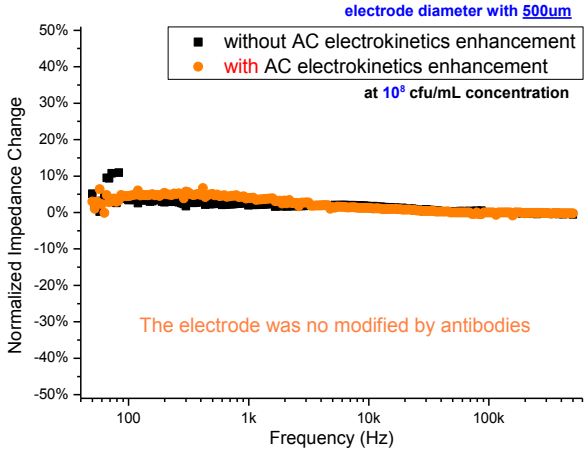

Figure 4-26 NIC spectra for *Vibrio Parahaemolyticus* binding with and without AC electrokinetics enhancement.

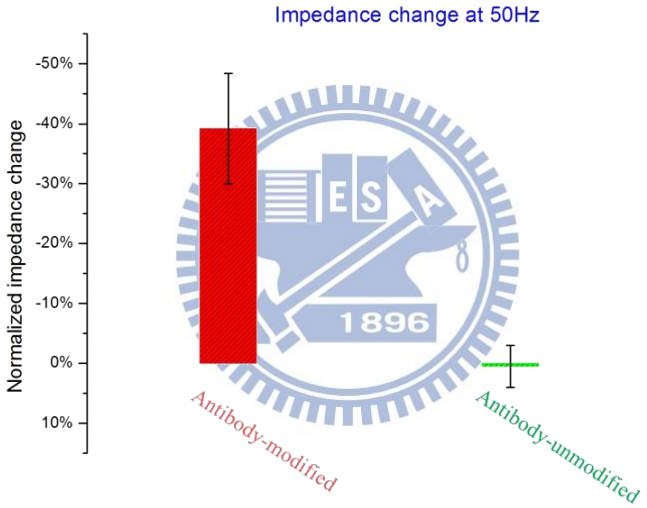

Figure 4-27 NIC between bacteria binding with and without modification of antibodies.

Appling the impedance spectra to the equivalent circuit model, the data fitting of three elements is collected by Table 4-3. The electrode with antibodies modification has biggest change on surface capacitance (CPEdl-T) after bacteria binding, 2.4 times of value from surface capacitance before binding, however, the chip without antibodies modification gives a change of 0.9 times in CPEdl-T. The impedance

spectra of each element for antibodies unmodification are shown in Figure 4-28. The magnitude of capacitance of electrode surface, resistance of solution, or capacitance of solution demonstrates a negligible change before and after bacteria binding.

Table 4-3 Data fitting for bacteria detection with and without antibodies modification.

	CPEdl-T	CPEdl-p	Rsol	CPEsol-T	CPEsol-p
With antibodies					
before detection	**8.7701×10^{-9}**	0.72793	68620	1.6052×10^{-10}	0.91754
After detection	**2.0848×10^{-8}**	0.6613	44204	2.3348×10^{-10}	0.8948
Without antibodies					
before detection	**1.2653×10^{-8}**	0.76104	94521	9.4923×10^{-11}	0.99394
After detection	**1.1471×10^{-8}**	0.76894	07305	9.5325×10^{-11}	0.99378

(a)

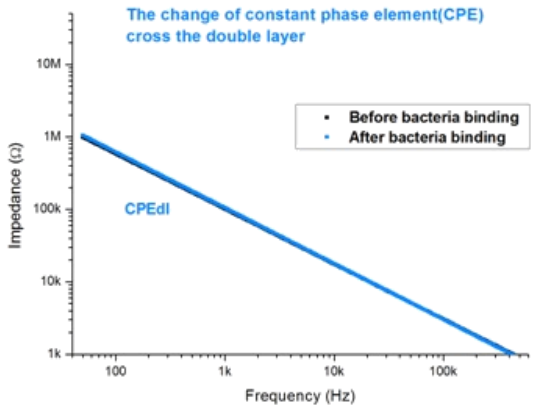

(b)

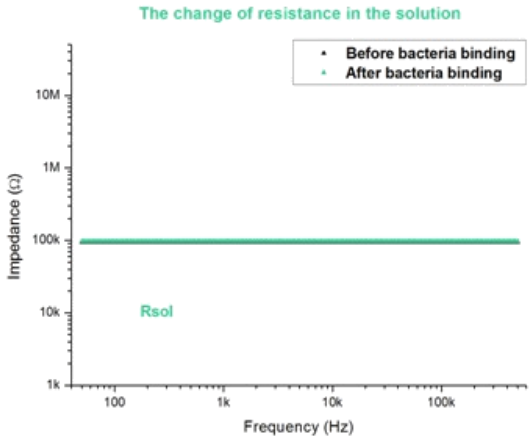

(c)

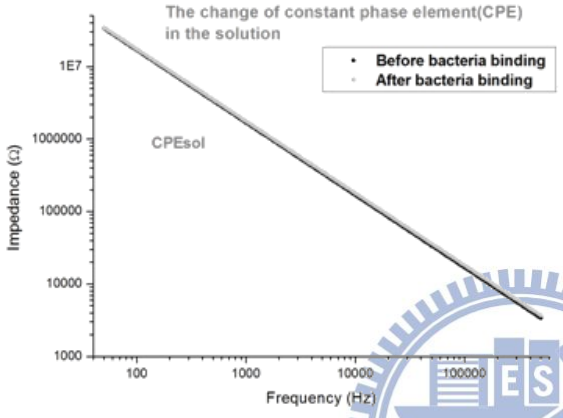

Figure 4-28 Impedance spectra of each element (a)impedance of CPE on electrode surface (b) impedance of solution(c) impedance of CPE in the solution.

4-3-3 Impedance analysis of various concentrations of *Vibrio Parahaemolyticus*

The study also utilized the functionalized chip, the electrode A, detect the *Vibrio Parahaemolyticus* in concentration ranging from 10^5 to 10^7cfu/mL, binding on inner electrode. The analysis was achieved in a comparison based on bacteria manipulation with AC electrokinetics without AC electrokinetics(control).

Figure 4-29(a), Figure 4-30(a), and Figure 4-31(a) stated the detection of *Vibrio Parahaemolyticus* at a concentration ranging from 10^5cfu/mL to 10^7cfu/mL. Figure 4-29(b)(c), Figure 4-30(b)(c), and Figure 4-31(b)(c) shows different concentration of the bacterial cells before and after binding with AC electrokinetics enhancement. Less concentration of bacteria means less bacteria binding on the electrode surface. In the same way, the immobilized bacteria have effect of the impedance change on the electrode surface at low frequency. Its changes indicate a negative value of Normalized impedance change (NIC) due to the decrease of the magnitude of impedance as well. Furthermore, the variation of the Normalized impedance change (NIC) is proportional to number of the bacterial reduction. Figure 4-32 thus depicts the impedance change for different number of *Vibrio Parahaemolyticus* at a fixed frequency of 50 Hz. The limitation of this system for low concentration of bacteria is greater than 10^5 cfu/mL. However, the infection dose of *Vibrio Parahaemolyticus* giving rise to symptoms of illness is at 10^6 cfu/mL.

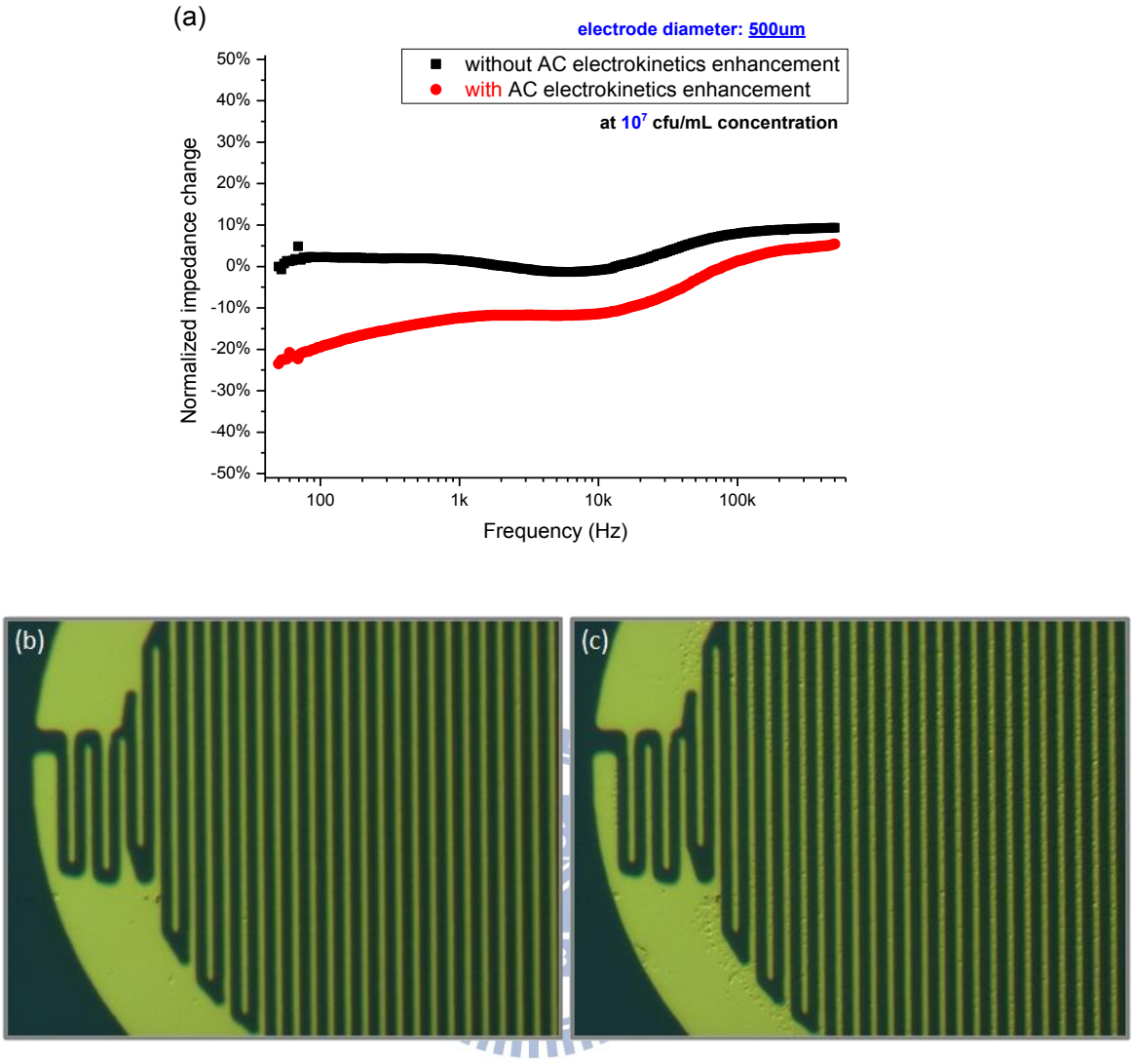

Figure 4-29 Optical images of *Vibrio Parahaemolyticus* at a concentration of 10^7cfu/mL (a) NIC spectra for binding with and without AC electrokinetics enhancement (b) optical microscopy before binding of bacteria (c) after binding with AC electrokinetics enhancement.

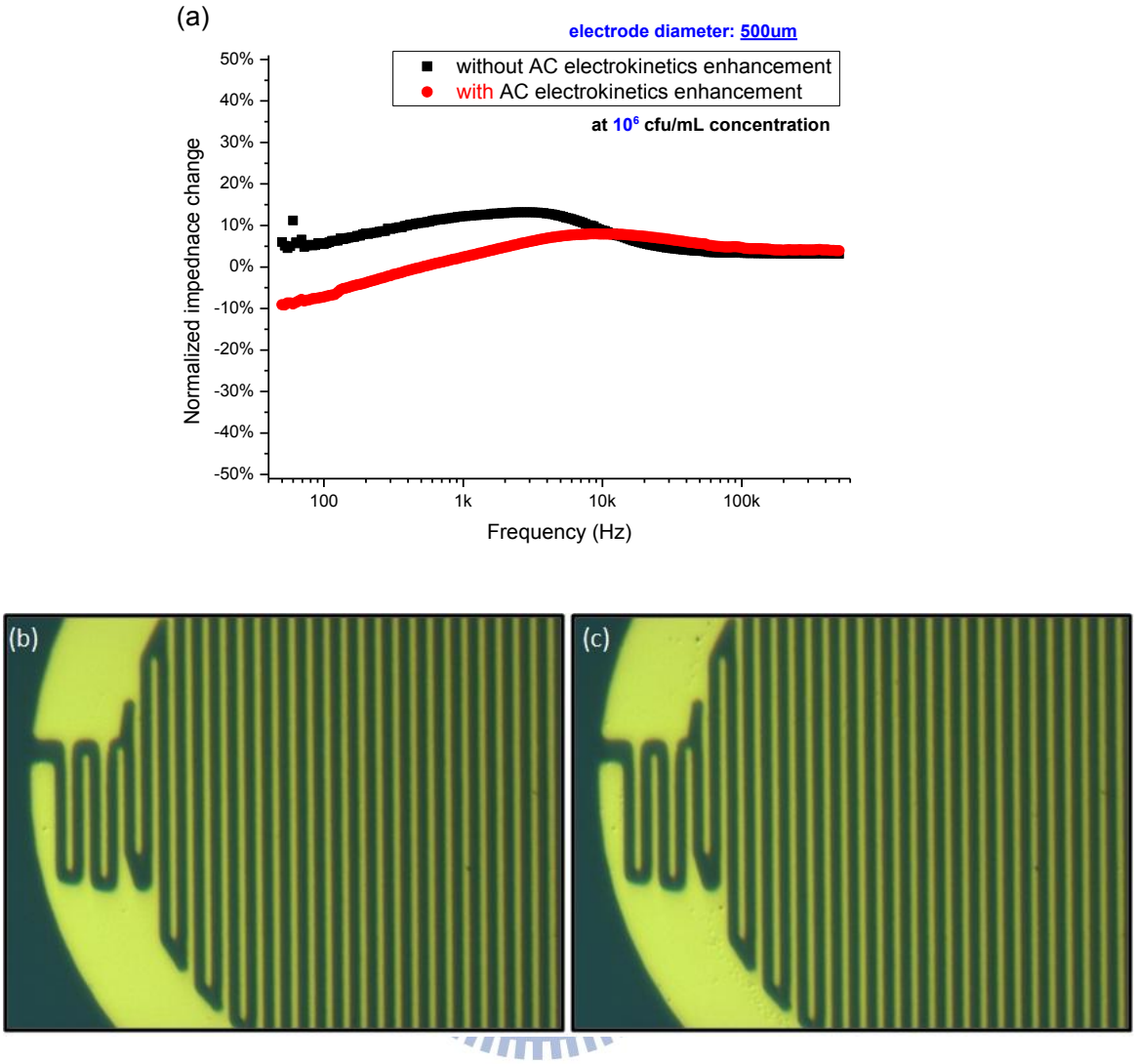

Figure 4-30 Optical images of *Vibrio Parahaemolyticus* at a concentration of 10^6cfu/mL (a) NIC spectra for binding with and without AC electrokinetics enhancement (b) optical microscopy before binding of bacteria (c) after binding with AC electrokinetics enhancement.

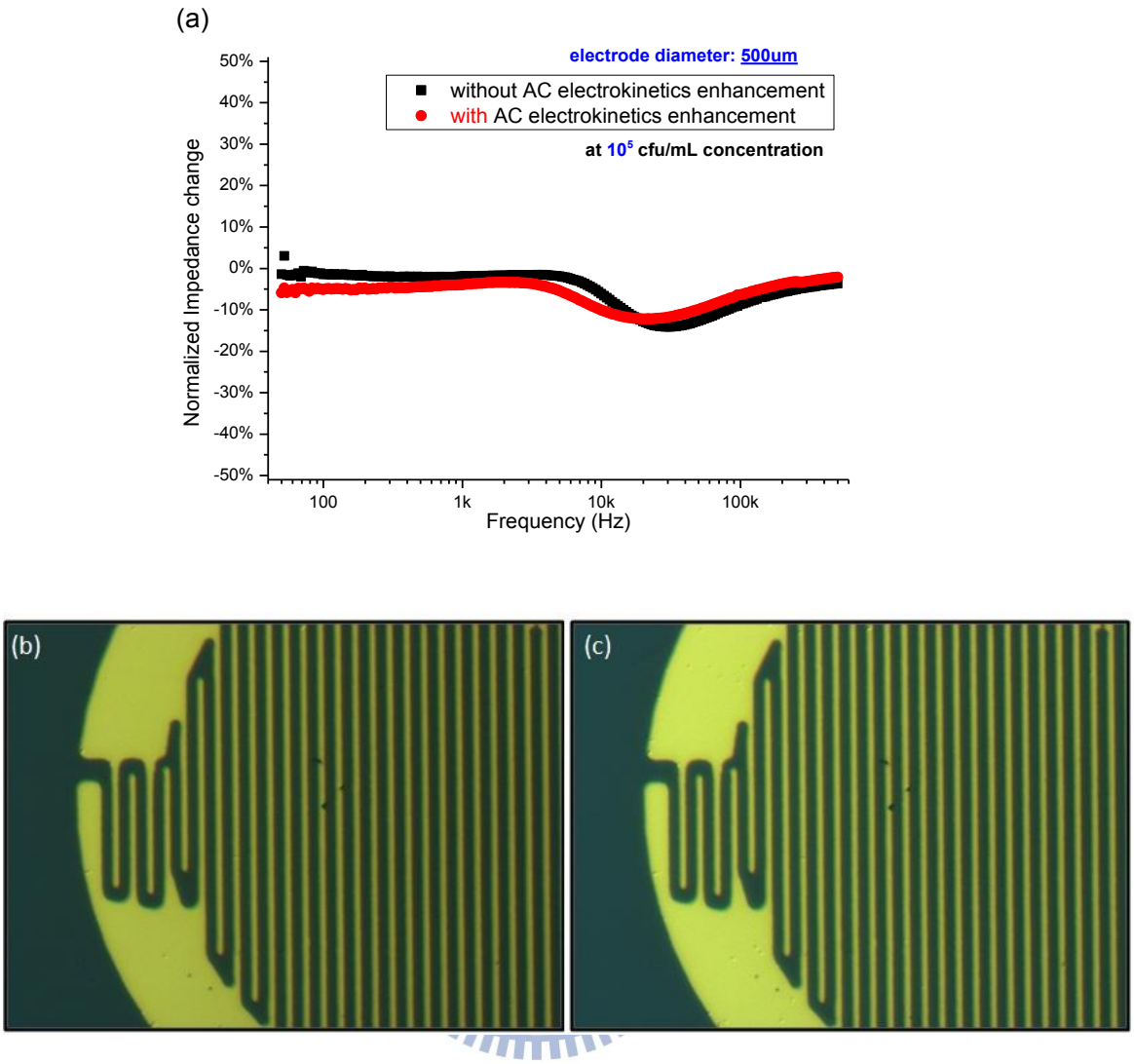

Figure 4-31 Optical images of *Vibrio Parahaemolyticus* at a concentration of 10^5cfu/mL (a) NIC spectra for binding with and without AC electrokinetics enhancement (b) optical microscopy before binding of bacteria (c)after binding with AC electrokinetics enhancement.

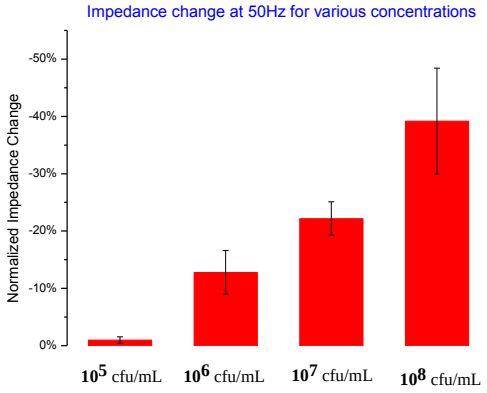

Figure 4-32 Impedance change of various concentrations of *Vibrio Parahaemolyticus* at 50 Hz

4-3-4 Selective detection between *Vibrio Parahaemolyticus* and XL1 blue *E. coli*

Bacteria detection has to be distinguishable in clinical diagnosis whereas the pathogenic bacteria always go along with many other non-pathogenic bacterial cells. In this experiments, ELISA method was utilized to perform the *Vibrio Parahaemolyticus* recognition by its specific antibodies. The assay also introduced XL1 blue *E coli* strain as nonpathogenic bacteria in the system. The indirect type ELISA was thus carried out. Two sorts of bacteria were incubated in plate separately. Figure 4-33 showed the TMB chromogenic result by using different dilution of concentration of antibodies immobilized in the plate. The darker color changes obviously in the columns (rightside) with *Vibrio Parahaemolyticus* differ from the columns with *E coli* (Figure 4-33(a)). The recognition of the antibodies is clearly specific for *Vibrio Parahaemolyticus,* enable the distinguish detection of bacteria selectively. The absorbency for each plate well measured at 450nm decrease progressively depends on concentration of antibodies, shown in Figure 4-33(b). Figure 4-34 is including the negative and positive control.

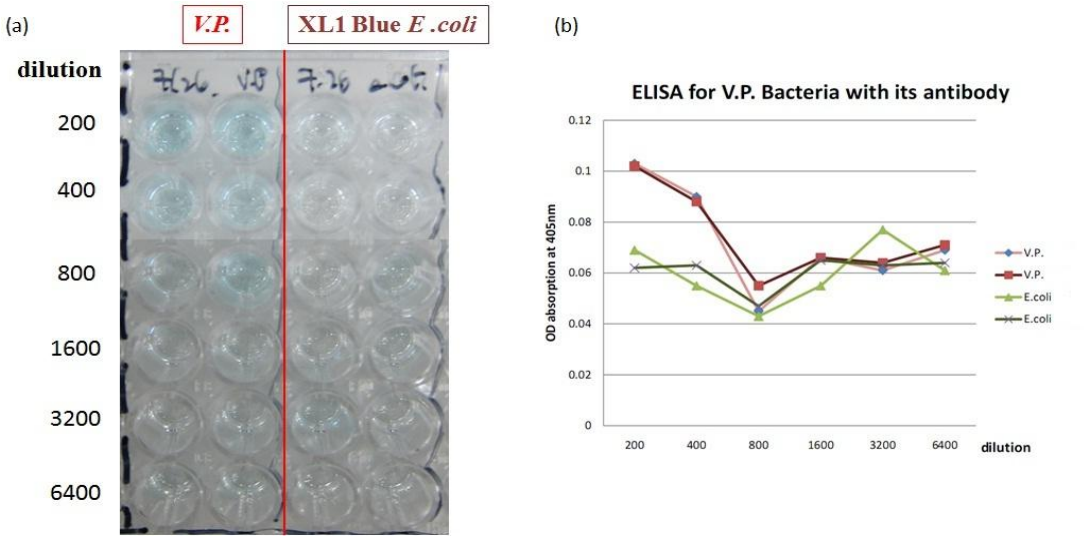

Figure 4-33 ELISA chromogenic result for XL blue *E coli* and *Vibrio Parahaemolyticus* detection with *Vibrio Parahaemolyticus*-specific antibodies (a) color change from TMB development (b) absorbency

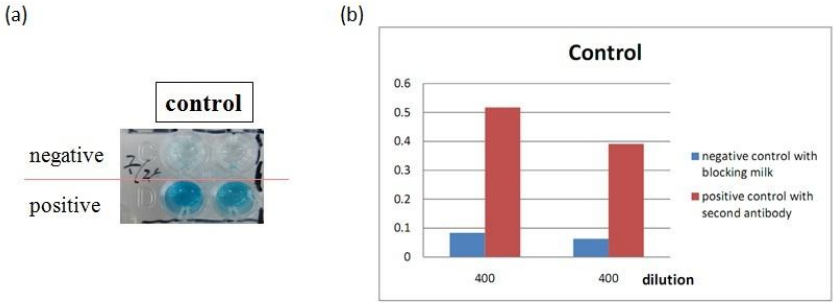

Figure 4-34 Negative/positive Control for ELISA.

The selective detection was further demonstrated by two assay systems. First, the mixed solution with *Vibrio Parahaemolyticus* and XL blue *E coli* at the same concentration of 5×10^7 cfu/mL was measured after bacteria binding with AC electrokinetics enhancement. The operational parameters for AC electrokinetics rely on *Vibrio Parahaemolyticus* trapping. Second, observed the performance of the antibodies' recognition, only XL blue *E coli* at concentration of 10^8 cfu/mL was trapped and measured.

The impedance spectra of mixed solution were shown in Figure 4-35. Bacteria binding can be also observed by optical microscopy in Figure 4-36. The shape of XL1 blue *E coli* and *Vibrio Parahaemolyticus* cannot tell difference apparently, so the AC electrokinetics for trapping may force on both bacteria. The measurement after bacteria binding with AC electrokinetics(Figure 4-35 (a)) has different scale compared to the binding without AC elctrokinetics(Figure 4-35(b)). The NIC for mixed solution is shown in Figure 4-37. However, the detections of *E coli* individually with and with AC electrokinetics depicted in Figure 4-38 vary no difference after bacteria binding and wash. The NIC of *E coli* measurement shown in Figure 4-40 also report the same drift. In Figure 4-39, few *E coli* attach to the electrode firmly due to DEP force even washed by buffer. The polarized force induced by DEP bring bacteria to touch the

edge of electrodes(Figure 4-39(b)). All the selective detection of bacteria including *Vibrio Parahaemolyticus*, *E. coli*, and *Vibrio Parahaemolyticus*+ *E. coli* compared together with impedance change at 50 Hz in Figure 4-41. The selectivity was particularly for *Vibrio Parahaemolyticus*, which show a slightly larger measurement relative to XL1 Blue *E coli*

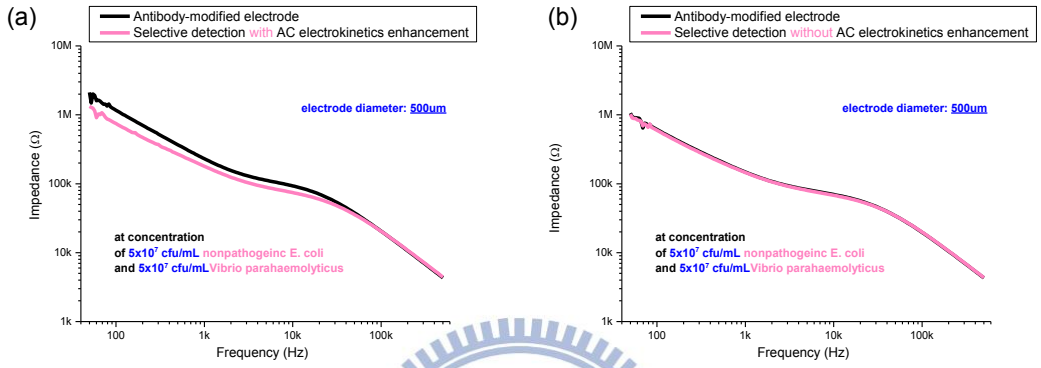

Figure 4-35 Impedance spectra (a)with AC electrokinetics (b) without AC electrokinetics.

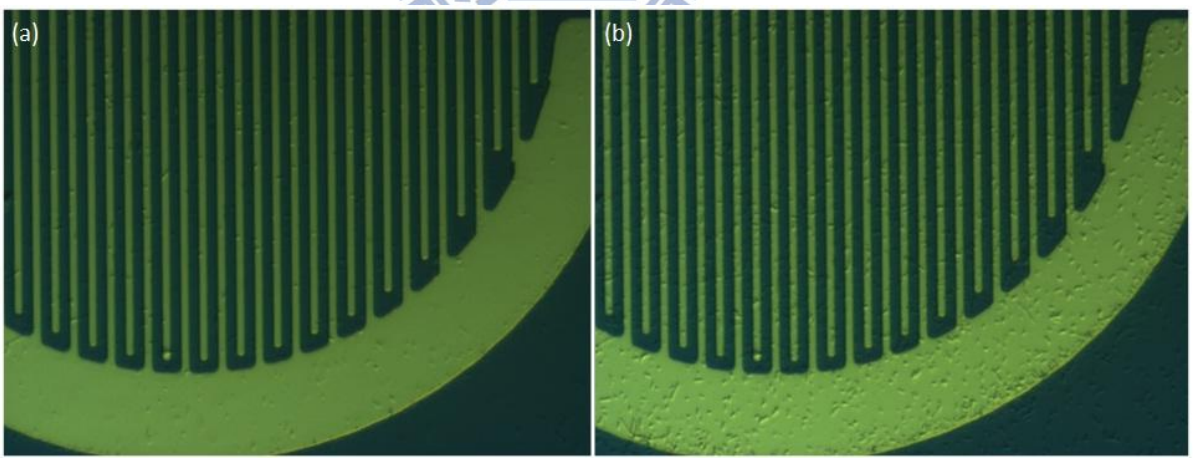

Figure 4-36 Optical images of *Vibrio Parahaemolyticus* ($5*10^7$cfu/mL) with XL1 blue *E. coli* ($5*10^7$cfu/mL) binding on electrode with AC electrokinetics enhancement. (a)before binding of bacteria (b) after binding.

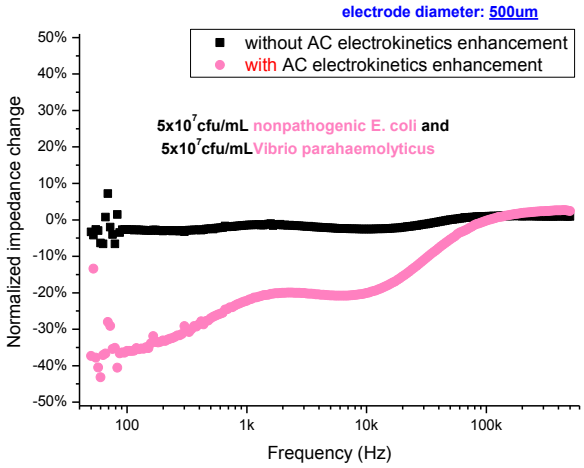

Figure 4-37 NIC spectra of *Vibrio Parahaemolyticus* ($7*10^5$cfu/mL) with XL1 blue *E. coli* ($7*10^5$cfu/mL) binding.

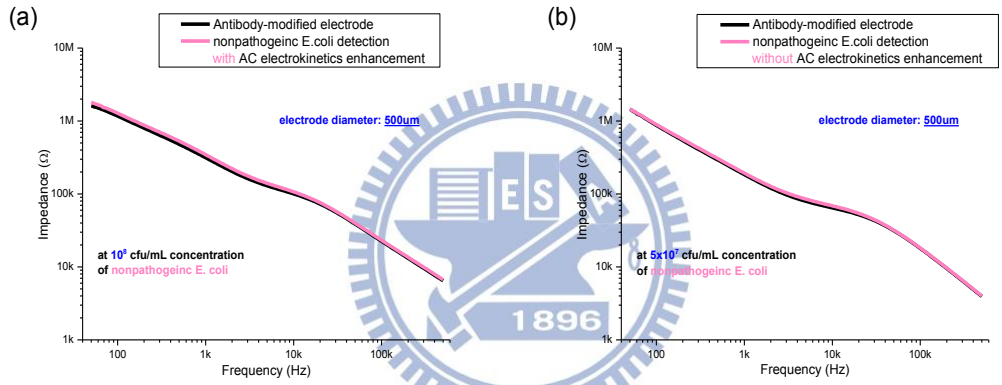

Figure 4-38 Impedance spectra (a)with AC electrokinetics (b) without AC electrokinetics.

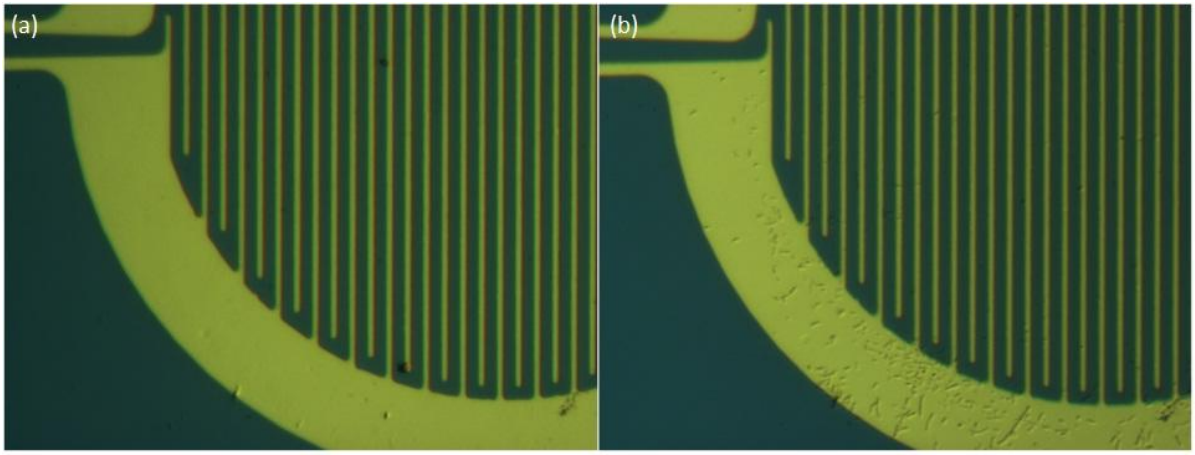

Figure 4-39 Optical images of XL1 blue *E. coli*(10^8cfu/mL) binding on electrode with AC electrokinetics enhancement. (a)before binding of bacteria (b) after binding.

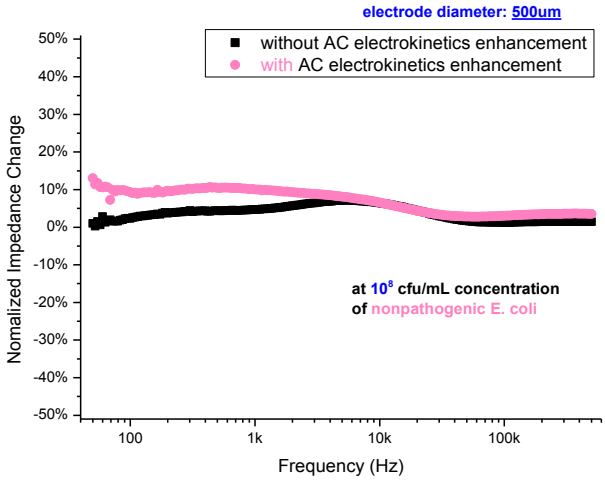

Figure 4-40 NIC spectra of XL1 blue *E. coli* (10^8cfu/mL) binding.

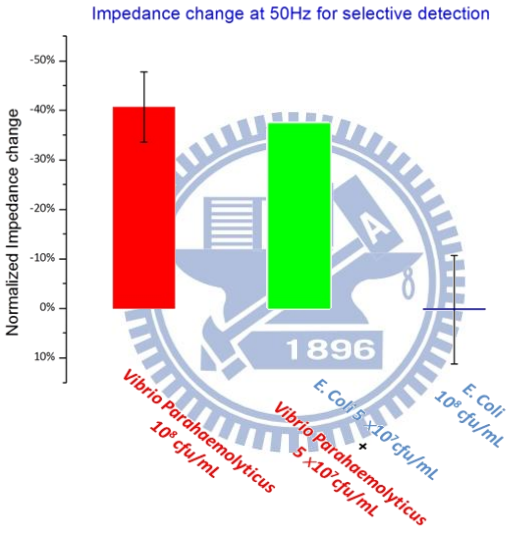

Figure 4-41 NIC related to two bacterial species at 50 Hz.

Appling the impedance spectra to the equivalent circuit model, the fitting data of three elements is collected by Table 4-4. Measurement of the *Vibrio Parahaemolyticus* binding in the presence of *Ecoli* change surface capacitance (CPEdl-T) as usual after bacteria binding both, 2.2 times of value from surface capacitance before binding, however, the chip for another detection of E coli gives a change of 1.1 times in CPEdl-T. The impedance spectra of each element for selective detection are shown in Figure 4-42 and Figure 4-43. For detection the magnitude of

electrode surface capacitance demonstrates a change, relative to detection of *E coli*, before and after bacteria binding at low frequency.

Table 4-4 Data fitting for selective detection.

	CPEdl-T	CPEdl-p	Rsol	CPEsol-T	CPEsol-p
***Vibrio parahaemolyticus* 10^{8} cfu/mL**					
before detection	**8.7701×10^{-9}**	0.72793	68620	1.6052×10^{-10}	0.91754
After detection	**2.0848×10^{-8}**	0.6613	44204	2.3348×10^{-10}	0.8948
***Vibrio parahaemolyticus* 5×10^{7} cfu/mL+ *nonpathogenic E. coli* 5×10^{7} cfu/mL**					
before detection	**5.0858×10^{-9}**	0.78937	102350	8.5359×10^{-11}	0.99052
After detection	**1.1316×10^{-8}**	0.7469	74774	9.2347×10^{-10}	0.98296
***nonpathogenic E. coli* 10^{8} cfu/mL**					
before detection	**4.2393×10^{-9}**	0.81075	73203	1.0449×10^{-10}	098239
After detection	**4.911×10^{-9}**	0.78692	86021	1.0268×10^{-10}	0.98189

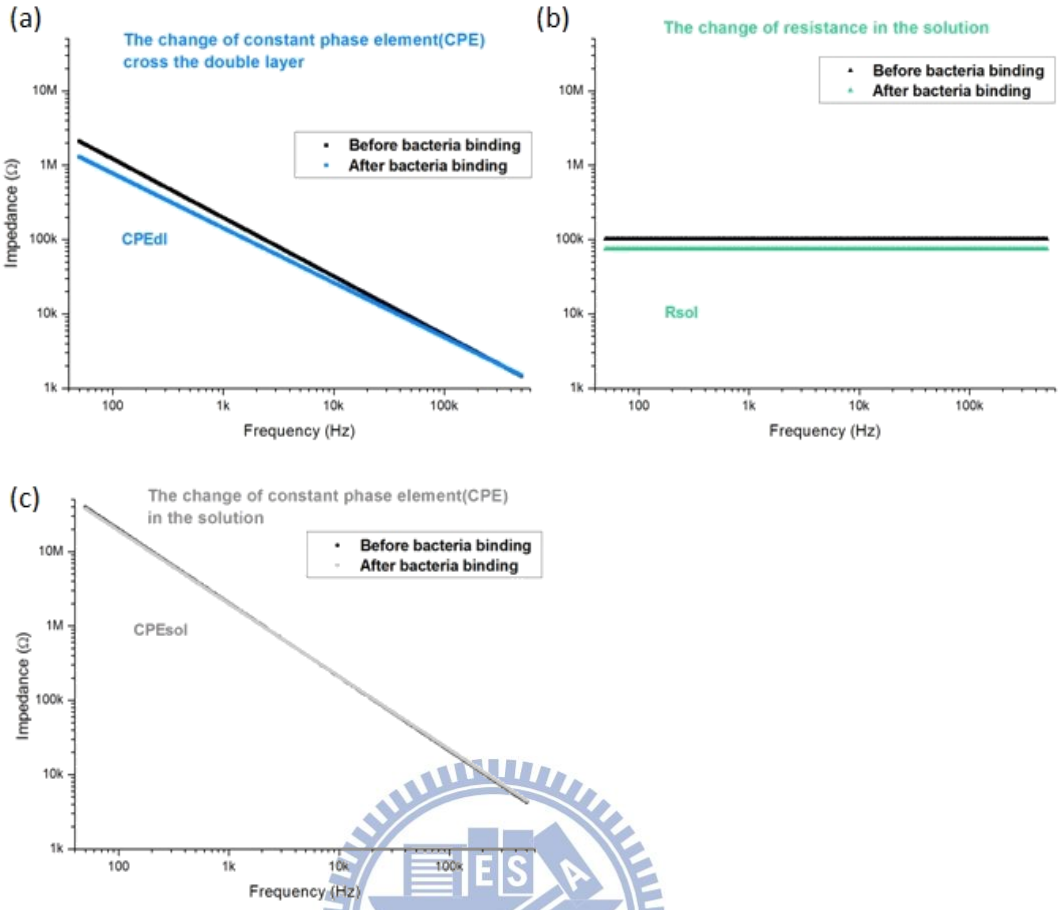

Figure 4-42 Impedance of each element (a)impedance of CPE on electrode surface (b) impedance of solution(c) impedance of CPE in the solution for *V.P.+E coli* detection.

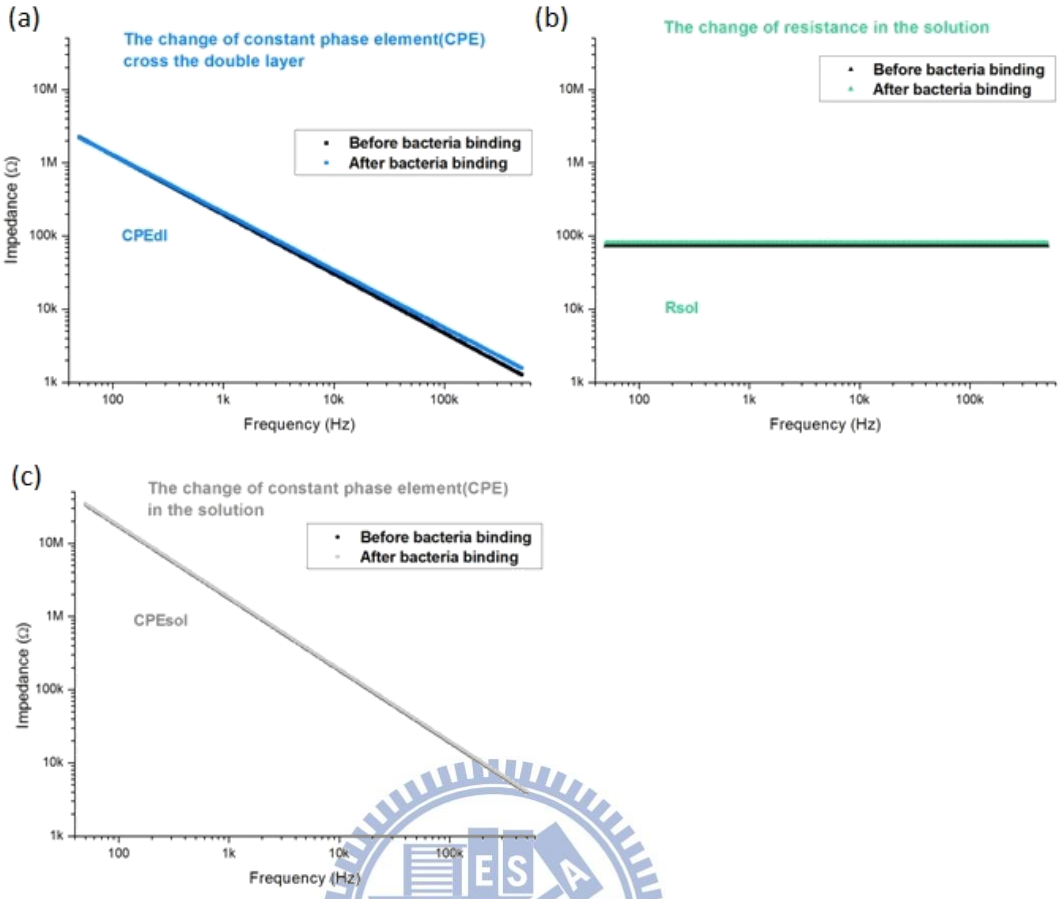

Figure 4-43 Impedance of each element (a)impedance of CPE on electrode surface (b) impedance of solution(c) impedance of CPE in the solution for *E coli* detection.

Chapter 5 Conclusion and Future work

5-1 Conclusion

In this study, impedance biosensor has been proposed for rapid detection of pathogenic bacteria, *Vibrio parahaemoltricus*. AC electrokinetics has been realized to concentrate the bacteria onto functionalized electrodes and detecting immobilized bacteria via impedance spectra in the microfluidic system. Binding of linker molecule and antibodies on gold electrode have been demonstated and justified by several methods. We have demonstrated the successful manipulation of *Vibrio parahaemoltricus* on the circular electrodes within interdigited configures via AC electrokinetics. The new electrode configuration successfully demonstrated the integration of bacteria concentration and its detection.

Compared to the bacteria binding without AC electrokinetics, the impedance change due to the *Vibrio parahaemoltricus* immobilization with AC electrokinetics greatly improved within a limited time. After the bacteria adhered to the surface of electrode, the total impedance changed at low frequency due to the decrease of impedance across the electrical double layer, resulting from the equivalent circuit fitting. The impedance analyzer detected a minimum of 10^5 cfu/mL of *Vibrio parahaemoltricus* in 0.01xPhosphate buffer. The analysis showed that the larger ratio of biosensing area to microfluidic channel the more sensitive on bacteria detection. Moreover, the selective detections were demonstrated via detection of mixing *Vibrio parahaemoltricus* with non-pathogenic bacteria, XL1 Blue *E. coli* with *Vibrio parahaemoltricus* antibodies-modified electrode.

5-2 Future work

Further exploration on this work will be on the increase of sensitivity down to 10^3 cfu/ml. The sensitivity of impedance detection depends on various parameters, including configure of electrode, binding affinity of biomolecule, dimension of microfluidic system, and ionic strength of buffer solution for detection. First, improvement of configure of the electrode for detection and for trapping influence using AC electrokinetics make it efficiently applicable to biosensing comprehensively. Second, SiO_2 substrate can be passivated with poly(ethylene glycol)(PEG). Due to its highly hydrated polymer chains and steric stabilization force, it may prevent the binding between SiO_2 and protein or fluorescent dye toward selectivity for gold-patterned SiO_2 surfaces. The concentration of antibodies also affect on the affinity of bacteria binding. Future experiments should cover the relation between concentration of antibodies and efficiency of bacteria binding. Third, for impedance detection in microfluidic system, carrying small resistance and large capacitance of solution can rise capacitance of the electrical double layer respectively. Hence, using narrow and elaborate microfluidic system may enhance the sensitivity of the bio-impedance analysis, especially for lower concentration detection. Further, the solution using higher conductivity for impedance analysis can reduce the background impedance. Figure 5-1 shows the background impedance (without antibodies modification) in the solution of 0.01*phosphate buffer and 1*phosphate buffer. With the above mentioned improvements, biosensors can be improved toward higher quality for impedance analysis in bacteria detection.

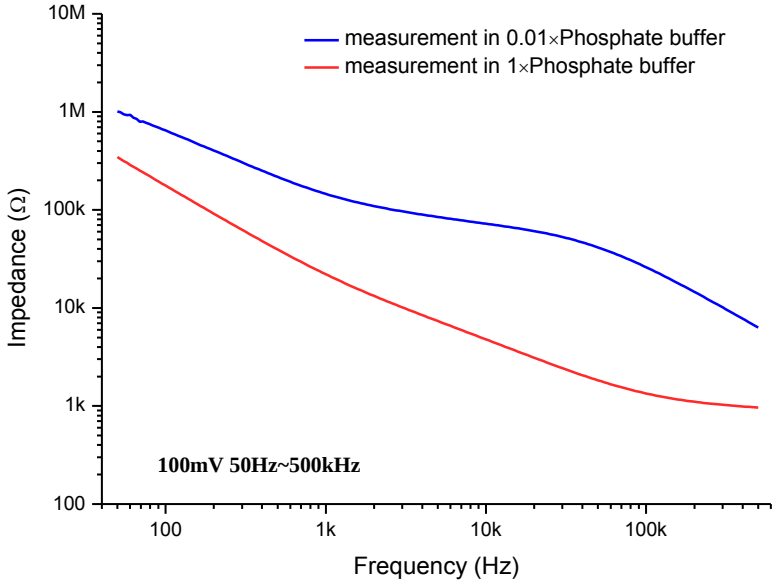

Figure 5-1 Comparison of background impedance spectra between 0.01xPB and 1xPB.

References

1. CDC *Foodborne illness: National Center for Emerging and Zoonotic Infectious Diseases* (Atlanta), (CDC); 2011.
2. 食品藥物管理局 "台灣食品中毒案件因物質統計表", 2010.
3. Velusamy V, Arshak K, Korostynska O, Oliwa K, & Adley C "An overview of foodborne pathogen detection: In the perspective of biosensors", *Biotechnology Advances* 28 2 pp. 232-254, 2009.
4. Yang L & Bashir R "Electrical/electrochemical impedance for rapid detection of foodborne pathogenic bacteria", *Biotechnology Advances* 26 2 pp. 135-150, 2007.
5. Daniels JS & Pourmand N "Label-free impedance biosensors: Opportunities and challenges", *Electroanalysis* 19 12 pp. 1239-1257, 2007.
6. Taylor AD, Yu Q, Chen S, Homola J, & Jiang S "Comparison of E. coli O157:H7 preparation methods used for detection with surface plasmon resonance sensor", *Sensors and Actuators B: Chemical* 107 1 pp. 202-208, 2005.
7. Su X-L & Li Y "A QCM immunosensor for Salmonella detection with simultaneous measurements of resonant frequency and motional resistance", *Biosensors and Bioelectronics* 21 6 pp. 840-848, 2005.
8. Johnson RP, *et al.* "Detection of Escherichia coli O157:H7 in meat by an enzyme-linked immunosorbent assay, EHEC-Tek", *Applied and Environmental Microbiology* 61 1 pp. 386-388, 1995.
9. González SF, Krug MJ, Nielsen ME, Santos Y, & Call DR "Simultaneous Detection of Marine Fish Pathogens by Using Multiplex PCR and a DNA Microarray", *Journal of Clinical Microbiology* 42 4 pp. 1414-1419, 2004.
10. Yang L, Li Y, Griffis CL, & Johnson MG "Interdigitated microelectrode (IME) impedance sensor for the detection of viable Salmonella typhimurium", *Biosensors and Bioelectronics* 19 10 pp. 1139-1147, 2004.
11. Yang L, Li Y, & Erf GF "Interdigitated Array Microelectrode-Based Electrochemical Impedance Immunosensor for Detection of Escherichia coli O157:H7", *Analytical Chemistry* 76 4 pp. 1107-1113, 2004.
12. Suehiro J, Ohtsubo A, Hatano T, & Hara M "Selective detection of bacteria by a dielectrophoretic impedance measurement method using an

antibody-immobilized electrode chip", *Sensors and Actuators B: Chemical* 119 1 pp. 319-326, 2006.

13. **Suehiro J, Noutomi D, Shutou M, & Hara M "Selective Detection of Bacteria by using Dielectrophoretic Impedance Measurement Method with Immobilized Antibody Electrode", *IEEE* pp. 1950-1955, 2001.**
14. **Suehiro J, Noutomi D, Shutou M, & Hara M "Selective detection of specific bacteria using dielectrophoretic impedance measurement method combined with an antigen–antibody reaction", *Journal of Electrostatics* 58 3-4 pp. 229-246, 2003.**
15. **Suehiro J, Hamada R, Noutomi D, Shutou M, & Hara M "Selective detection of viable bacteria using dielectrophoretic impedance measurement method", *Journal of Electrostatics* 57 2 pp. 157-168, 2003.**
16. **Bown M & Meinhart C "AC electroosmotic flow in a DNA concentrator", *Microfluidics and Nanofluidics* 2 6 pp. 513-523, 2006.**
17. **Sin MLY, Gau V, Liao JC, Haake DA, & Wong PK "Active Manipulation of Quantum Dots using AC Electrokinetics", *The Journal of Physical Chemistry C* 113 16 pp. 6561-6565, 2009.**
18. **Wong PK, Chen C-Y, Wang T-H, & Ho C-M "Electrokinetic Bioprocessor for Concentrating Cells and Molecules", *Analytical Chemistry* 76 23 pp. 6908-6914, 2004.**
19. **Varshney M & Li Y "Interdigitated array microelectrodes based impedance biosensors for detection of bacterial cells", *Biosensors and Bioelectronics* 24 10 pp. 2951-2960, 2009.**
20. **Ramos A, Morgan H, Green NG, & Castellanos A "Ac electrokinetics: a review of forces in microelectrode structures", *Journal of Physics D: Applied Physics* 31 18 pp. 2338, 1998.**
21. **Castellanos A, Ramos A, González A, Green NG, & Morgan H "Electrohydrodynamics and dielectrophoresis in microsystems: scaling laws", *Journal of Physics D: Applied Physics* 36 20 pp. 2584, 2003.**
22. **Oh J, Hart R, Capurro J, & Noh H "Comprehensive analysis of particle motion under non-uniform AC electric fields in a microchannel", *Lab on a Chip* 9 1 pp. 62-78, 2009.**
23. **Green NG, Ramos A, & Morgan H "Ac electrokinetics: a survey of sub-micrometre particle dynamics", *Journal of Physics D: Applied Physics***

33 6 pp. 632, 2000.

24. **Morgan H, Hughes MP, & Green NG "Separation of Submicron Bioparticles by Dielectrophoresis", *Biophysical Journal* 77 1 pp. 516-525, 1999.**
25. **Kai FH, Martin BM, & Michael PH "Use of combined dielectrophoretic/electrohydrodynamic forces for biosensor enhancement", *Journal of Physics D: Applied Physics* 36 20 pp. L101, 2003.**
26. **Liju Y "Dielectrophoresis assisted immuno-capture and detection of foodborne pathogenic bacteria in biochips", *Talanta* 80 2 pp. 551-558, 2009.**
27. **Kirby BJ *Micro- and Nanoscale Fluid Mechanics: Transport in Microfluidic Devices*, Cambrigde University Press 2009.**
28. **Bard LRFAJ *ELECTROCHEMICAL METHODS Fundamentals and Applications*, 2001.**
29. **Schoch RB, Han J, & Renaud P "Transport phenomena in nanofluidics", *Reviews of Modern Physics* 80 3 pp. 839-883, 2008.**
30. **Ramos A, Morgan H, Green NG, & Castellanos A "AC Electric-Field-Induced Fluid Flow in Microelectrodes", *Journal of Colloid and Interface Science* 217 2 pp. 420-422, 1999.**
31. **H.Morgan NGG *AC electrokinetics: colloids and nanoparticles*, RESEARCH STUDIES PRESS LTD. 2001.**
32. **Aldaeus F, Lin Y, Roeraade J, & Amberg G "Superpositioned dielectrophoresis for enhanced trapping efficiency", *ELECTROPHORESIS* 26 22 pp. 4252-4259, 2005.**
33. **Morgan H & Green NG "Dielectrophoretic manipulation of rod-shaped viral particles", *Journal of Electrostatics* 42 3 pp. 279-293, 1997.**
34. **Fischer LM, *et al.* "Gold cleaning methods for electrochemical detection applications", *Microelectronic Engineering* 86 4-6 pp. 1282-1285, 2008.**
35. **Canaria CA, *et al.* "Formation and removal of alkylthiolate self-assembled monolayers on gold in aqueous solutions", *Lab on a Chip* 6 2 pp. 289-295, 2006.**
36. **Samanta D & Sarkar A "Immobilization of bio-macromolecules on self-assembled monolayers: methods and sensor applications", *Chemical***

Society Reviews **40 5 pp. 2567-2592, 2011.**

37. **Choi SH, Lee JW, & Sim SJ "Enhanced performance of a surface plasmon resonance immunosensor for detecting Ab–GAD antibody based on the modified self-assembled monolayers",** ***Biosensors and Bioelectronics*** **21 2 pp. 378-383, 2005.**
38. **Lan S, Veiseh M, & Zhang M "Surface modification of silicon and gold-patterned silicon surfaces for improved biocompatibility and cell patterning selectivity",** ***Biosensors and Bioelectronics*** **20 9 pp. 1697-1708, 2005.**
39. **Hong J,** ***et al.*** **"AC frequency characteristics of coplanar impedance sensors as design parameters",** ***Lab on a Chip*** **5 3 pp. 270-279, 2005.**
40. **Varshney M & Li Y "Interdigitated array microelectrode based impedance biosensor coupled with magnetic nanoparticle–antibody conjugates for detection of Escherichia coli O157:H7 in food samples",** ***Biosensors and Bioelectronics*** **22 11 pp. 2408-2414, 2007.**